Effect of Processing Parameters on Bond Strength and Effective Plasticity in Al_2O_3-TiB_2 Composites

Susan Marie Holt

Thesis submitted to the faculty of the Virginia Polytechnic Institute and State University in partial fulfillment of the requirements for the degree of

Master of Science
In
Materials Science and Engineering

Kathryn V. Logan
Gary R. Pickrell
William T. Reynolds

September 9, 2011
Blacksburg, Virginia

Keywords: Bond strength, Effective plasticity, Alumina, Titanium Diboride

Effect of Processing Parameters on Bond Strength and Effective Plasticity in Al_2O_3-TiB_2 Composites

Susan Marie Holt

ABSTRACT

Alumina-titanium diboride (Al_2O_3-TiB_2) composites have high temperature, wear, and impact resistance that could be useful in high performance applications. Determining the effect of processing parameters on relative bond strength and effective plasticity may contribute to optimization and predictability of performance in the Al_2O_3-TiB_2 system. Al_2O_3-TiB_2 composites were obtained from a collection of samples that were created during a separate ongoing research program being conducted by Dr. Kathryn V. Logan. The Logan samples were initially formed by hot pressing powders produced using Self-Propagating High Temperature synthesis (SHS) of Al, TiO_2, and B_2O_3 powders or manual mixing (MM) of Al_2O_3 and TiB_2 powders. Samples were then fractured using standard single edge notched beam (SENB) fracture toughness testing. The obtained fractured surfaces were examined using Scanning Electron Microscopy (SEM) and Energy Dispersive X-ray Spectroscopy (EDS). Relative amounts of transgranular and intergranular fracture of Al_2O_3 and TiB_2 grains were determined. Transgranular fracture was used as a measure of relative bond strength. Other samples were obtained from the Logan collection to conduct nano-indentation measurements on polished sample surfaces in Al_2O_3 grains and in TiB_2 grains. Indent locations were verified using SEM. Reduced modulus, final displacements, and fracture toughness for indents in Al_2O_3 grains and in TiB_2 grains were determined from nano-indentation curves. Reduced modulus was used as a measure of relative bond strength. Final displacement and fracture toughness were used as measures of relative effective plasticity. Analysis of Variance (ANOVA) using Taguchi arrays was conducted using the powder processing factor (SHS vs. MM) and the predominant microstructure factor (TiB_2 grains surrounding Al_2O_3 grains vs. TiB_2 grains distributed amongst Al_2O_3 grains) when examining the effect of processing parameters on relative bond strength as measured by amount of transgranular fracture. Analysis of Variance (ANOVA) using Taguchi arrays was conducted using the powder processing factor (SHS vs. MM), the predominant microstructure factor (TiB_2 grains surrounding Al_2O_3 grains vs. TiB_2 grains distributed amongst Al_2O_3 grains), and the indented phase factor (Al_2O_3 vs. TiB_2) when examining the effect of processing parameters on relative bond strength as measured by nano-indentation reduced modulus and both measures of relative effective plasticity. Powder processing was significant for the relative bond strength measures, but was not significant for the relative effective plasticity measures. Predominant microstructure was significant for all measures except relative effective plasticity as measured by fracture toughness, for which none of the factors and interactions were significant. The interaction between powder processing and predominant microstructure was significant for most of the relative bond strength measures and for relative effective plasticity as measured by final displacements. Indented phase was significant for the nano-indentation measures except nano-indentation fracture toughness, although the significance for nano-indentation fracture toughness was just below the critical level. The interaction between powder processing

and indented phase and the interaction between predominant microstructure and indented phase were only significant for the relative bond strength measure using nano-indentation reduced modulus. The interaction between powder processing, predominant microstructure, and indented phase was significant for the nano-indentation measures except nano-indentation fracture toughness. The optimum level for powder processing was predominantly manual mixing. The optimum level for predominant microstructure was predominantly TiB_2 grains surrounding Al_2O_3 grains. The optimum level for indented phase was predominantly TiB_2.

Dedication

To my family, Chris, Laz, and Ki. Without their love and support, during the past several years, this research would not have been completed.

Acknowledgements

The author wishes to sincerely thank Dr. Kathryn V. Logan, chairperson of the thesis committee, for her guidance, encouragement, and support throughout this research. The author also wishes to thank the other members of the committee, Dr. Gary R. Pickrell and Dr. William T. Reynolds, for their advice throughout this research endeavor.

The author wishes to acknowledge the National Institute of Aerospace for their funding (Grant Award# VT-03-01) of this work. The author also wishes to acknowledge the use of facilities at the ICTAS Nanoscale Characterization and Fabrication Laboratory and the valuable assistance of John McIntosh and Stephen McCartney when using the SEM, EDS, and nano-indentation equipment.

The author wishes to thank the Multifunctional Materials Research Group for their insightful questions and encouragement throughout this research.

Finally, the author wishes to thank her extended family for their love, support, and encouragement throughout this research.

Table of Contents

Figures

Tables

1. Introduction and Background

This thesis describes the effect of processing parameters on relative bond strength and relative effective plasticity. The introduction and background provide information about the objective and goals of this research as well as background information about bond strength, fracture mode, effective plasticity, Alumina-Titanium diboride (Al_2O_3-TiB_2) composites, Scanning Electron Microscopy (SEM), Energy Dispersive X-ray Spectroscopy (EDS), nano-indentation, Taguchi methods, and Analysis of Variance (ANOVA). The experimental methods section provides information about the techniques used to obtain relative measures of bond energy and effective plasticity as well as analysis techniques. The results and discussion section provide a summary of the measurement results for comparative bond energy and effective plasticity as well as a discussion of the results. The conclusions section provides a concise summary of findings in this research. The future work section describes information that would clarify or provide further depth into findings of this research.

1.1. Research Objective and Goals

This section presents the research objective and goals. The objective of this research is to explore the effect of processing parameters on bond strengths and effective plasticity in Al_2O_3-TiB_2 composites. The justification for this research is that previous research on Al_2O_3-TiB_2 composites studied behavior of composites, produced using Self-Propagating High Temperature Synthesis (SHS) and using manual mixing, with respect to dynamic properties. Atomic scale properties of Al_2O_3-TiB_2 composites have not yet been studied. Correlations between processing parameters and atomic scale properties, such as bond strength and effective plasticity, would provide understanding that would allow optimization of properties in Al_2O_3-TiB_2 composites. The information may also be useful in understanding the behavior of other high performance materials such as carbides, nitrides, and other borides.

This research presents new methods for determining the relative bond strength and relative effective plasticity of samples, which can be used to determine the influence of processing parameters on materials characteristics.

The following is a list of goals for this research that will be accomplished to achieve the stated objective.

1. Determine fracture mode (intergranular, transgranular, or mixed mode) for various samples
2. Determine nano-indentation reduced modulus, final displacements, and fracture toughness for various samples
3. Determine relative bond strengths of various samples
4. Determine effect of processing parameters on relative bond strength
5. Determine relative effective plasticity of various samples

6. Determine effect of processing parameters on relative effective plasticity
7. Determine correlations between relative bond strength as measured by fracture mode, relative bond strength as measured by nano-indentation reduced modulus, relative effective plasticity as measured by nano-indentation final displacement, and relative effective plasticity as measured by nano-indentation fracture toughness.

1.2. Bond Strength and Fracture Mode

This section presents background information for bond strength and fracture mode. This section includes a description of bond strength, an explanation of fracture mode, and a description of how fracture mode relates to bond strength.

1.2.1. Bond Strength

This section presents background information about bond strength. On an atomic level, bond strength is a measure of the force it takes to break a bond between two atoms[1]. When two atoms get close enough to each other, the atoms exert both attractive and repulsive forces on each other.[2,3,4] The strength of the forces are a function of interatomic spacing as shown in Figure 1.1.[2,3,4,5]

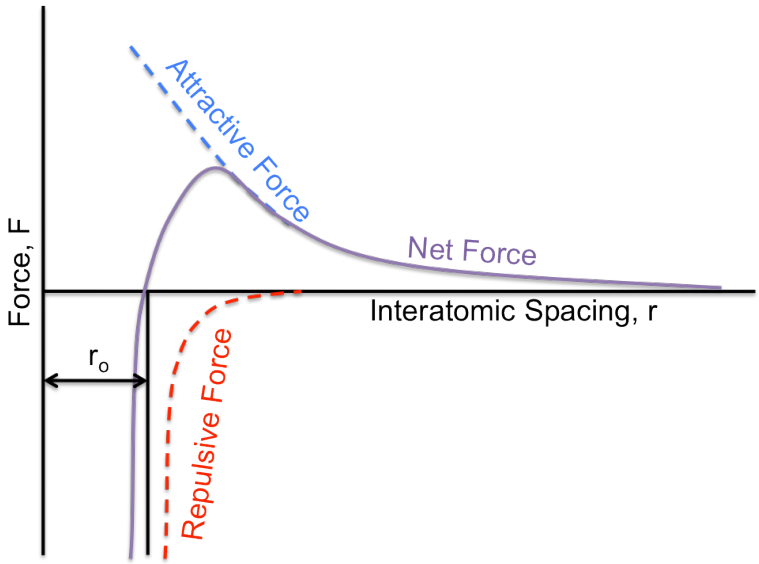

Figure 1.1 Force Versus Interatomic Spacing Between Two Atoms

When the attractive and repulsive forces are balanced, the atoms will be in equilibrium, indicated by r_o in Figure 1.1, and resist any forces that try to pull atoms apart or push them closer together.[2] The resistance to motion can be quantified by a relation with the elastic modulus as shown in Equation 1.1.[2,3] A weakly bonded material has a smaller elastic modulus than a strongly bonded material because of the slope of the Force versus Interatomic Spacing curve as the curve crosses zero force as shown in Figure 1.2.[2,3,4] A

strongly bonded material has a steeper slope as the curve crosses zero Force, and therefore a strongly bonded material has a higher elastic modulus. [2,3,4]

$$E \propto \left(\frac{dF}{dr}\right) \tag{1.1}$$

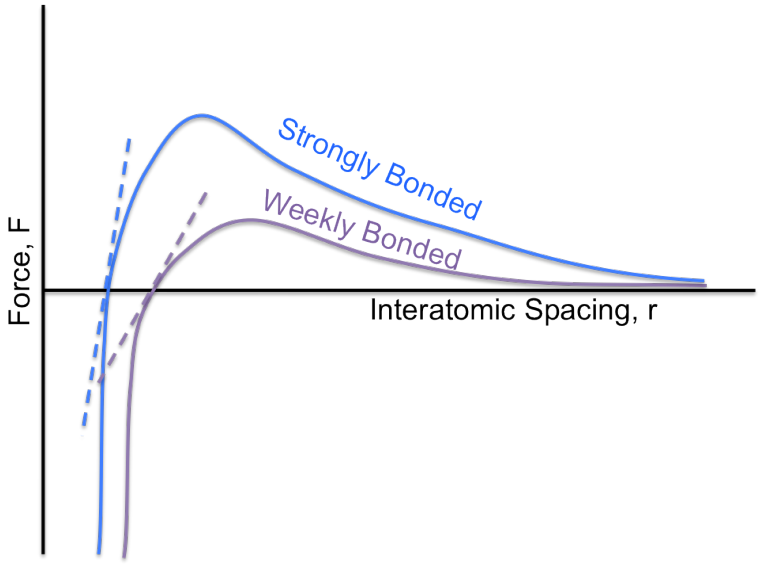

Figure 1.2 Force versus Interatomic Spacing for Weakly Bonded and Strongly Bonded Materials

A typical way to determine bulk elastic modulus is to measure the stress-strain response during tensile testing. The elastic modulus is determined from the initial linear response as shown in Figure 1.3.[1,2,3] As the stress increases, the strain increases linearly in the elastic portion of the stress-strain curve where the material has complete recovery of the strain if the stress is removed.[2,6] Ceramic materials generally do not show significant plastic deformation before failure, therefore the stress-strain curve for most ceramics only shows linear elastic behavior.[2,3]

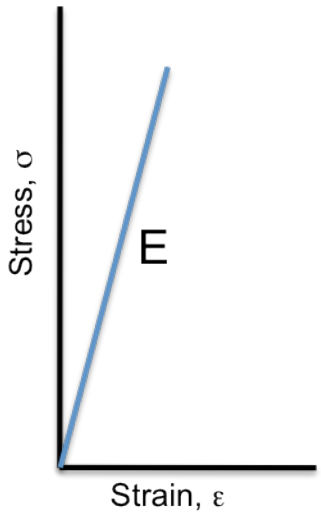

Figure 1.3 Stress-Strain Curve

The elastic modulus is calculated from the initial linear response on the stress-strain curve using Equation 1.2.[2,6] Elastic modulus determined using a tensile stress-strain curve could be inaccurate because of "material creep and deflection of the testing machine".[1]

$$E = \frac{\sigma}{\varepsilon} \tag{1.2}$$

The bond strength determined by relating the force between atoms and the distance between atoms, as shown in Figure 1.2 and Equation 1.1, are relations, at the atomic level, in two dimensions. The elastic modulus that is proportional to the atomic bond strength is also a relation in two dimensions. The elastic modulus that is determined from a stress-strain diagram is a bulk measure of the material properties in three dimensions. Therefore the elastic modulus measured from stress-strain diagrams is related to bond strength at the atomic level.

1.2.2. Fracture Mode

This section presents background information about fracture mode and how fracture mode relates to bond strength. Two main types of fracture are ductile fracture and brittle fracture.[2] Ductile fracture involves significant plastic deformation before failure.[2,12] Brittle fracture involves little or no plastic deformation before fracture and occurs in most ceramic materials.[2,3,5,7] The two main brittle fracture modes are transgranular and intergranular fracture.[6,8,9] Transgranular fracture occurs when fracture travels through grains.[2,3,8,9] Intergranular fracture occurs when fracture travels around grains, along grain boundaries.[2,8,9] Intergranular fracture has a very jagged appearance whereas transgranular fracture appears much more smooth.[3,6,8,9,10]

The fracture path between components in a ceramic matrix composite influences the fracture strength of a material.[11] If cracks are propagated at an angle away from the original crack direction, the crack tip can be blunted.[12,13] When a crack propagates in an intergranular mode, the crack is more likely to deflect along the boundary between the grains, which increases the fracture strength of the material.[12,13]

The bond strength between two grains or phases can be optimized to cause more transgranular or intergranular failure.[12] Intergranular fracture is more common when the bond strength between grains is less than the bond strength inside grains.[3] The three dimensional microscopic bond strength between grains is a measure of the grain boundary interface strength and is typically referred to as grain boundary strength. The three dimensional microscopic bond strength inside grains will be referred to as grain strength.

The ratio of transgranular fracture to intergranular fracture may correlate with bond strength as measured by grain boundary strength and grain strength.[14] An increase in the amount of transgranular fracture indicates an increase in the grain boundary strength relative to the grain strength. A material with a higher amount of transgranular fracture

than intergranular fracture would have higher grain boundary strength than a material with a higher amount of intergranular fracture than transgranular fracture.

The correlation between fracture mode and grain boundary strength may be confounded by the tendency for small grains sizes to show intergranular fracture and for larger grains to show transgranular fracture due to residual stresses or impurities and porosity at grain boundaries.[6,14]

1.3. Effective Plasticity

This section presents background information for effective plasticity. This section includes a description of effective plasticity, crack formation, crack propagation, and fracture toughness.

The bulk elastic-inelastic response, "effective" plasticity, was used to describe the microscopic behavior, which caused a plastic-like response on a bulk scale through cracking and deformation on a microscopic scale. Plastic deformation is permanent deformation that remains after a load is removed.[2,3,4,5,6,15]

One of the ways plastic deformation can occur is by dislocation motion.[2,3,4,5,15,16] Dislocations are lines of defects.[2,3,5,15] Defects are imperfections in a material at an atomic level and can include point defects such as vacancies, interstitial atoms, and impurities, and linear defects such as screw and edge dislocations.[2,3,5,15]

Dislocations can move by gliding along a slip plane.[2,3,5,6,17] A slip plane is a crystallographic orientation on which atomic motion is easier.[3] The slip plane usually occurs on the plane where the atoms are packed closely together, but the slip plane can be influenced by the charge of the atoms around the slip plane.[2,3,4,6] The crystal structure of ceramics causes slip to be difficult.[2,4,6] For ceramics with ionic bonding, some atoms have a positive charge and some have a negative charge.[2,5] During slip in certain directions, atoms of the same charge are in close proximity, which makes slip in specific directions difficult.[2] For ceramics with covalent bonding, the atomic bond strength is very high, there are a very small number of slip systems, and the dislocation movement is very complex. [2,15]

A polycrystalline material, such as a ceramic matrix composite, has grain boundaries, which can act as a barrier to dislocation motion.[3,4] If there are many dislocations in one area, then the dislocations can interfere with each other, making dislocation movement difficult.[4]

The Hall-Petch effect shows that finer grain material has a larger volume of grain boundaries, which decreases dislocation movement.[2] The decrease in dislocation movement can cause an increase in hardness and fracture strength.[2]

During plastic deformation, atomic bonds are broken, then atoms move, and new atomic bonds are formed.[2,5,15] If new atomic bonds are not formed, then fracture occurs.[5] Many ceramic materials fracture before plastic deformation occurs. [2]

The fracture strength of a material is dependent upon the atomic bond strength in the material.[2] When cracks grow, bonds are broken along the length of the crack.[1,6,16,18] The theoretical fracture strength of a material can be approximated as *E/10*, where *E* is the elastic modulus.[1,2,5,16] Experimental measurements of fracture strength show fracture strengths 10-100 times less than the expected fracture strength from elastic modulus approximations.[2,16] The decrease in measured fracture strength could be due to defects and flaws.[2,14,16,18] Defects can include pores, inhomogeneity, and impurities.[14]

Defects and flaws can act as a stress raiser, which means that the stress at the tip of the defect or flaw is higher than the stress in the bulk of the material.[2] Stress risers include not only microscopic defects and flaws, but also include macroscopic features such as corners.[2] One way to explain the effect of a stress raiser is to examine stresses for an elliptical crack in the interior of a material as shown in Figure 1.4.[2,6,16,18]

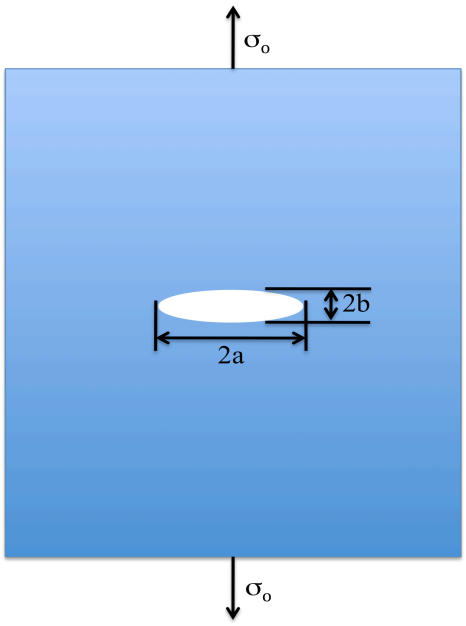

Figure 1.4 Elliptical Crack as an Example Stress Raiser

The two stages of fracture are crack formation and crack propagation.[2] Formation of cracks occur when the stress at a specific point in the material, like at a crack tip or another stress raiser, exceed the fracture strength of the material.[2]

The maximum stress at the edge of the elliptical crack, the crack tip, is given by σ_m.[2,6] The maximum stress at the crack tip is related to the tensile stress applied to the bulk of the material, σ_o, as shown in Equation 1.3.[2,6,16] The radius of curvature of a crack tip is given by ρ_t as shown in Equation 1.4, and is a function of *a,* one half the length of an interior crack, and *b*, one half the width of an interior crack.[5,6,16]

$$\sigma_m = \sigma_o \left[1 + 2\left(\frac{a}{\rho_t} \right)^{1/2} \right] \tag{1.3}$$

$$\rho_t = b^2 / a \tag{1.4}$$

If the crack is very long, then the ratio of crack length to radius of curvature of the crack tip becomes much greater than one.[2] Therefore, the second term on the right hand side of Equation 1.3 becomes dominant and the equation can be simplified as shown in Equation 1.5, which shows the maximum stress that can be accommodated without fracture.[2,3,16]

$$\sigma_m = 2\sigma_o \left(\frac{a}{\rho_t} \right)^{1/2} \tag{1.5}$$

Griffith showed that for crack propagation to occur in brittle materials, which show no plastic deformation, a critical stress, σ_c, must be exceeded.[2,3,6] The equation to determine the critical stress is shown in Equation 1.6.[2,3,6,16] The modulus of elasticity is given by E, the surface energy per unit area is given by γ_s.[2,3,5,16]

$$\sigma_c = \left(\frac{2E\gamma_s}{\pi a} \right)^{1/2} \tag{1.6}$$

Fracture toughness, K_c, is the stress intensity factor for the critical stress necessary to cause crack propagation as shown in Equation 1.7.[2,16] Y is a dimensionless parameter, which is related to the crack length, the component width, and the direction(s) of applied load.[2,16]

$$K_c = Y\sigma_c \sqrt{\pi a} \tag{1.7}$$

For ceramics, the most commonly reported fracture toughness is the Mode I fracture toughness, K_{Ic}, as shown in Equation 1.8.[2,6,16] In Mode I fracture, the sample is thick enough that the value for fracture toughness is no longer affected by the thickness of the sample. The stress is also applied normal to the crack plane in Mode I fracture, as shown in Figure 1.4.[2] The Mode I fracture toughness, also called the plain strain fracture toughness, is expected to be the most important mode of fracture in ceramics.[2,6,16]

$$K_{Ic} = Y\sigma_c \sqrt{\pi a} \tag{1.8}$$

One way to increase fracture toughness is to create a material with interfaces between phases or grains, which can act as crack propagation barriers by redirecting the crack along the interface.[6,12,17,19,20] The strength of the interface between grains, referred to in this research as grain boundary strength, would need to be weaker than the strength within the grains, referred to in this research as grain strength, to cause the crack to deflect along the interface but not so weak as to cause a reduction in overall fracture strength of the material.[12]

In brittle materials, like ceramics, small cracks, called microcracks, may form at the crack tip.[4] Microcracks act to reduce the stress at the crack tip and increase the material's resistance to further cracking.[4] Microcracks cause a plastic-like response on a bulk scale through cracking and deformation on a microscopic scale, which is an example of phenomenon included in effective plasticity. Other mechanisms, which decrease the stress at the crack tip, include crack deflection and crack bridging.[21]

1.4. Al_2O_3-TiB_2 composites

This section presents background information for Al_2O_3-TiB_2 composites. This section discusses properties of Al_2O_3, TiB_2, and the Al_2O_3-TiB_2 composites. The properties include chemical structure, bonding characteristics, fracture toughness, elastic modulus, hardness, and Poisson's ratio.

1.4.1. Al_2O_3

This section presents background information about Al_2O_3 materials. Al_2O_3 is a low cost material, which can be produced using many different processing techniques.[22] Al_2O_3 has a high melting temperature, 2050°C, and high strength at elevated temperatures.[23] The coefficient of thermal expansion for Al_2O_3 from 0°C to 20°C is 4.6E-6 1/K.[23] The coefficient of thermal expansion for Al_2O_3 from 0°C to 1500°C is 8.6E-6 1/K.[23]

Al_2O_3 consists of a hexagonal structure with the following lattice parameters: a is 4.761 and c is 12.991 Angstroms.[23] The structure is formed by alternating layers of oxygen and aluminum, with aluminum occupying two-thirds of the available sites to maintain charge balance as shown in Equation 1.9.[3,6,15,23]

$$2Al^{+3} = 3O^{-2} \tag{1.9}$$

The bonds between Al and O in Al_2O_3 are covalent bonds, which are very strong, and are the reason the material has a high melting point.[3,24] The primary slip plane in Al_2O_3 is the basal plane.[3,15] Single crystal Al_2O_3 was found to have cleavage fracture on the basal plane.[25] During deformation, Al_2O_3 has formed twins.[25]

1.4.2. TiB_2

This section presents background information about TiB_2 materials. TiB_2 has a high hardness, low density and high melting point, 3225°C.[26,27,28,29,30] TiB_2 is also oxidation resistant even at high temperatures.[26,29,31] TiB_2 has good wear resistance and chemical stability.[27,28,29,30] A table of the TiB_2 coefficients of thermal expansion from 0°C to the temperature listed is shown in Table 1.1. The coefficient of thermal expansion is higher for the c lattice parameter than for the a lattice parameter.

Table 1.1 TiB_2 Coefficients of Thermal Expansion

Lattice parameter	Temperature	
	20°C	1500°C
a	6.4	8.3
c	9.2	11.0

TiB_2 forms a hexagonal structure with lattice parameters as follows: a is 3.024 to 3.040 and c is 3.213 to 3.234 Angstroms.[28,32,33,34] The Ti and B atoms form alternate layers.[15,29,32,34] In order to have a charge balance, there must be one Ti and two B in the TiB_2 material, as shown in Equation 1.10.

$$1Ti^{+4} = 2B^{-2} \tag{1.10}$$

TiB_2 is strong and brittle due to covalent bonding.[26] One of the main slip planes is the basal plane.[15,32] During deformation, TiB_2 has formed twins.[35]

1.4.3. Al_2O_3-TiB_2 composites

This section presents background information about Al_2O_3-TiB_2 composites under study in this research. Al_2O_3-TiB_2 composites have high temperature, wear, and impact resistance, which could be useful in high performance applications.[13,36,37,38] Previous research indicates that there may be a eutectic formed between Al_2O_3 and TiB_2 at a temperature near 1925°C.[39,40]

In addition to properties useful for high performance applications, Al_2O_3-TiB_2 composites have the added advantage of production using a SHS reaction with inexpensive precursors.[13,37,38,41,42] During SHS reactions, processing parameters including particle size influence the final properties of the composite, including grain sizes, phase formation, density, porosity, hardness, and other physical and mechanical properties.[36,37] Table 1.2 shows a summary of properties for Al_2O_3, TiB_2, and Al_2O_3-TiB_2 composites. The range of values for properties of Al_2O_3-TiB_2 composites overlaps the ranges of values for properties of Al_2O_3 and TiB_2 bulk materials as would be expected from a rule of mixtures.

Table 1.2 Summary of Properties for Al_2O_3, TiB_2, and Al_2O_3-TiB_2 Composites

Material	Fracture Toughness ($MPa\text{-}m^{1/2}$)	Elastic Modulus (GPa)	Hardness (GPa)	Poisson's Ratio
Al_2O_3	2.5-4.5[22,23,43]	280-450[22,23,34,44]	15-24[22,23,34,42,45]	0.230-0.231[23,44]
TiB_2	3.2-8.0[22,28,31,46]	347-570[13,22,28,34,44]	18-35[22,28,31,34,42,45]	0.108-0.130[28,44]
Al_2O_3-TiB_2	1.0-7.2[13,21]	151-425[13,21,42,44,47]	18-27[42,47]	N/A

Al_2O_3-TiB_2 composites were created during a separate ongoing research program being conducted by Dr. Kathryn V. Logan. The Logan samples were initially formed by hot pressing powders produced using SHS of Aluminum (Al), Titanium Dioxide (TiO_2), and

Boron Anhydride (B_2O_3) powders or manual mixing (MM) of Al_2O_3 and TiB_2 powders.[21,36,40,48] The reaction is shown in Equation 1.11.[21,40,48] The SHS reaction which forms Al_2O_3-TiB_2 composites has an adiabatic temperature of 2175-2200°C.[41,51]

$$10Al + 3B_2O_3 + 3TiO_2 \rightarrow 5Al_2O_3 + 3TiB_2 \quad (1.11)$$

Manually mixed samples were mixed with 70 wt % Al_2O_3 and 30 wt % TiB_2 powders, which corresponded with the stoichiometric composition shown in Equation 1.11.[21,48] The SHS and MM powders were hot pressed at varying times ranging from 150 to 240 minutes at pressures ranging from 500 to 5000 psi at a temperature of 1620°C.[21]

A summary of processing parameters for the samples under study in this research is shown in Table 1.3.[21,49] Samples A and B were produced using SHS.[21,49] Samples C and D were produced using manual mixing, MM.[21,48] The predominant microstructure for Sample A and Sample C was TiB_2 grains surrounding Al_2O_3 grains.[36,49] The predominant microstructure for Sample B and Sample D was TiB_2 grains distributed amongst Al_2O_3 grains.[36,49] Hot pressing pressure that shows 500/5000 psi indicates that 500 psi was applied to the sample while ramping temperature up to the hold temperature, 1620°C, at which point 5000 psi was applied to the sample.[21] The hold time was 150 or 240 minutes.[21] A detailed description of the processing methods can be found in Carney's thesis.[21]

Table 1.3 Summary of Processing Parameters for Samples A-D

Sample	Powder Processing	Predominant Microstructure	Hot Pressing Pressure	Hot Pressing Hold Time
A	SHS	TiB_2 grains surround Al_2O_3 grains	5000 psi	240 min
B	SHS	TiB_2 grains distributed amongst Al_2O_3 grains	500/5000 psi	240 min
C	MM	TiB_2 grains surround Al_2O_3 grains	500/5000 psi	150 min
D	MM	TiB_2 grains distributed amongst Al_2O_3 grains	500/5000 psi	240 min

Previous research indicated the size of the Al_2O_3 and TiB_2 grains or phases in each sample.[21,40,50] Carney and others stated that Samples A and B had smaller grains than Samples C and D.[21,50] Logan indicated grain size ranges for each sample as shown in Table 1.4.[40] Sample C had a much larger Al_2O_3 grain size than the other samples. Sample B had a smaller TiB_2 grain size than the other samples.

Table 1.4 Grain Size of Al_2O_3 and TiB_2 in Al_2O_3-TiB_2 composites

Sample	Al_2O_3	TiB_2
A	20-40 μm	1-10 μm
B	10-20 μm	1-5 μm
C	up to 100 μm	1-10 μm
D	avg 12.3 μm	1-10 μm

Other research measured the phase size instead of the grain size as shown in Table 1.5.[36] The measurement was conducted in terms of the linear intercept length.[36] Sample C had a much larger areas of Al_2O_3 than the other samples, with Sample A also having large Al_2O_3 areas. Sample B had smaller TiB_2 areas than the other samples and Sample D had the largest TiB_2 areas. Depending upon the methods used to characterize the grain or phase size, a difference comparison of the phases can be obtained.

Table 1.5 Phase Size of Al_2O_3 and TiB_2 in Al_2O_3-TiB_2 composites

Sample	Al_2O_3	TiB_2
A	10.30 ±11.08 μm	5.06 ±5.33 μm
B	5.88 ±5.86 μm	2.43 ±2.45 μm
C	24.77 ±35.62 μm	11.31 ±14.89 μm
D	8.17 ±8.72 μm	3.09 ±2.75 μm

X-ray diffraction testing of Samples A, C, and D had no peaks unaccounted for by Al_2O_3 and TiB_2 patterns.[21] X-Ray diffraction of Sample B had one small peak unaccounted for by Al_2O_3 and TiB_2 patterns which may have been caused by an aluminum borate (9 Al_2O_3 -2 B_2O_3).[21]

A single-edge notched beam (SENB) method was used to test bars for fracture toughness.[21] After pressing, test samples were cut from discs according to MIL-STD-1942B.[21] A detailed description of the fracture toughness testing method can be found in Carney's thesis.[21]

Previous testing determined the effect of parameters such as particle size, milling time, hot pressing pressure, hot pressing hold time, phase distribution, and phase size on materials properties including the microstructure.[13,36,40,49,51,52] Results from SENB fracture toughness testing, elastic modulus, and density of test bars for Samples A-D are shown in Table 1.6. Density measurements were calculated using 4.14 g/cc as the theoretical density.[21] The density of Sample B was lower than the other three samples. The elastic modulus of Sample B was generally lower than the other three samples, but the fracture toughness of Sample B was similar to the fracture toughness of sample C.

Table 1.6 Summary of Previous Testing Results for Samples A-D

Sample	K_{Ic} (MPa*√m)[21]	E (GPa)[21,50]	Density (% th) [21]
A (22)	4.14 +/- 0.37	408.6-505.8	98.7
B (23)	3.49 +- 0.26	356.8-420.8	94.8
C (13)	3.45 +/- 0.00	433.6-478.8	99.1
D (24)	4.14 +/- 0.75	421.2-473.9	98.9

Bars used to test SENB fracture toughness were mounted in epoxy and polished according to the schedule shown in Table 1.7 during previous testing.[21] A detailed description of polishing can be found in Carney's thesis. [21]

Table 1.7 Previous Polishing Schedule

Suspension	Load	Time
15 μm	By hand	3-4 minutes
15 μm	5 N	3-4 minutes
9 μm	30 N	6 minutes
3 μm	35 N	4 minutes
Silica	45 N	2 minutes

Previous testing reported variable results for fracture modes for Al_2O_3 grains and TiB_2 grains in Al_2O_3-TiB_2 composites using the same samples under study in this research. A summary of results is shown in Table 1.8. Logan reported dynamic testing fracture modes for Al_2O_3 grains as transgranular fracture and for TiB_2 grains as transgranular and intergranular fracture.[40]

Keller and Zhou showed results similar to Logan during dynamic testing using split Hopkins pressure bars.[36,53] Keller and Zhou reported transgranular cleavage for Al_2O_3 grains in Samples A, B, C, and D.[36,53] The fracture mode for TiB_2 grains in Sample A and B was intergranular pullout.[36,53] Fracture modes for TiB_2 grains in Sample C and D were mainly transgranular fracture with some intergranular pullout.[36,53] Keller noted that there was a higher percentage of Al_2O_3 on fracture surfaces of Samples A and C, which indicated a preference for failure in Al_2O_3.[53]

Keller and Zhou noted that fracture modes for TiB_2 grains in Sample C were mainly intergranular pullout with some transgranular fracture.[36] Fracture modes for TiB_2 grains in Sample D were mainly transgranular fracture with some intergranular pullout.[36]

In sample D, there were more TiB_2 fracture surfaces than would have been expected to exist from the volume fraction of TiB_2 in the composite.[36] The higher amount of TiB_2 fracture surfaces indicated that more failures occurred in the TiB_2 phase.[36]

Carney examined fracture surfaces created during modulus of rupture testing with a crosshead speed of 0.05 cm/min (0.02 in/min).[21] The fracture mode for Al_2O_3 grains in Samples A and B was transgranular fracture.[21] The fracture mode for Al_2O_3 grains in Samples C and D was intergranular fracture.[21] The fracture mode for TiB_2 grains in Samples A, B, and C was intergranular fracture.[21] The fracture mode for TiB_2 grains in Sample D was transgranular fracture.[21]

Table 1.8 Fracture Modes from Previous Research

Research	Logan[40]		Keller and Zhou[36]		Carney[21]	
Sample	Al_2O_3	TiB_2	Al_2O_3	TiB_2	Al_2O_3	TiB_2
A	T	T & I	T	I	T	I
B	T	T & I	T	I	T	I
C	T	T & I	T	T & I	I	I
D	T	T & I	T	T & I	I	T

*T for Transgranular; I for Intergranular

When the fracture mode is transgranular, then the grain strength is lower than the grain boundary strength.[38] When the fracture mode is intergranular, then the grain boundary strength is lower than the grain strength.[38] Depending upon which of the previous research results were used for analysis, the relative grain strength may be higher or lower than the grain boundary strength.

1.5. Analytical Characterization Methods

This section describes background information about analytical characterization methods used in this research. This section includes a description of SEM and EDS characterization methods as well as Taguchi methods and ANOVA analysis.

1.5.1. SEM and EDS

This section describes SEM and EDS characterization methods. SEM analysis uses an electron beam, which is scattered by interactions with the atoms in the material.[8,16] During the scattering, secondary electrons, back-scattered electrons, and X-rays are created.[8,16] Secondary electrons are mainly produced close to the surface of the material.[16,54] The area in which the secondary electrons are created is about the same as the diameter of the electron beam, back-scattered electrons are emitted from a slightly larger volume, and X-rays are emitted from a much larger volume as shown in Figure 1.5.[16] Secondary and back-scattered electrons provide information about the surface topography while X-rays provide information about the atoms in the interaction volume.[16,54]

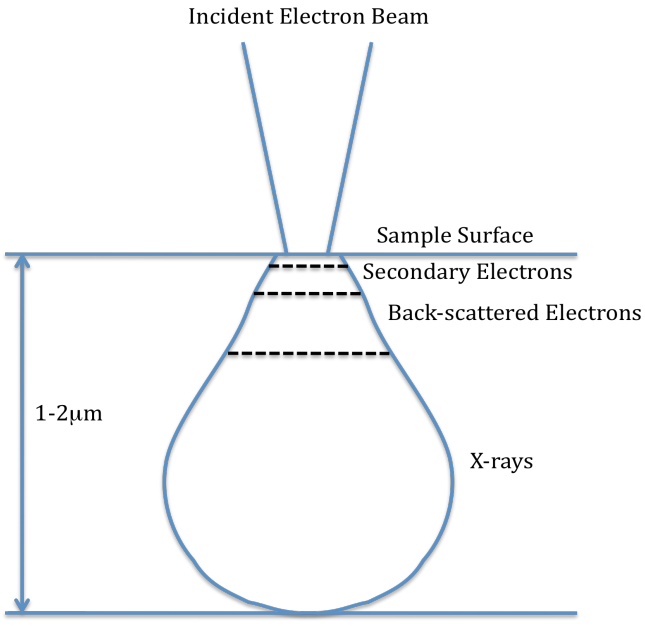

Figure 1.5 Area of Interaction Between Electron Beam and Atoms in Material

The spot size of the electron beam is an indication of how much of the sample will interact with the electron beam.[8] Spot sizes generally range from 5 to 20 μm with the smaller spot size being more useful for high-resolution imagery and the larger spot size being more useful for EDS (using an X-ray detector).[8]

Samples should be mounted such that there is a grounded path between the sample surface under examination and the sample holder.[2,8,9,54] Grounding can be accomplished by applying a coating of a conductive material such as Gold-Palladium (Au-Pd) to the surface and using conductive tape or paint to provide a path from the sample surface to the sample holder.[8,9]

Because of the way secondary electrons are detected, surface features, which are shielded by other surface features, show as dark areas on the display, similar to how outcroppings cause shadows on the ground around them in bright sunlight.[16]

SEM is very commonly used in fractography.[16] Identification of intergranular and transgranular fracture modes can be made using SEM micrographs.[9,10,14] The magnification and the location at which microscopy is conducted is very important in determinations of fracture mode.[16] For fractographic analysis, magnifications should be limited to less than 20,000x due to resolution limitations of current SEM instruments.[16]

1.5.2. Nano-indentation

This section presents background information about nano-indentation, how nano-indentation reduced modulus relates to bond strength, and how nano-indentation final displacement and fracture toughness relate to effective plasticity. Nano-indentation is an indentation test conducted on the nanometer scale.[3,55] Indentation testing measures a material's resistance to deformation.[1,2,5,6,56]

Loads used in nano-indentation are on the order of millinewtons (10^{-3} N).[55] In conventional indentation testing, the size of the indent is used to calculate the area of contact and the hardness of the material.[1,3,4,55] In nano-indentation, the contact area is calculated from the depth of the indent and the actual shape of the indenter, as determined through calibration.[55]

During nano-indentation testing, a load versus displacement curve is recorded during loading and unloading as shown in Figure 1.6.[3,55] A straight line with a slope identical to the initial unloading slope shows the plastic recovery, h_p, of the sample.[55]

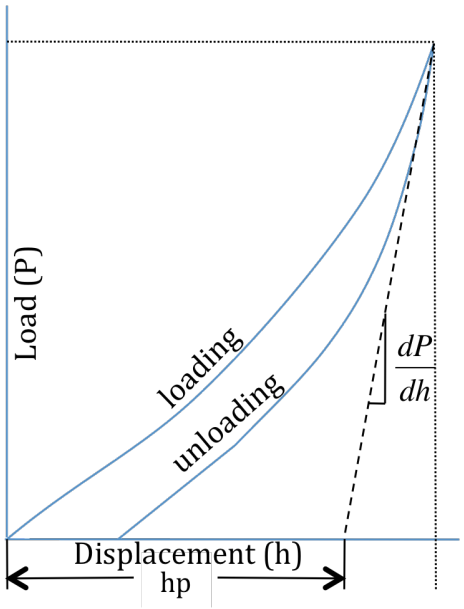

Figure 1.6 Nano-indentation Load-Displacement Curve

The indentation modulus, also referred to as reduced modulus, E_r, is related to the load-displacement slope, dP/dh, and contact area, A, as shown in Equation 1.12.[55] The derivation of Equation 1.12 makes the assumption that the indenter is symmetric.[55]

$$E_r = \frac{1}{2}\sqrt{\frac{\pi}{A}} * \frac{dP}{dh} \tag{1.12}$$

Nano-indentation can be conducted using a Berkovich indenter, which is a three-sided pyramid.[55] The Berkovich indenter was designed to allow testing of very hard materials.[55] Because of the shape of the indenter, the load-displacement curve is shaped as shown in Figure 1.7. Three measurements of displacement as shown in Figure 1.7 are the elastic displacement, h_e, plastic displacement, h_p, and final displacement, h_f.[55] Final displacements are a measure of the amount of unrecovered displacement and are an indication of the inelastic response of the material.[55]

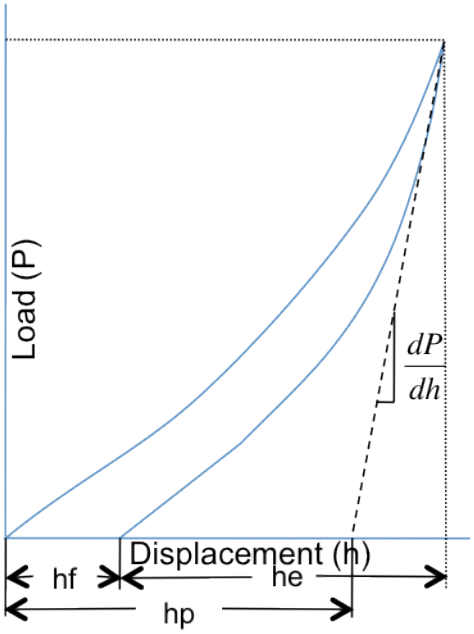

Figure 1.7 Nano-indentation Load-Displacement Curve for Berkovich Indenter

The contact area is determined from the plastic displacement, h_p, as shown in Equation 1.13 using the face angle, θ.[55]

$$A = 3\sqrt{3}h_p^2 \tan^2\theta \tag{1.13}$$

For a Berkovich indenter, the face angle is 65.27, which makes the projected area-to-depth ratio the same for a Berkovich indenter as for a Vickers indenter.[55] Equation 1.14 shows the contact area using a Berkovich indenter.[55]

$$A = 24.494h_p^2 \tag{1.14}$$

Therefore, the equation for reduced modulus using a symmetric Berkovich indenter is as shown in Equation 1.15.[55]

$$E_r = \frac{1}{2h_p}\sqrt{\frac{\pi}{24.494}} * \frac{dP}{dh} \tag{1.15}$$

A real Berkovich indenter may be non-symmetrical.[55] A correction factor, β, is used to account for the actual asymmetry of a real Berkovich indenter as shown in Equation 1.16.[55] The correction factor for a real Berkovich indenter is 1.034.[55]

$$\frac{dP}{dh} = \frac{1}{\beta}\frac{dP}{dh}_{measured} \tag{1.16}$$

Therefore, the equation for reduced modulus using a real Berkovich indenter is as shown in Equation 1.17.[55]

$$E_r = \frac{1}{2(1.034)h_p}\sqrt{\frac{\pi}{24.494}} * \frac{dP}{dh}_{measured} \tag{1.17}$$

The plastic displacement, h_p, can be determined from the location of a straight line drawn from the initial slope of the load-displacement, *dP/dh*, curve during unloading, as shown in Figure 1.7.[55] The equation of the slope line is shown in Equation 1.18.

$$y = mx + b \tag{1.18}$$

The equation is then solved for *x* as shown in Equation 1.19.

$$x = \frac{y - b}{m} \tag{1.19}$$

The plastic displacement, h_p, is then input for *x*, using the slope intercept, *b*, and the slope, *dP/dh*, as shown in Equation 1.20.

$$h_p = x = \frac{y - b}{m} = \frac{0 - (\text{slope intercept})}{dP/dh} \tag{1.20}$$

Reduced modulus is related to the indenter modulus, E_i, and Poisson's ratio, ν_i, as well as the sample's elastic modulus, E_s, and Poisson's ratio, υ_s, as shown in Equation 1.21.[55,57] The elastic modulus for the diamond Berkovich indenter used in this research was 1140 GPa and the Poisson's ratio was 0.07.[58]

$$\frac{1}{E_r} = \frac{\left(1 - \nu_s^2\right)}{E_s} + \frac{\left(1 - \nu_i^2\right)}{E_i} \tag{1.21}$$

Equation 1.21 was rearranged to obtain an equation to determine the bulk modulus of a sample from the nano-indentation reduced modulus as shown in Equation 1.22.

$$E_s = \frac{E_r E_i\left(1 - \nu_s^2\right)}{E_i - E_r\left(1 - \nu_i^2\right)} \tag{1.22}$$

Equation 1.21 was also rearranged to obtain an equation to determine the reduced modulus as shown in Equation 1.23.

$$E_r = \frac{E_s E_i}{E_i\left(1 - \nu_s^2\right) - E_s\left(1 - \nu_i^2\right)} \tag{1.23}$$

The bulk values for each material and the indenter are shown in Table 1.9 and were used to calculate the expected reduced modulus, which are also shown in Table 1.9.

Table 1.9 Calculation of Expected Reduced Modulus for Al_2O_3 and TiB_2

Material	E	ν	Calculated Reduced Modulus (GPa)
Diamond	1000[55]	0.07[55]	N/A
Al_2O_3	280-450	0.230-0.231	248.2-355.9
TiB_2	347-570	0.108-0.130	279.3-381.4

The nano-indentation reduced modulus is related to the bulk elastic modulus. The bulk elastic modulus is related to the two dimensional elastic modulus, which is related to the two dimensional atomic bond strength.

Nano-indentation can be used to measure fracture toughness, K_c, as shown in Equation 1.24.[6,55,59] Values for constants k are between 0.0120 and 0.216, and the value for n is 0.5.[6,55,59,60] Values for each constant are shown in Table 1.10. The bulk elastic modulus, (not the indentation modulus), is indicated by E.[55] Hardness, as measured through nano-indentation, is indicated by H.[55] Indentation load is indicated by P.[55] The crack length, c, is measured from the center of the indent to the end of the surface crack.[55]

$$K_c = k\left(\frac{E}{H}\right)^n \frac{P}{c^{3/2}} \tag{1.24}$$

Table 1.10 Fracture Toughness Constants

Source	n	k
Experimental[60]	0.5	0.0120-0.0200
Numerical[60]		0.0135-0.0185
Analytical[60]		0.0130-0.0216

Nano-indentation hardness is a measure of the mean contact pressure as determined the indentation load and the contact area, A, as shown in Equation 1.25.[5,6,55]

$$H = \frac{P}{A} \tag{1.25}$$

When the contact area for a Berkovich indenter, as shown in Equation 1.14, is combined with Equation 1.25, the nano-indentation hardness as obtained using a Berkovich indenter is as shown in Equation 1.26.[55]

$$H = \frac{P}{24.494 h_p^2} \tag{1.26}$$

It may be possible to measure fracture toughness from pop in events if crack lengths are not measurable.[61] The crack length, c, was determined using Equation 1.27.[61] Q was experimentally determined to be 4.55 for fused silica and 4.91 for glassy carbon.[61] It is possible that Q is a constant independent of material.[61] The maximum displacement with pop-in, h_m, and the anticipated maximum displacement without pop-in, h_t, were used to

calculate h_x as shown in Equation 1.28.[61] The notation *E'* indicates a function of elastic modulus and Poisson's ratio, ν, as shown in Equation 1.29.[61] The original derivation of Equation 1.27 was conducted for cube corner geometry and may require adjustment for absolute comparisons using the Berkovich indenter geometry.

$$c = \sqrt{2h_m} + \left(Q\frac{E'}{H} - \sqrt{2}\right)h_x \tag{1.27}$$

$$h_x = h_m - h_t \tag{1.28}$$

$$E' = \frac{E}{1-\nu^2} \tag{1.29}$$

Nano-indentation final displacement measures the amount of deformation on a microscopic scale. Nano-indentation fracture toughness measures the resistance to fracture on a microscopic scale. Therefore both nano-indentation final displacement and nano-indentation fracture toughness can be used as measures of relative effective plasticity since both measure the microscopic behavior, which can cause a plastic-like response on a bulk scale.

One limitation of using nano-indentation is the necessity for a smooth sample surface.[5,15,55] If the sample surface is rough, then the contact area may be artificially elevated due to localized deformation.[15,55] Surface roughness effects are decreased for sharp indenters like the Berkovich indenter.[55] Polishing is recommended with the smallest grit being around 1 μm to reduce surface roughness effects on nano-indentation.[55]

Another limitation of nano-indentation is that the contact area and the plastic displacement, h_p, are calculated rather than measured.[55] During indentation of brittle materials, pile-up or sinking-in of material around the indenter is possible as shown in Figure 1.8.[55] Pile-up could lead to an over-estimation of the contact area and an overestimation of the plastic displacement as compared to the actual displacement, h_t.[55] Sinking-in could lead to an under-estimation of the contact area of the indenter and an underestimation of the plastic displacement.[55]

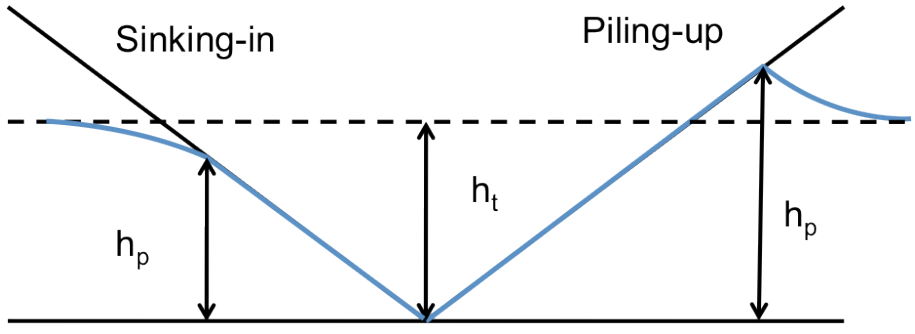

Figure 1.8 Sinking-in and Piling-up Around Nano-indentation Indent

Some authors state that fracture toughness obtained from indentation, K_c, should not be compared directly with K_{Ic}, but may be used to compare fracture toughness values obtained using indentation.[17,59]

Another consideration in the analysis of indentation data is the relative size of the grain and dislocation defects in relation to the size of the indentation.[15,55,59]

1.5.3. Taguchi and ANOVA

This section describes background information about Taguchi methods and ANOVA analysis. Statistical analysis can be conducted to determine the effect of processing parameters on materials properties.[62,63,64] One way to perform statistical analysis is to use orthogonal arrays as promoted by Dr. Genechi Taguchi.[62,64,65] ANOVA can be used to perform analysis of an array created using Taguchi's methods.[62,63,64]

A Taguchi array appropriate for use with two two-level factors is an L4 array as shown in Table 1.11.[64,65] The first two-level factor, labeled 'A' in Table 1.11 is placed in column 1.[64,65] The '1' indicates the first of two levels, and the '2' indicates the second of two levels. The second two-level factor, labeled 'B', is placed in column 2.[64,65] The interaction between factors A and B, labeled 'AxB', will be reflected in the calculations for column 3.[64,65]

Table 1.11 L4 Taguchi Array

Test Run	Column 1: A	Column 2: B	Column 3: AxB
1	1	1	1
2	1	2	2
3	2	1	2
4	2	2	1

A Taguchi array appropriate for use with three two-level factors is an L8 array as shown in Table 1.12.[64,65] The first two-level factor, labeled 'A' in Table 1.12 is placed in column 1.[64,65] The second two-level factor, labeled 'B', is placed in column 2.[64,65] The interaction between factors A and B, labeled 'AxB', will be reflected in the calculations for column 3 during analysis.[64,65] The third two-level factor, labeled 'C', is placed in column 4.[64,65] The interaction between factors A and C, labeled 'AxC', will be reflected in the calculations for column 5 during analysis.[64,65] The interaction between factors B and C, labeled 'BxC', will be reflected in the calculations for column 6 during analysis.[64,65] The interaction between factors A, B, and C, labeled 'AxBxC', will be reflected in the calculations for column 7 during analysis.[64,65]

Table 1.12 L8 Taguchi Array

Test Run	Col 1 A	Col 2 B	Col 3 AxB	Col 4 C	Col 5 AxC	Col 6 BxC	Col 7 AxBxC
1	1	1	1	1	1	1	1
2	1	1	1	2	2	2	2
3	1	2	2	1	1	2	2
4	1	2	2	2	2	1	1
5	2	1	2	1	2	1	2
6	2	1	2	2	1	2	1
7	2	2	1	1	2	2	1
8	2	2	1	2	1	1	2

ANOVA is conducted through an analysis of the responses for a particular Taguchi array.[65] The responses for a particular array are obtained through experimentation and would form a table similar to Table 1.13.[63,65]

Table 1.13 Responses for ANOVA analysis

Test Run	Response 1	Response 2	…	Response n
1	y_{11}	y_{12}	…	y_{1b}
2	y_{21}	y_{22}	…	y_{2b}
…	…	…	…	…
a	y_{a1}	y_{a2}	…	y_{ab}

After obtaining the responses for factor levels as determined by the Taguchi array, calculations are performed to complete the ANOVA analysis. [65] The first step is to determine the total sum of the squares, SS_T, as shown in Equation 1.30.[63,65] Each individual response, y_{ij}, was obtained and shown in Table 1.13. The number of test runs is indicated by a.[63] The number of responses for each test run is indicated by b.[63] The total average, $\bar{y}_{total}$, is obtained from Equation 1.31.[63] The grand total, y_{total}, is obtained from Equation 1.32.[63] The total number of responses, N, is obtained from Equation 1.33.[63] The number of degrees of freedom for the total sum of the squares is obtained by subtracting one from the total number of responses as shown in Equation 1.34.

$$SS_T = \sum_{i=1}^{a}\sum_{j=1}^{b}\left(y_{ij} - \bar{y}_{total}\right)^2 = \sum_{i=1}^{a}\sum_{j=1}^{b}\left(y_{ij}\right)^2 - \frac{\left(y_{total}\right)^2}{N} \tag{1.30}$$

$$\bar{y}_{total} = \left\{\sum_{i=1}^{a}\left[\left(\sum_{j=1}^{b} y_{ij}\right)\Big/ b\right]\Big/ a\right\} \tag{1.31}$$

$$y_{total} = \sum_{i=1}^{a}\sum_{j=1}^{b} y_{ij} \tag{1.32}$$

$$N = a * b \tag{1.33}$$

$$DF_T = N - 1 \tag{1.34}$$

The second step in ANOVA analysis is to determine the sum of the squares for each factor, SS_{factor}, as shown in Equation 1.35.[63] Equation 1.35 shows the equation if there are only two levels for the factor under study.[63] The subscript *a(1)* refers to all values of *a* for which the factor is at level 1. The subscript *a(2)* refers to all values of *a* for which the factor is at level 2. The number of degrees of freedom for each factor is obtained by subtracting one from the number of levels for that factor as shown in Equation 1.36.[63]

$$SS_{factor} = \frac{1}{b}\left[\left(\sum_{j=1}^{b} y_{a(1)j}\right)^2 + \left(\sum_{j=1}^{b} y_{a(2)j}\right)^2\right] - \frac{\left(y_{total}\right)^2}{N} \tag{1.35}$$

$$DF_{factor} = \left(Number\ of\ levels\right)_{factor} - 1 \tag{1.36}$$

The third step in ANOVA analysis is to determine the sum of the squares for the error term, SS_E, as shown in Equation 1.37.[63] The number of degrees of freedom for the error term is obtained by subtracting the number of degrees of freedom for each factor from the number of degrees of freedom for the total sum of the squares as shown in Equation 1.38.[63]

$$SS_E = \sum_{i=1}^{a}\sum_{j=1}^{b}\left[\left(y_{ij} - \bar{y}_i\right)^2\right] = SS_T - \sum_{i=1}^{a} SS_{Factor} \tag{1.37}$$

$$DF_E = DF_T - \sum DF_{factor} \tag{1.38}$$

The mean square is calculated by dividing the sum of the squares by the degrees of freedom for that sum of the squares as shown in Equation 1.39.[63] An example calculation using factor A is shown in Equation 1.40.[63]

$$MS_{factor} = SS_{factor} / DF_{factor} \tag{1.39}$$

$$MS_A = SS_A / DF_A \tag{1.40}$$

In order to determine if a factor has a significant effect, a calculated F value is obtained and compared to a tabulated F value.[63] The F value is calculated as shown in Equation 1.41.[63] The tabulated F value is obtained by looking up the F value for the degrees of freedom of the factor and the degrees of freedom of the error as shown in Equation 1.42.[63] The value of α in Equation 1.42 is an indication of the confidence level.[63] If α is 0.10, then the confidence level, *C.L.*, is 0.9 as shown in Equation 1.43.[63]

$$F_{factor} = MS_{factor} / MS_E \tag{1.41}$$

$$F_{tabulated} = F_{\alpha, DF_{factor}, DF_{error}} \tag{1.42}$$

$$C.L. = 1 - \alpha \tag{1.43}$$

When the calculated F-value is larger than the tabulated F-value then the factor is significant to at least the confidence level used to obtain the tabulated F-value.[63]

Another way to determine the confidence level is to determine the value for alpha that returns a value for tabulated F that matches the calculated value for F.[63] The value of alpha is displayed as the P-value.[63] The probability that the factor is significant is calculated and shown as the confidence level in the C.L. column in Table 1.14. When a specific confidence level is desired, the alpha value is compared with the P-value. When the P-value is smaller than the alpha level then the factor is significant at that confidence level.[63] The results of the calculations on an L4 array would form a table similar to Table 1.14.[63]

Table 1.14 Calculation of Sum of the Squares for L4 Taguchi Array

Source of Variation	Sum of Squares	Degrees of Freedom	Mean Square	F_0	P-Value	C.L.
A: Powder Processing	SS_A	1	MS_A	F_A	P_A	$C.L._A$
B: Predominant Microstructure	SS_B	1	MS_B	F_B	P_B	$C.L._B$
AxB: Interaction between powder processing and predominant microstructure	SS_{AxB}	1	MS_{AxB}	F_{AxB}	P_{AxB}	$C.L._{AxB}$
Error	SS_E	4	MS_E			
Total	SS_T	7				

An optimum condition can be calculated by using the contribution of each significant factor to determine the best estimated value, which may be the highest, lowest, or closest to a target value.[64] The contribution of a factor can be determined from Equation 1.44 where $\overline{T}(2)$ is the average value when the factor is at the second level, $\overline{T}(1)$ is the average value when the factor is at the first level, and $\overline{T}$ is the overall average value for all runs. [64]

$$Contribution_{factor} = \left(\overline{T}(2)_{factor} - \overline{T}(1)_{factor}\right) - \overline{T} \tag{1.44}$$

The contribution of each factor is set so that the contribution causes the total to increase or decrease towards the optimum value. [64] Interaction contributions are determined from the levels of the factors determined to increase or decrease the optimum value above. [64] The optimum value is determined from the contributions of each main effect and interactions. [64]

Some benefits of using Taguchi arrays and ANOVA analyses include providing an objective analysis, determination of the relative significance of each factor, examination of interactions between factors, prediction of the most desirable conditions for optimum behavior, and determination of error.[62,63] The error term could include factors that were not examined during the analysis, uncontrollable factors, and experimental or measurement error.[63,64] Limitations of using Taguchi with ANOVA include the assumption of independent main effects, normal distribution of data, and random sampling.[62,63] Other limitations are that analysis can only provide probable effects not proven effects and analysis can show correlation, but do not prove causation.[64]

2. Experimental Methods

This section describes experimental methods used determine relative bond strength and relative effective plasticity as well as a description of analysis methods used to determine the effect of processing parameters on relative bond strength and relative effective plasticity. An examination of fracture surfaces, created during previous notched edge fracture toughness measurements and obtained from Dr. Logan, was conducted to determine relative amounts of intergranular and transgranular fracture of Al_2O_3 grains and TiB_2 grains in each sample. Nano-indentation was conducted in Al_2O_3 grains and in TiB_2 grains on metallographically polished samples. Indent locations were verified using SEM. Nano-indentation reduced modulus, final displacements, and fracture toughness were determined using nano-indentation curves. The relative amounts of transgranular fracture and nano-indentation reduced modulus were used as measures of relative bond strength. Nano-indentation final displacements and fracture toughness were used as measures of relative effective plasticity. Statistical analysis was conducted to determine the effect of processing parameters on relative bond strength and relative effective plasticity. A comparison was performed to determine similarities and differences between effects of processing parameters on relative bond strength and relative effective plasticity using each different measurement method.

2.1. Bond Strength

This section describes experimental methods used to perform relative bond strength analysis. Fracture surfaces, created during previous notched edge fracture toughness measurements, obtained from Dr. Logan, were examined using SEM and EDS. Relative amounts of transgranular fracture and intergranular fracture of Al_2O_3 grains and TiB_2 grains in each sample were determined. The relative amount of transgranular fracture was used as a measure of relative bond strength in each sample. Nano-indentation was conducted on polished samples in Al_2O_3 grains and in TiB_2 grains. Indent locations were verified using SEM. Reduced modulus for indents in Al_2O_3 grains and in TiB_2 grains were determined from nano-indentation curves. Statistical analysis was conducted to determine the effect of processing parameters on relative bond strength using relative amounts of transgranular fracture and nano-indentation reduced modulus as responses under study.

2.1.1. Transgranular Fracture and Intergranular Fracture

This section describes experimental methods used to determine relative amounts of transgranular and intergranular fracture for Al_2O_3 grains and TiB_2 grains in each sample. Fracture surfaces created during previous notched edge fracture toughness testing were examined using SEM and EDS. Several interior locations on each sample were imaged using SEM and EDS. Relative amounts of transgranular and intergranular fracture for Al_2O_3 grains and TiB_2 grains were determined using SEM and EDS micrographs.

Statistical analysis was conducted to determine the effect of processing parameters on relative bond strength using relative amounts of transgranular fracture as the response under study.

2.1.1.1. Determination of Amounts of Transgranular Fracture

This section describes experimental methods used to determine amounts of transgranular and intergranular fracture for Al_2O_3 grains and TiB_2 grains in each sample. Fracture surfaces created during previous notched edge fracture toughness testing were examined using SEM and EDS. Several interior locations on each sample were imaged using SEM and EDS. Relative amounts of transgranular and intergranular fracture for Al_2O_3 grains and TiB_2 grains were determined using SEM and EDS micrographs and image analysis software.

A notched edge fracture toughness bar for each sample was mounted on an SEM stub using double sided tape so that the fracture surface would be observable when each stub was mounted as shown in Figure 2.1(a). The fracture surfaces were coated with 3.0 nm of Au-Pd using a sputter coater.

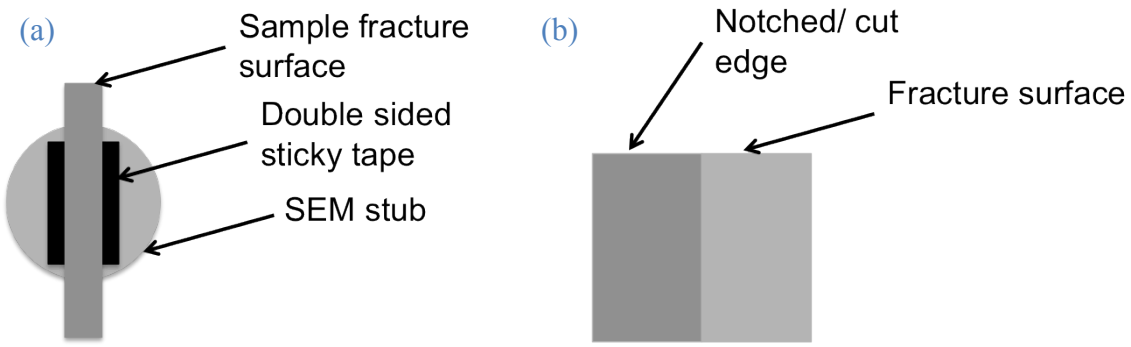

Figure 2.1 SEM (a) Sample Mount (b) Fracture Surface Orientation

Fracture surfaces were examined using SEM on a FEI Quanta 600 FEG and EDS with a Bruker EDX. The spot size was 5.0 μm, the voltage was 20kV, and the working distance was around 12 mm. Samples were oriented so the fracture surface was perpendicular to the electron beam. The SEM stage was oriented such that the notched surface was on the left and the fracture surface was on the right as shown in Figure 2.1(b). The sample dimensions were measured using distance tools in the SEM software. The horizontal midpoint (between the notched/fracture edge and the edge of the sample) was determined. Two points, one-third of the vertical distance and two-thirds of the vertical distance, were located as shown in Figure 2.2(a). Four micrographs were taken at the intersections of the horizontal midpoint with the vertical thirds to attain eight micrographs on the interior of each sample as shown in Figure 2.2(b). EDS maps were acquired at the intersections of the horizontal midpoint with the vertical thirds, as shown in Figure 2.2(a), to verify the identity of the phases on each fracture surface. EDS was conducted with Aluminum (Al) and Titanium (Ti) as the selected elements since previous X-ray diffraction did not show significant formation of phases other than Al_2O_3 and TiB_2.

Al was displayed on the EDS map in red, and Ti was displayed on the EDS map in green. Table 2.1 lists the samples that were used for fracture surface analysis.

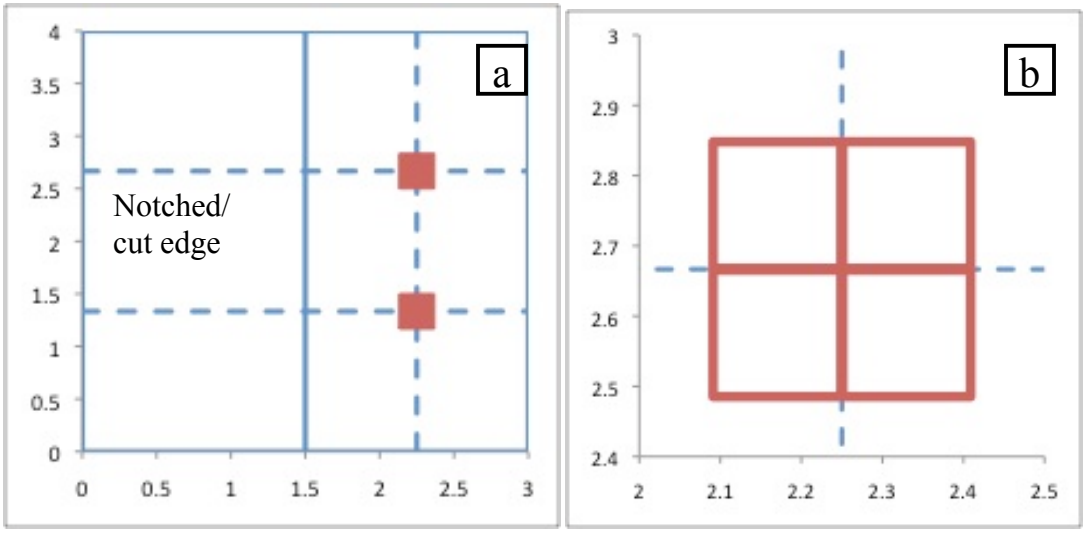

Figure 2.2 SEM Micrograph Locations on Fracture Surfaces (a) General Locations (b) Detail of Upper Location

Table 2.1 Sampling List for Fracture Surfaces

Test #	Sample	Location
1	A	Upper middle
2	A	Lower middle
3	B	Upper middle
4	B	Lower middle
5	C	Upper middle
6	C	Lower middle
7	D	Upper middle
8	D	Lower middle

Qualitative visual observation of fracture modes using SEM and EDS micrographs of each sample was conducted. The qualitative observations were compared with the previous results from other research.

EDS maps were exported from the EDS software as a .doc file. EDS maps were then saved individually as .jpg files for each location. ImageJ software was used to perform micrograph analysis on each EDS .jpg micrograph. The first step in the analysis was to determine the total area of the micrograph, which was accomplished by selecting Measure from the Analyze menu in ImageJ, which measured the whole area of the .jpg and displayed the result. The total area of the micrograph was recorded. Then the total area of TiB_2 grains in each micrograph was determined by setting the threshold color to pass hues in the range of 34-210 as shown in Figure 2.3(a). Figure 2.3(b) shows a filtered image with only the passing hues. Once the color filter range was set, the color filter was set as a threshold, which provided an image as shown in Figure 2.3(c). Next the total area

of TiB_2 grains was determined by using the Analyze Particles function. Then the total area for TiB_2 grains was recorded.

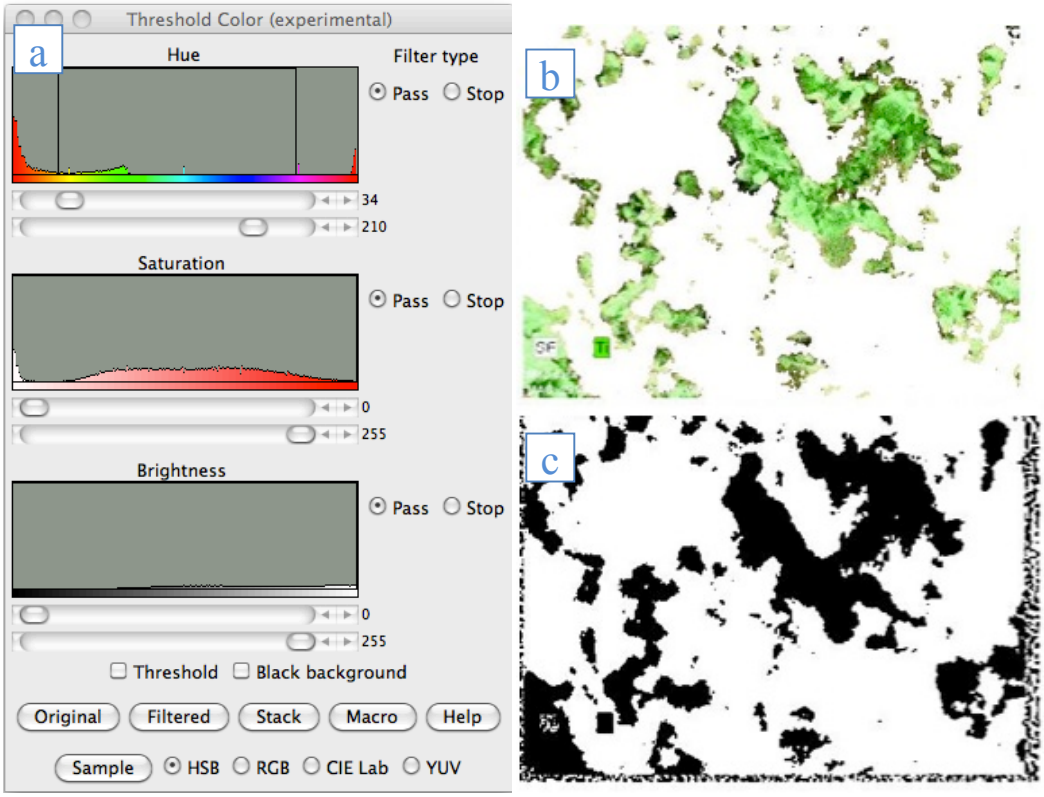

Figure 2.3 Setting Color Threshold (a) Color Threshold Window (b) Filtered Image (c) Threshold Image

The third step was to determine the total area of Al_2O_3 grains in each micrograph by setting the color threshold to stop hues in the range of 34-210, which eliminated the green hues and showed only the red color. The image was once again filtered using the color threshold and the area was measured using the Analyze Particles function. Then the total area of Al_2O_3 grains was recorded. The total area of Al_2O_3 grains and TiB_2 grains was compared with the total area of the micrograph to verify that the whole micrograph was measured.

The threshold was turned off so the .jpg filtered image showed only Al_2O_3 grains. Areas of transgranular fracture in Al_2O_3 grains were identified on the EDS micrograph by comparison with the appropriate SEM micrographs. The Freehand Selection tool was used to hand draw selection areas one at a time as shown in yellow (thin line) in Figure 2.4. After one selection area was drawn, the Measurement tool was used to determine the area of that selection, and then the measured area was recorded. The Pencil tool was used to mark the area as measured so that when the next selection area was drawn, previous measured areas would be visible as shown in grey (thick line) in Figure 2.4. Individual area selection, measurement, recording, and marking were continued until all transgranular fracture areas in Al_2O_3 grains were measured and marked. The intergranular

fracture area in Al_2O_3 grains was determined by subtracting the total transgranular fracture areas of Al_2O_3 grains from the total Al_2O_3 grain area.

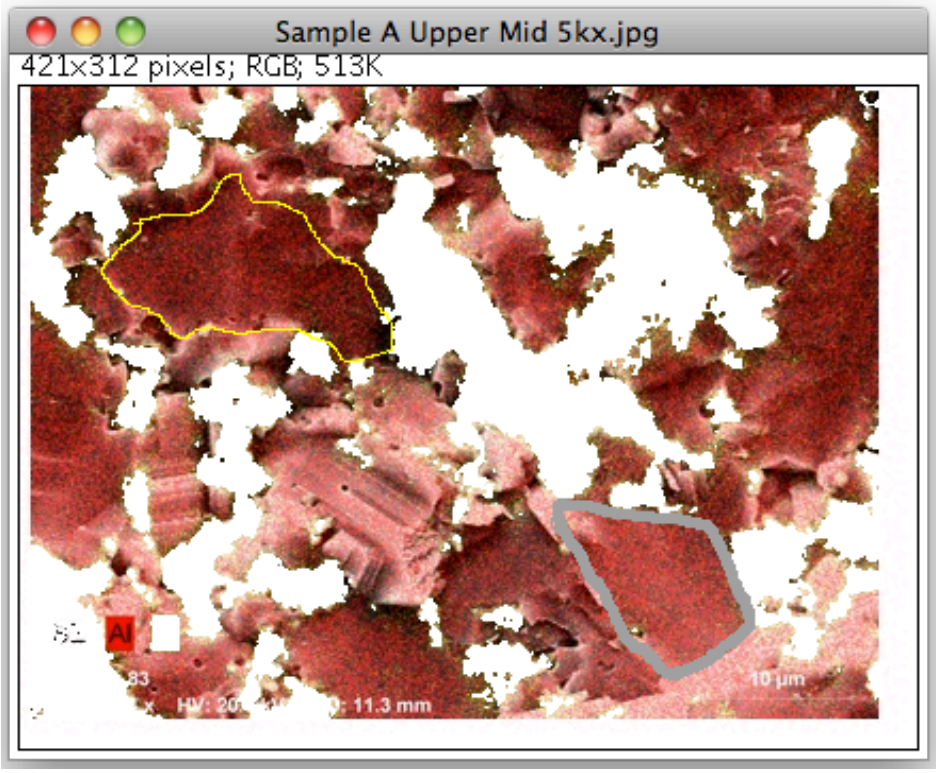

Figure 2.4 Example of Freehand Selection Tool and Pencil Tool Selections

The same process was used to determine transgranular fracture of TiB_2 grains, after the filter was changed from 'stop' to 'pass' so that hues in the range of 34-210 were visible including green colors indicating TiB_2 grains. An example summary of the data is shown in Table 2.2.

Table 2.2 Example Summary of Measured Fracture Areas

Location	Al_2O_3 grains			TiB_2 grains		
	Total area	Trans-granular area	Inter-granular area	Total area	Trans-granular area	Inter-granular area
Upper middle	$A_{Al_2O_3,Total}$	A_{Trans,Al_2O_3}	A_{Inter,Al_2O_3}	$A_{TiB_2,Total}$	A_{Trans,TiB_2}	A_{Inter,TiB_2}

2.1.1.2. Relative Bond Strength from Transgranular Fracture

This section describes experimental methods used to determine relative bond strengths from amounts of transgranular fracture in each sample. Total amounts of transgranular fracture in each location were determined by adding the area of transgranular fracture in Al_2O_3 grains and transgranular fracture in TiB_2 grains as shown in Equation 2.1.

$$A_{Trans,Total} = A_{Trans,Al_2O_3} + A_{Trans,TiB_2} \quad (2.1)$$

The relative amount of transgranular fracture in each location was calculated by dividing the total amount of transgranular fracture by the total area of Al_2O_3 grains plus TiB_2 grains, then converting the decimal to a percent, as shown in Equation 2.2. The relative amount of total transgranular fracture in each location was used to determine the relative bond strength for each sample.

$$A_{Rel.Trans.} = A_{Trans,Total} / \left(A_{Al_2O_3,Total} + A_{TiB_2,Total} \right) \quad (2.2)$$

The relative amount of transgranular fracture of Al_2O_3 grains was determined by dividing the relative amount of transgranular fracture for Al_2O_3 grains by the total area of Al_2O_3 grains for each location, then converting the decimal to a percent, as shown in Equation 2.3. The relative bond strength in Al_2O_3 grains for each sample was determined from the amount of transgranular fracture for Al_2O_3 grains at each location.

$$A_{Rel.Trans,Al_2O_3} = A_{Trans,Al_2O_3} / A_{Al_2O_3,Total} \quad (2.3)$$

The same calculations were performed for transgranular fracture in TiB_2 grains as shown in Equation 2.4. The relative bond strength in TiB_2 grains for each sample was determined from the amount of transgranular fracture of TiB_2 grains at each location.

$$A_{Rel.Trans,Al_2O_3} = A_{Trans,TiB_2} / A_{TiB_2,Total} \quad (2.4)$$

2.1.1.3. Effect of Processing Parameters on Relative Bond Strength using Transgranular Fracture

This section describes experimental methods used to determine the effect of processing parameters on relative bond strength as determined by relative amounts of transgranular fracture. Statistical analysis was conducted to determine the effect of processing parameters on relative bond strength.

Minitab was used to perform ANOVA on L4 Taguchi arrays. Results of relative bond strength determinations were organized to match the factor levels shown in Table 2.3 for each test run. The L4 array was input with powder processing (SHS vs. MM) and predominant microstructure (TiB_2 grains surrounding Al_2O_3 grains vs. TiB_2 grains distributed amongst Al_2O_3 grains) as the factors under study as shown in Table 2.3. Powder processing was placed in factor column 1 and predominant microstructure was placed in factor column 2. Factor column 3 showed interactions between the powder processing and predominant microstructure factors. ANOVA analysis was initially conducted using relative bond strength as measured by total transgranular fracture as the response under study.

Table 2.3 L4 for Effect of Processing Parameter on Relative Bond Strength as Measured by Total Transgranular Fracture

	Factor A Column 1	Factor B Column 2	Factor AxB Column 3	Results	
Test Run	Powder processing	Predominant Microstructure	Interaction between powder processing and predominant microstructure	Upper	Lower
1	SHS	TiB_2 grains surround Al_2O_3 grains	Level not controlled – Interaction determined from calculations	y_{11}	y_{12}
2	SHS	TiB_2 grains distributed amongst Al_2O_3 grains		y_{21}	y_{22}
3	MM	TiB_2 grains surround Al_2O_3 grains		y_{31}	y_{32}
4	MM	TiB_2 grains distributed amongst Al_2O_3 grains		y_{41}	y_{42}

Example calculations were used to verify results obtained from Minitab. The first step in ANOVA analysis was to calculate the grand total, y_{total}, of all results as shown in Equation 2.5.

$$y_{total} = \sum_{i=1}^{a}\sum_{j=1}^{b} y_{ij} \tag{2.5}$$

Then, the total sum of the squares, SS_T, was calculated as shown in Equation 2.6. The total number of results, N, was calculated from the total number of runs, a, and the total number of results for each run, b, as shown in Equation 2.7.

$$SS_T = y_{11}^2 + y_{12}^2 + y_{21}^2 + y_{22}^2 + y_{31}^2 + y_{32}^2 + y_{41}^2 + y_{42}^2 - \frac{y_{total}^2}{N} \tag{2.6}$$

$$N = a * b = 4 * 2 = 8 \tag{2.7}$$

In order to calculate the sum of the squares for each factor, it was necessary to determine which result values corresponded with each level of that factor. For the Factor A, the values y_{11}, y_{12}, y_{21}, and y_{22} corresponded to level 1 of factor A. The values y_{31}, y_{32}, y_{41}, *and* y_{42} corresponded to level 2 of factor A. The sum of the squares for factor A was calculated by adding the values for the first level, then squaring that total, then adding the values for the second level and squaring the second level total. Then the whole total was divided by the number of results for each run, c, and then subtracting the grand total squared divided by the total number of results. The sum of the squares was calculated

using Equation 2.8. The number of results for each run, c, was calculated using Equation 2.9

$$SS_A = \frac{1}{c}\left[\left(y_{11}+y_{12}+y_{21}+y_{22}\right)^2+\left(y_{31}+y_{32}+y_{41}+y_{42}\right)^2\right]-\frac{y_{total}^2}{N} \quad (2.8)$$

$$c = \frac{a}{2} * b = \frac{4}{2} * 2 = 4 \quad (2.9)$$

The same method was used to calculate the sum of the squares for the other factors, SS_B and SS_{AxB}, as shown in Equations 2.10 and 2.11.

$$SS_B = \frac{1}{c}\left[\left(y_{11}+y_{12}+y_{31}+y_{32}\right)^2+\left(y_{21}+y_{22}+y_{41}+y_{42}\right)^2\right]-\frac{y_{total}^2}{N} \quad (2.10)$$

$$SS_{AxB} = \frac{1}{c}\left[\left(y_{11}+y_{12}+y_{41}+y_{42}\right)^2+\left(y_{21}+y_{22}+y_{31}+y_{32}\right)^2\right]-\frac{y_{total}^2}{N} \quad (2.11)$$

The sum of the squares for the error, SS_E, was calculated using Equation 2.12.

$$SS_E = SS_T - SS_A - SS_B - SS_{AxB} \quad (2.12)$$

The number of degrees of freedom, DF_F, for the total was calculated as shown in Equation 2.13.

$$DF_T = N - 1 = 8 - 1 = 7 \quad (2.13)$$

The number of degrees of freedom for each factor, DF_A, DF_B, and DF_{AxB}, was calculated as shown in Equation 2.14.

$$DF_A = DF_B = DF_{AxB} = (number\,of\ levels) - 1 = 2 - 1 = 1 \quad (2.14)$$

The number of degrees of freedom for the error term was calculated as shown in Equation 2.15.

$$DF_E = DF_T - \sum DF_{factor} = 7 - 3 = 4 \quad (2.15)$$

The mean square for each factor, MS_A, MS_B, and MS_{AxB}, was calculated as shown in Equations 2.16, 2.17, and 2.18.

$$MS_A = SS_A / DF_A \quad (2.16)$$

$$MS_B = SS_B / DF_B \quad (2.17)$$

$$MS_{AxB} = SS_{AxB} / DF_{AxB} \quad (2.18)$$

The mean square for the error, MS_E, term was calculated as shown in Equation 2.19.

$$MS_E = SS_E / DF_E \tag{2.19}$$

The F-value for each factor, F_A, F_B, and F_{AxB}, was calculated as shown in Equations 2.20, 2.21, and 2.22.

$$F_A = MS_A / MS_E \tag{2.20}$$

$$F_B = MS_B / MS_E \tag{2.21}$$

$$F_{AxB} = MS_{AxB} / MS_E \tag{2.22}$$

The F-value was compared with a tabulated F-value to determine the probability of significance, $(1-\alpha)$, of the factor. For a probability of significance of 90%, the confidence interval, α, would be 10%, as shown in Equation 2.23.

$$\alpha = 100\% - 90\% = 10\% = 0.10 \tag{2.23}$$

The tabulated F-value was determined according to Equation 2.24.

$$F_{tabulated} = F_{\alpha, DF_{factor}, DF_{error}} = F_{0.10,1,4} = 4.55 \tag{2.24}$$

The Minitab software displayed the confidence interval as the P-value. A summary of results was shown in a table like Table 2.4.

Table 2.4 Calculation of Sum of the Squares for L4 Taguchi Array

Source of Variation	Sum of Squares	Degrees of Freedom	Mean Square	F_0	P-Value
A: Powder Processing	SS_A	1	MS_A	F_A	P_A
B: Predominant Microstructure	SS_B	1	MS_B	F_B	P_B
AxB: Interaction between powder processing and predominant microstructure	SS_{AxB}	1	MS_{AxB}	F_{AxB}	P_{AxB}
Error	SS_E	4	MS_E		
Total	SS_T	7			

The effect of each factor, $E_{Factor,level}$, was determined from the average of the values for each level of that factor, as shown in Equations 2.25 and 2.26.

$$E_{Factor,2} = L_{Factor,2} - L_{Factor,1} \tag{2.25}$$

$$E_{Factor,1} = L_{Factor,1} - L_{Factor,2} \tag{2.26}$$

The average of the values for each level of each factor, $L_{factor,level}$, was calculated as shown in Equations 2.27 and 2.28.

$$L_{A,1} = \frac{1}{c}(y_{11} + y_{12} + y_{21} + y_{22}) \tag{2.27}$$

$$L_{A,2} = \frac{1}{c}(y_{31} + y_{32} + y_{41} + y_{42}) \tag{2.28}$$

Once the effect of each factor was determined, an optimum value was determined as shown in Equation 2.29. The optimum value, *Opt*, was calculated using the overall average value, $Avg_{Overall}$, as shown in Equation 2.30.

$$Opt = Avg_{Overall} + E_{A,Level} + E_{B,Level} + E_{AxB,Level} \tag{2.29}$$

$$Avg_{Overall} = \frac{y_{total}}{a * b} \tag{2.30}$$

A summary of optimization results was shown in a table like Table 2.5.

Table 2.5 Optimization of Relative Bond strength as Measured by Total Transgranular Fracture.

A	B	AxB	Effect A	Effect B	Effect AxB	Optimize
1	1	1	$E_{A,1}$	$E_{B,1}$	$E_{AxB,1}$	Opt
1	2	2	$E_{A,1}$	$E_{B,2}$	$E_{AxB,2}$	Opt
2	1	2	$E_{A,2}$	$E_{B,1}$	$E_{AxB,2}$	Opt
2	2	1	$E_{A,2}$	$E_{B,2}$	$E_{AxB,1}$	Opt

ANOVA analysis was also conducted using relative amounts of transgranular fracture in Al_2O_3 grains and relative amounts of transgranular fracture in TiB_2 grains as separate measures of relative bond strength.

2.1.2. Nano-indentation Reduced Modulus

This section describes experimental methods used to determine relative bond strength as determined by nano-indentation reduced modulus. Nano-indentation was conducted on polished samples in Al_2O_3 grains and in TiB_2 grains. Indent locations were verified using SEM. Reduced modulus for indents in Al_2O_3 grains and in TiB_2 grains were determined from nano-indentation curves. Statistical analysis was conducted to determine the effect of processing parameters on relative bond strength as measured by nano-indentation reduced modulus.

2.1.2.1. Determination of Nano-indentation Reduced Modulus

This section describes experimental methods used to determine nano-indentation reduced modulus. Nano-indentation was conducted on polished samples in Al_2O_3 grains and in TiB_2 grains. Indent locations were verified using SEM. Reduced modulus for indents in Al_2O_3 grains and in TiB_2 grains were determined from nano-indentation curves.

Some of the fracture toughness bars described in Section 2.1.1 were used for studies of reduced modulus. Since samples may have been scratched during transportation, samples were repolished according to the schedule shown in Table 2.6. An Ecomet 3 and Automet 2 were used to perform automated polishing. Clean eight-inch polishing discs (Leco part #810-648) were used for each step. A strip of diamond polishing paste, one inch long, was added to the clean polishing disc at the start of each step. Then, the paste was mixed with Microid Extender (Leco part #811-002). During each polishing step, Microid Extender was added every 30 seconds. After each polishing step, the samples were rinsed with water, cleaned in an ultrasonic bath for 10 minutes, and rinsed again with water. The ultrasonic bath consisted of one part General Purpose Cleaner (Leco part #810-698-HAZ) and nine parts water in a Branson 2510 ultrasonic cleaner. The automatic sample holder was suspended in the bath, with the sample surface face down, so that the samples were covered in cleaning solution.

Table 2.6 Polishing Schedule

Step	Diamond Polishing Paste	Force	Rotation Speed	Time
1	15 μm	4 lbs	150 rpm	3 min
2	9 μm	7 lbs	150 rpm	6 min
3	3 μm	8 lbs	150 rpm	4 min
4	1 μm	10 lbs	150 rpm	2 min

Each sample was marked with a Sharpie on the side near the intended nano-indentation test area. The mounting epoxy above the intended nano-indentation test area was scratched and covered with Sharpie ink so that marks would be visible optically and in an SEM as shown in Figure 2.5. Samples were capped with protective covers when not in use.

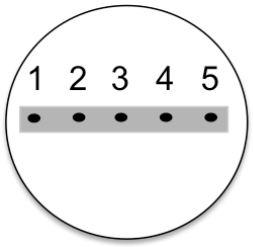

Figure 2.5 Nano-indentation Sample

Nano-indentation locations were chosen using the optical microscope attached to the nano-indenter (Hysitron Triboindenter). Twelve locations were chosen on each sample, six locations in Al_2O_3 grains and six locations in TiB_2 grains. Nano-indentation was

conducted by applying a load over a ten second interval up to a maximum of 10,000 μN, then removing the load over a ten second interval. The load-displacement curve during loading and unloading was recorded. A pattern of 3x3 indentations was conducted at each location for Al_2O_3 grains and TiB_2 grains respectively. The spacing between indents in the pattern was 7.5 μm.

Indent locations were verified using SEM. Since the nano-indentation curves were numbered and the order in which the indents were conducted was known, it was possible to identify which curves applied to each indentation point on the SEM micrographs. Indentation curves were chosen for which surface effects (such as scratches) and boundary effects (such as grain boundaries, phase boundaries, and pores) were minimized.

Five curves for Al_2O_3 grains and five curves for TiB_2 grains for each sample were analyzed to determine reduced modulus for each phase in each sample. Reduced modulus, E_r, was calculated using Equation 2.31.

$$E_r = \frac{1}{2(1.034)h_p}\sqrt{\frac{\pi}{24.494}} * \frac{dP}{dh}_{measured} \tag{2.31}$$

The plastic displacement, h_p, was determined using Equation 2.32.

$$h_p = x = \frac{y-b}{m} = \frac{0-(\text{slope intercept})}{dP/dh} \tag{2.32}$$

The initial slope of the load-displacement curve, and the slope intercept were determined from the load-displacement curve during unloading, as shown in Figure 2.6. The reduced modulus obtained through calculations was compared with the values in the nano-indenter summary file.

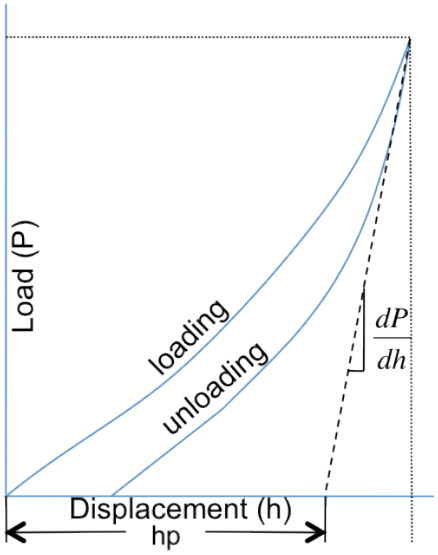

Figure 2.6 Plastic Displacement on the Load-Displacement Curve

2.1.2.2. Effect of Processing Parameters on Relative Bond Strength using Nano-indentation Reduced Modulus

This section describes experimental methods used to determine the effect of processing parameters on relative bond strength using nano-indentation reduced modulus as a measure of relative bond strength. Statistical analysis was conducted to determine the effect of processing parameters on relative bond strength.

Minitab was used to perform ANOVA on an L8 Taguchi array. The L8 array was input using powder processing (SHS vs. MM), predominant microstructure (TiB_2 grains surrounding Al_2O_3 grains vs. TiB_2 grains distributed amongst Al_2O_3 grains), and the indented phase (Al_2O_3 vs. TiB_2) as the factors under study as shown in Table 2.7. Powder processing was placed in factor column 1, predominant microstructure was placed in factor column 2, and indented phase was placed in factor column 4. Factor column 3 showed interactions between powder processing and predominant microstructure. Factor column 5 showed interactions between powder processing and indented phase. Factor column 6 showed interactions between predominant microstructure and indented phase. Factor column 7 was used to determine interactions between all three factors.

Table 2.7 L8 for Effect of Processing Parameter on Relative Bond Strength as Measured by Nano-indentation Reduced Modulus

	Factor A Column 1	Factor B Column 2	Factor AxB Column 3	Factor C Column 4	Factor AxC Column 5	Factor BxC Column 6	Factor AxBxC Column 7
Test Run	Powder Processing	Predominant Microstructure	Interaction	Indented Phase	Interaction	Interaction	Interaction
1	SHS	TiB_2 grains surround Al_2O_3 grains	Interaction between powder processing and predominant microstructure – Levels are not controlled – Interactions determined from calculations	Al_2O_3	Interaction between powder processing and indented phase – Levels are not controlled – Interactions determined from calculations	Interaction between predominant microstructure and indented phase – Levels are not controlled – Interactions determined from calculations	Interaction between powder processing, predominant microstructure, and indented phase – Levels are not controlled – Interactions determined from calculations
2	SHS	TiB_2 grains surround Al_2O_3 grains		TiB_2			
3	SHS	TiB_2 grains distributed amongst Al_2O_3 grains		Al_2O_3			
4	SHS	TiB_2 grains distributed amongst Al_2O_3 grains		TiB_2			
5	MM	TiB_2 grains surround Al_2O_3 grains		Al_2O_3			
6	MM	TiB_2 grains surround Al_2O_3 grains		TiB_2			
7	MM	TiB_2 grains distributed amongst Al_2O_3 grains		Al_2O_3			
8	MM	TiB_2 grains distributed amongst Al_2O_3 grains		TiB_2			

ANOVA analysis was conducted using relative bond strength as measured by nano-indentation reduced modulus as the response under study. Results of relative bond strength determinations were organized to match the factor levels shown in Table 2.7 for each test run. The results were entered into Minitab as shown in Table 2.8.

Table 2.8 L8 of Relative Bond Strength Results as Measured by Nano-indentation Reduced Modulus

Test Run	Result 1	Result 2	Result 3	Result 4	Result 5
1	y_{11}	y_{12}	y_{13}	y_{14}	y_{15}
2	y_{21}	y_{22}	y_{23}	y_{24}	y_{25}
3	y_{31}	y_{32}	y_{33}	y_{34}	y_{35}
4	y_{41}	y_{42}	y_{43}	y_{44}	y_{45}
5	y_{51}	y_{52}	y_{53}	y_{54}	y_{55}
6	y_{61}	y_{62}	y_{63}	y_{64}	y_{65}
7	y_{71}	y_{72}	y_{73}	y_{74}	y_{75}
8	y_{81}	y_{82}	y_{83}	y_{84}	y_{85}

Example calculations were used to verify results obtained from Minitab. The first step in ANOVA analysis was to calculate the grand total, y_{total}, of all results as shown in Equation 2.33. The total number of results, N, was calculated as shown in Equation 2.34, where a is the number of runs and b is the number of results for each run.

$$y_{total} = \sum_{i=1}^{a}\sum_{j=1}^{b} y_{ij} \tag{2.33}$$

$$N = a * b = 8 * 5 = 40 \tag{2.34}$$

The sum of the squares for each factor, SS_A, SS_B, SS_C , SS_{AxB}, SS_{BxC}, SS_{BxC}, and SS_{AxBxC}, was calculated as shown in Equations 2.35 through 2.41. The sum of the squares for each factor was determined by adding all the values for the first level of that factor, then squaring the result. Then the values for the second level of that factor were added together and the result was squared. Then the summation of the squares was divided by the number of results per run. Finally the square of the grand total was divided by the total number of results and subtracted from the previous total.

$$SS_A = \frac{1}{b}\left[\left(\sum_{i=1}^{4}\sum_{j=1}^{b} y_{ij}\right)^2 + \left(\sum_{i=5}^{8}\sum_{j=1}^{b} y_{ij}\right)^2\right] - \frac{y_{total}^2}{N} \tag{2.35}$$

$$SS_B = \frac{1}{b}\left[\begin{array}{l}\left(\sum_{j=1}^{b} y_{1j} + \sum_{j=1}^{b} y_{2j} + \sum_{j=1}^{b} y_{5j} + \sum_{j=1}^{b} y_{6j}\right)^2 \\ +\left(\sum_{j=1}^{b} y_{3j} + \sum_{j=1}^{b} y_{4j} + \sum_{j=1}^{b} y_{7j} + \sum_{j=1}^{b} y_{8j}\right)^2\end{array}\right] - \frac{y_{total}^2}{N} \quad (2.36)$$

$$SS_C = \frac{1}{b}\left[\begin{array}{l}\left(\sum_{j=1}^{b} y_{1j} + \sum_{j=1}^{b} y_{3j} + \sum_{j=1}^{b} y_{5j} + \sum_{j=1}^{b} y_{7j}\right)^2 \\ +\left(\sum_{j=1}^{b} y_{2j} + \sum_{j=1}^{b} y_{4j} + \sum_{j=1}^{b} y_{6j} + \sum_{j=1}^{b} y_{8j}\right)^2\end{array}\right] - \frac{y_{total}^2}{N} \quad (2.37)$$

$$SS_{AxB} = \frac{1}{b}\left[\begin{array}{l}\left(\sum_{j=1}^{b} y_{1j} + \sum_{j=1}^{b} y_{2j} + \sum_{j=1}^{b} y_{7j} + \sum_{j=1}^{b} y_{8j}\right)^2 \\ +\left(\sum_{i=1}^{b} y_{3j} + \sum_{i=1}^{b} y_{4j} + \sum_{i=1}^{b} y_{5j} + \sum_{i=1}^{b} y_{6j}\right)^2\end{array}\right] - \frac{y_{total}^2}{N} \quad (2.38)$$

$$SS_{AxC} = \frac{1}{b}\left[\begin{array}{l}\left(\sum_{j=1}^{b} y_{1j} + \sum_{j=1}^{b} y_{3j} + \sum_{j=1}^{b} y_{6j} + \sum_{j=1}^{b} y_{8j}\right)^2 \\ +\left(\sum_{j=1}^{b} y_{2j} + \sum_{j=1}^{b} y_{4j} + \sum_{j=1}^{b} y_{5j} + \sum_{j=1}^{b} y_{7j}\right)^2\end{array}\right] - \frac{y_{total}^2}{N} \quad (2.39)$$

$$SS_{BxC} = \frac{1}{b}\left[\begin{array}{l}\left(\sum_{j=1}^{b} y_{1j} + \sum_{j=1}^{b} y_{4j} + \sum_{j=1}^{b} y_{5j} + \sum_{j=1}^{b} y_{8j}\right)^2 \\ +\left(\sum_{j=1}^{b} y_{2j} + \sum_{j=1}^{b} y_{3j} + \sum_{j=1}^{b} y_{6j} + \sum_{j=1}^{b} y_{7j}\right)^2\end{array}\right] - \frac{y_{total}^2}{N} \quad (2.40)$$

$$SS_{AxBxC} = \frac{1}{b}\left[\begin{array}{l}\left(\sum_{j=1}^{b} y_{1j} + \sum_{j=1}^{b} y_{4j} + \sum_{j=1}^{b} y_{6j} + \sum_{j=1}^{b} y_{7j}\right)^2 \\ +\left(\sum_{j=1}^{b} y_{2j} + \sum_{j=1}^{b} y_{3j} + \sum_{j=1}^{b} y_{5j} + \sum_{j=1}^{b} y_{8j}\right)^2\end{array}\right] - \frac{y_{total}^2}{N} \quad (2.41)$$

The sum of the squares for the error, SS_E, was calculated using Equation 2.42.

$$SS_E = SS_T - SS_A - SS_B - SS_C - SS_{AxB} - SS_{AxC} - SS_{BxC} - SS_{AxBxC} \quad (2.42)$$

The number of degrees of freedom, DF_F, for the total was calculated as shown in Equation 2.43.

$$DF_T = N - 1 = 40 - 1 = 39 \quad (2.43)$$

The number of degrees of freedom for each factor, DF_A, DF_B, DF_C, DF_{AxB}, DF_{BxC}, DF_{AxC}, and DF_{AxBxC}, was calculated as shown in Equation 2.44.

$$DF_{Factor} = (number\,of\ levels) - 1 = 2 - 1 = 1 \quad (2.44)$$

The number of degrees of freedom for the error term was calculated as shown in Equation 2.45.

$$DF_E = DF_T - \sum DF_{factor} = 39 - 7 = 32 \quad (2.45)$$

The mean square for each factor, MS_{factor}, was calculated as shown in Equation 2.46. For example, the equation for the mean square for factor A, MS_A, was calculated as shown in Equation 2.47.

$$MS_{factor} = SS_{factor} / DF_{factor} \quad (2.46)$$

$$MS_A = SS_A / DF_A \quad (2.47)$$

The mean square for the error, MS_E, term was calculated as shown in Equation 2.48.

$$MS_E = SS_E / DF_E \quad (2.48)$$

The F-value for each factor, F_{factor}, was calculated as shown in Equation 2.49.

$$F_{factor} = MS_{factor} / MS_E \quad (2.49)$$

The F-value was compared with a tabulated F-value to determine the probability of significance, $(1-\alpha)$, of the factor. For a probability of significance of 90%, the confidence interval, α, would be 10%, as shown in Equation 2.50.

$$\alpha = 100\% - 90\% = 10\% = 0.10 \quad (2.50)$$

The tabulated F-value was determined according to Equation 2.51.

$$F_{tabulated} = F_{\alpha, DF_{factor}, DF_{error}} = F_{0.10,1,32} = 2.869 \quad (2.51)$$

The Minitab software displayed the confidence interval as the P-value. An example summary of results is shown in Table 2.9.

Table 2.9 Calculation of Sum of the Squares for L8 Taguchi Array

Source of Variation	Sum of Squares	Degrees of Freedom	Mean Square	F_0	P-Value
A: Powder Processing	SS_A	1	MS_A	F_A	P_A
B: Predominant Microstructure	SS_B	1	MS_B	F_B	P_B
C: Indented Phase	SS_C	1	MS_C	F_C	P_C
AxB: Interaction between powder processing and predominant microstructure	SS_{AxB}	1	MS_{AxB}	F_{AxB}	P_{AxB}
AxC: Interaction between powder processing and indented phase	SS_{AxC}	1	MS_{AxC}	F_{AxC}	P_{AxC}
BxC: Interaction between predominant microstructure and indented phase	SS_{BxC}	1	MS_{BxC}	F_{BxC}	P_{BxC}
AxBxC: Interaction between powder processing, predominant microstructure, and indented phase	SS_{AxBxC}	1	MS_{AxBxC}	F_{AxBxC}	P_{AxBxC}
Error	SS_E	32	MS_E		
Total	SS_T	39			

The effects of each factor and the optimized result were calculated and summarized in a table like Table 2.10

Table 2.10 Optimization of Bond Strength as Measured by Nano-indentation Reduced Modulus

A	B	C	A xB	A xC	B xC	A xB xC	E_A	E_B	E_C	E_{AxB}	E_{AxC}	E_{BxC}	E_{AxBxC}	Opt
1	1	1	1	1	1	1	$E_{A,1}$	$E_{B,1}$	$E_{C,1}$	$E_{AxB,1}$	$E_{AxC,1}$	$E_{BxC,1}$	$E_{AxBxC,1}$	Opt
1	1	2	1	2	2	2	$E_{A,1}$	$E_{B,1}$	$E_{C,2}$	$E_{AxB,1}$	$E_{AxC,2}$	$E_{BxC,2}$	$E_{AxBxC,2}$	Opt
1	2	1	2	1	2	2	$E_{A,1}$	$E_{B,2}$	$E_{C,1}$	$E_{AxB,2}$	$E_{AxC,1}$	$E_{BxC,2}$	$E_{AxBxC,2}$	Opt
1	2	2	2	2	1	1	$E_{A,1}$	$E_{B,2}$	$E_{C,2}$	$E_{AxB,2}$	$E_{AxC,2}$	$E_{BxC,1}$	$E_{AxBxC,1}$	Opt
2	1	1	2	2	1	2	$E_{A,2}$	$E_{B,1}$	$E_{C,1}$	$E_{AxB,2}$	$E_{AxC,2}$	$E_{BxC,1}$	$E_{AxBxC,2}$	Opt
2	1	2	2	1	2	1	$E_{A,2}$	$E_{B,1}$	$E_{C,2}$	$E_{AxB,2}$	$E_{AxC,1}$	$E_{BxC,2}$	$E_{AxBxC,1}$	Opt
2	2	1	1	2	2	1	$E_{A,2}$	$E_{B,2}$	$E_{C,1}$	$E_{AxB,1}$	$E_{AxC,2}$	$E_{BxC,2}$	$E_{AxBxC,1}$	Opt
2	2	2	1	1	1	2	$E_{A,}$	$E_{B,2}$	$E_{C,2}$	$E_{AxB,1}$	$E_{AxC,1}$	$E_{BxC,1}$	$E_{AxBxC,2}$	Opt

2.2. Effective Plasticity

This section describes experimental methods used to perform effective plasticity analysis. Nano-indentation curves obtained during reduced modulus testing were analyzed to determine nano-indentation final displacements and nano-indentation fracture toughness. Statistical analysis was conducted to determine the effect of processing parameters on relative effective plasticity using nano-indentation final displacements and fracture toughness as separate measures of relative effective plasticity.

2.2.1. Nano-indentation Final Displacements

This section describes experimental methods used to determine nano-indentation final displacements. Nano-indentation curves obtained during reduced modulus testing were analyzed to determine nano-indentation final displacements. Statistical analysis using ANOVA of Taguchi arrays was conducted to determine the effect of processing parameters on relative effective plasticity using nano-indentation final displacement as a measure of relative effective plasticity.

2.2.1.1. Determination of Nano-indentation Final Displacements

This section describes experimental methods used to determine nano-indentation final displacements using nano-indentation curves obtained during reduced modulus testing. Five curves for Al_2O_3 grains and five curves for TiB_2 grains for each sample were analyzed to determine final displacements for each phase in each sample. Indentation curves were chosen for which surface effects (such as scratches) and boundary effects (such as grain boundaries, phase boundaries, and pores) were minimized. Final displacements, h_f, were obtained from the intersection between the unloading curve and the zero load line, as shown in Figure 2.7.

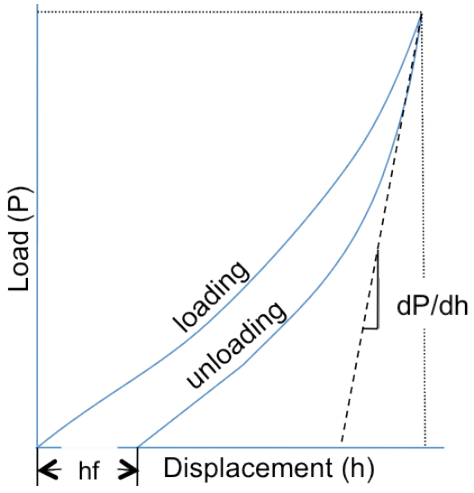

Figure 2.7 Final Displacement on Load-Displacement Curve

2.2.1.2. Effect of Processing Parameters on Relative Effective Plasticity using Nano-indentation Final Displacements

This section describes experimental methods used to determine the effect of processing parameters on relative effective plasticity using nano-indentation final displacement as a measure of effective plasticity. Statistical analysis was conducted to determine the effect of processing parameters on relative effective plasticity using nano-indentation final displacement as a measure of relative effective plasticity.

Minitab was used to perform ANOVA on an L8 Taguchi array. The L8 array was input using powder processing (SHS vs. MM), predominant microstructure (TiB_2 grains surrounding Al_2O_3 grains vs. TiB_2 grains distributed amongst Al_2O_3 grains), and the indented phase (Al_2O_3 vs. TiB_2) as the factors under study as shown in Table 2.11. Powder processing was placed in factor column 1, predominant microstructure was placed in factor column 2, and indented phase was placed in factor column 4. Factor column 3 showed interactions between powder processing and predominant microstructure. Factor column 5 showed interactions between powder processing and indented phase. Factor column 6 showed interactions between predominant microstructure and indented phase. Factor column 7 could be used to determine interactions between all three factors.

Table 2.11 L8 for Effect of Processing Parameter on Relative Effective Plasticity

	Factor A Column 1	Factor B Column 2	Factor AxB Column 3	Factor C Column 4	Factor AxC Column 5	Factor BxC Column 6	Factor AxBxC Column 7
Test Run	Powder Processing	Predominant Microstructure	Interaction	Indented Phase	Interaction	Interaction	Interaction
1	SHS	TiB_2 grains surround Al_2O_3 grains	Interaction between powder processing and predominant microstructure – Levels are not controlled – Interactions determined from calculations	Al_2O_3	Interaction between powder processing and indented phase – Levels are not controlled – Interactions determined from calculations	Interaction between predominant microstructure and indented phase – Levels are not controlled – Interactions determined from calculations	Interaction between powder processing, predominant microstructure, and indented phase – Levels are not controlled – Interactions determined from calculations
2	SHS	TiB_2 grains surround Al_2O_3 grains		TiB_2			
3	SHS	TiB_2 grains distributed amongst Al_2O_3 grains		Al_2O_3			
4	SHS	TiB_2 grains distributed amongst Al_2O_3 grains		TiB_2			
5	MM	TiB_2 grains surround Al_2O_3 grains		Al_2O_3			
6	MM	TiB_2 grains surround Al_2O_3 grains		TiB_2			
7	MM	TiB_2 grains distributed amongst Al_2O_3 grains		Al_2O_3			
8	MM	TiB_2 grains distributed amongst Al_2O_3 grains		TiB_2			

ANOVA analysis was conducted using relative effective plasticity as measured by final displacements as the response under study. Results of relative effective plasticity determinations were organized to match the factor levels shown in Table 2.11 for each test run. The results were entered into Minitab as shown in Table 2.12.

Table 2.12 L8 of Effective Plasticity Results as Measured by Final Displacements

Test Run	Result 1	Result 2	Result 3	Result 4	Result 5
1	y_{11}	y_{12}	y_{13}	y_{14}	y_{15}
2	y_{21}	y_{22}	y_{23}	y_{24}	y_{25}
3	y_{31}	y_{32}	y_{33}	y_{34}	y_{35}
4	y_{41}	y_{42}	y_{43}	y_{44}	y_{45}
5	y_{51}	y_{52}	y_{53}	y_{54}	y_{55}
6	y_{61}	y_{62}	y_{63}	y_{64}	y_{65}
7	y_{71}	y_{72}	y_{73}	y_{74}	y_{75}
8	y_{81}	y_{82}	y_{83}	y_{84}	y_{85}

Minitab output was obtained as shown in Table 2.13.

Table 2.13 Minitab Sum of the Squares for L8 Taguchi Array of Effect of Processing Parameters on Relative Effective Plasticity as Measured by Nano-indentation Final Displacements

Source of Variation	Sum of Squares	Degrees of Freedom	Mean Square	F_0	P-Value
A: Powder Processing	SS_A	1	MS_A	F_A	P_A
B: Predominant Microstructure	SS_B	1	MS_B	F_B	P_B
C: Indented Phase	SS_C	1	MS_C	F_C	P_C
AxB: Interaction between powder processing and predominant microstructure	SS_{AxB}	1	MS_{AxB}	F_{AxB}	P_{AxB}
AxC: Interaction between powder processing and indented phase	SS_{AxC}	1	MS_{AxC}	F_{AxC}	P_{AxC}
BxC: Interaction between predominant microstructure and indented phase	SS_{BxC}	1	MS_{BxC}	F_{BxC}	P_{BxC}
AxBxC: Interaction between powder processing, predominant microstructure, and indented phase	SS_{AxBxC}	1	MS_{AxBxC}	F_{AxBxC}	P_{AxBxC}
Error	SS_E	32	MS_E		
Total	SS_T	39			

The effects of each factor and the optimized value were obtained and summarized in a table like Table 2.14.

Table 2.14 Optimization of Relative Effective Plasticity as Measured by Nano-indentation Final Displacements

A	B	C	A xB	A xC	B xC	A xB xC	E_A	E_B	E_C	E_{AxB}	E_{AxC}	E_{BxC}	E_{AxBxC}	Opt
1	1	1	1	1	1	1	$E_{A,1}$	$E_{B,1}$	$E_{C,1}$	$E_{AxB,1}$	$E_{AxC,1}$	$E_{BxC,1}$	$E_{AxBxC,1}$	Opt
1	1	2	1	2	2	2	$E_{A,1}$	$E_{B,1}$	$E_{C,2}$	$E_{AxB,1}$	$E_{AxC,2}$	$E_{BxC,2}$	$E_{AxBxC,2}$	Opt
1	2	1	2	1	2	2	$E_{A,1}$	$E_{B,2}$	$E_{C,1}$	$E_{AxB,2}$	$E_{AxC,1}$	$E_{BxC,2}$	$E_{AxBxC,2}$	Opt
1	2	2	2	2	1	1	$E_{A,1}$	$E_{B,2}$	$E_{C,2}$	$E_{AxB,2}$	$E_{AxC,2}$	$E_{BxC,1}$	$E_{AxBxC,1}$	Opt
2	1	1	2	2	1	2	$E_{A,2}$	$E_{B,1}$	$E_{C,1}$	$E_{AxB,2}$	$E_{AxC,2}$	$E_{BxC,1}$	$E_{AxBxC,2}$	Opt
2	1	2	2	1	2	1	$E_{A,2}$	$E_{B,1}$	$E_{C,2}$	$E_{AxB,2}$	$E_{AxC,1}$	$E_{BxC,2}$	$E_{AxBxC,1}$	Opt
2	2	1	1	2	2	1	$E_{A,2}$	$E_{B,2}$	$E_{C,1}$	$E_{AxB,1}$	$E_{AxC,2}$	$E_{BxC,2}$	$E_{AxBxC,1}$	Opt
2	2	2	1	1	1	2	$E_{A,}$	$E_{B,2}$	$E_{C,2}$	$E_{AxB,1}$	$E_{AxC,1}$	$E_{BxC,1}$	$E_{AxBxC,2}$	Opt

2.2.2. Nano-indentation Fracture Toughness

This section describes experimental methods used to determine nano-indentation fracture toughness. Nano-indentation curves obtained during reduced modulus testing were analyzed to determine nano-indentation fracture toughness. Statistical analysis was conducted to determine the effect of processing parameters on relative effective plasticity as measured by nano-indentation fracture toughness.

2.2.2.1. Determination of Nano-indentation Fracture Toughness

This section describes experimental methods used to perform determine nano-indentation fracture toughness. Nano-indentation curves obtained during reduced modulus testing were reused to determine nano-indentation fracture toughness. The same five curves for Al_2O_3 grains and five curves for TiB_2 grains for each sample used to determine final displacements were used to determine fracture toughness for each phase in each sample.

A sample calculation using the five nano-indentation load-displacement curves for Al_2O_3 grains in Sample A is shown. Nano-indentation fracture toughness was calculated using Equation 2.52. The elastic modulus, E_s, is the bulk modulus that was calculated from the nano-indentation reduced modulus using the indenter modulus, E_i, indenter Poisson's ratio, ν_i, and material bulk Poisson's ratio, ν_s, as shown in Equation 2.53. The load, P, was the maximum load from the load-displacement curve. The hardness, H, was obtained using Equation 2.54. The plastic displacement, h_p, as shown in Figure 2.8, was obtained during the nano-indentation reduced modulus calculations.

$$K_c = 0.016\left(\frac{E_s}{H}\right)^{0.5}\frac{P}{c^{3/2}} \tag{2.52}$$

$$E_s = \frac{E_r E_i \left(1 - \nu_s^2\right)}{E_i - E_r \left(1 - \nu_i^2\right)} \tag{2.53}$$

$$H = \frac{P}{24.494 h_p^2} \tag{2.54}$$

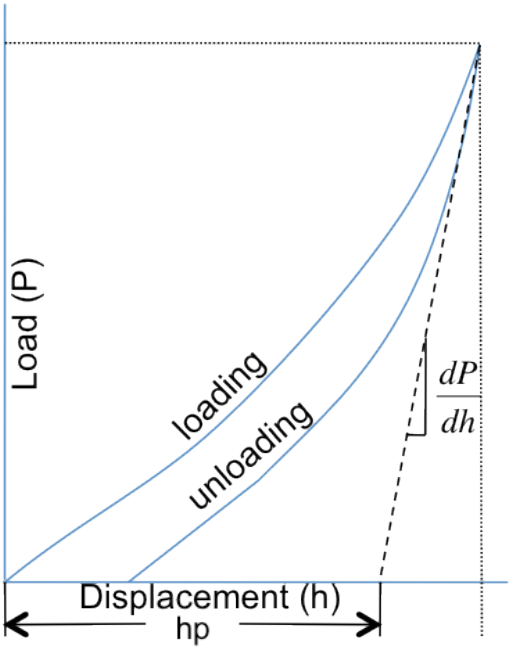

Figure 2.8 Plastic Displacement for Nano-indentation Fracture Toughness

Since nano-indentation cracks could not be seen using SEM, crack lengths, c, were approximated using Equation 2.55. The displacement, h_x, was calculated using Equation 2.56. The maximum displacement with pop-in, h_m, and maximum displacement without pop-in, h_t, were obtained from load-displacement curves. A value of 4.73 was used for Q since that was the average of previously obtained values. E_r is the reduced modulus that was calculated above.

$$c = \sqrt{2h_m} + \left(Q\frac{E_r}{H} - \sqrt{2}\right)h_x \tag{2.55}$$

$$h_x = h_m - h_t \tag{2.56}$$

2.2.2.2. Effect of Processing Parameters on Effective Plasticity using Nano-indentation Fracture Toughness

This section describes experimental methods used to determine the effect of processing parameters on effective plasticity using nano-indentation fracture toughness as a measure of effective plasticity. Statistical analysis was conducted to determine the effect of processing parameters on effective plasticity as measured by nano-indentation fracture toughness.

Minitab was used to perform ANOVA on an L8 Taguchi array. The L8 array was input using powder processing (SHS and MM), predominant microstructure (TiB_2 grains surrounding Al_2O_3 grains and TiB_2 grains distributed amongst Al_2O_3 grains), and the indented phase (Al_2O_3 and TiB_2) as the factors under study as shown in Table 2.15. Powder processing was placed in factor column 1, predominant microstructure was placed in factor column 2, and indented phase was placed in factor column 4. Factor column 3 showed interactions between powder processing and predominant microstructure. Factor column 5 showed interactions between powder processing and indented phase. Factor column 6 showed interactions between predominant microstructure and indented phase. Factor column 7 was used to determine interactions between all three factors.

Table 2.15 L8 for Effect of Processing Parameter on Effective Plasticity as Measured by Nano-indentation Fracture Toughness

	Factor A Column 1	Factor B Column 2	Factor AxB Column 3	Factor C Column 4	Factor AxC Column 5	Factor BxC Column 6	Factor AxBxC Column 7
Test Run	Powder Processing	Predominant Microstructure	Interaction	Indented Phase	Interaction	Interaction	Interaction
1	SHS	TiB_2 grains surround Al_2O_3 grains	Interaction between powder processing and predominant microstructure – Levels are not controlled – Interactions determined from calculations	Al_2O_3	Interaction between powder processing and indented phase – Levels are not controlled – Interactions determined from calculations	Interaction between predominant microstructure and indented phase – Levels are not controlled – Interactions determined from calculations	Interaction between powder processing, predominant microstructure, and indented phase – Levels are not controlled – Interactions determined from calculations
2	SHS	TiB_2 grains surround Al_2O_3 grains		TiB_2			
3	SHS	TiB_2 grains distributed amongst Al_2O_3 grains		Al_2O_3			
4	SHS	TiB_2 grains distributed amongst Al_2O_3 grains		TiB_2			
5	MM	TiB_2 grains surround Al_2O_3 grains		Al_2O_3			
6	MM	TiB_2 grains surround Al_2O_3 grains		TiB_2			
7	MM	TiB_2 grains distributed amongst Al_2O_3 grains		Al_2O_3			
8	MM	TiB_2 grains distributed amongst Al_2O_3 grains		TiB_2			

ANOVA analysis was conducted using relative effective plasticity as measured by fracture toughness as the response under study. Results of relative effective plasticity determinations were organized to match the factor levels shown in Table 2.15 for each test run. The results were entered into Minitab as shown in Table 2.16.

Table 2.16 L8 of Effective Plasticity Results as Measured by Fracture Toughness

Test Run	Result 1	Result 2
1	y_{11}	y_{12}
2	y_{21}	y_{22}
3	y_{31}	y_{32}
4	y_{41}	y_{42}
5	y_{51}	y_{52}
6	y_{61}	y_{62}
7	y_{71}	y_{72}
8	y_{81}	y_{82}

Minitab results were obtained and shown in a table like Table 2.17.

Table 2.17 Minitab Sum of the Squares for L8 Taguchi Array of Effect of Processing Parameters on Relative Effective Plasticity as Measured by Nano-indentation Fracture Toughness

Source of Variation	Sum of Squares	Degrees of Freedom	Mean Square	F_0	P-Value
A: Powder Processing	SS_A	1	MS_A	F_A	P_A
B: Predominant Microstructure	SS_B	1	MS_B	F_B	P_B
C: Indented Phase	SS_C	1	MS_C	F_C	P_C
AxB: Interaction between powder processing and predominant microstructure	SS_{AxB}	1	MS_{AxB}	F_{AxB}	P_{AxB}
AxC: Interaction between powder processing and indented phase	SS_{AxC}	1	MS_{AxC}	F_{AxC}	P_{AxC}
BxC: Interaction between predominant microstructure and indented phase	SS_{BxC}	1	MS_{BxC}	F_{BxC}	P_{BxC}
AxBxC: Interaction between powder processing, predominant microstructure, and indented phase	SS_{AxBxC}	1	MS_{AxBxC}	F_{AxBxC}	P_{AxBxC}
Error	SS_E	32	MS_E		
Total	SS_T	39			

The effect and optimized value calculations were summarized in a table like Table 2.18.

Table 2.18 Optimization of Relative Effective Plasticity as Measured by Nano-indentation Fracture Toughness

A	B	C	A xB	A xC	B xC	A xB xC	E_A	E_B	E_C	E_{AxB}	E_{AxC}	E_{BxC}	E_{AxBxC}	Opt
1	1	1	1	1	1	1	$E_{A,1}$	$E_{B,1}$	$E_{C,1}$	$E_{AxB,1}$	$E_{AxC,1}$	$E_{BxC,1}$	$E_{AxBxC,1}$	Opt
1	1	2	1	2	2	2	$E_{A,1}$	$E_{B,1}$	$E_{C,2}$	$E_{AxB,1}$	$E_{AxC,2}$	$E_{BxC,2}$	$E_{AxBxC,2}$	Opt
1	2	1	2	1	2	2	$E_{A,1}$	$E_{B,2}$	$E_{C,1}$	$E_{AxB,2}$	$E_{AxC,1}$	$E_{BxC,2}$	$E_{AxBxC,2}$	Opt
1	2	2	2	2	1	1	$E_{A,1}$	$E_{B,2}$	$E_{C,2}$	$E_{AxB,2}$	$E_{AxC,2}$	$E_{BxC,1}$	$E_{AxBxC,1}$	Opt
2	1	1	2	2	1	2	$E_{A,2}$	$E_{B,1}$	$E_{C,1}$	$E_{AxB,2}$	$E_{AxC,2}$	$E_{BxC,1}$	$E_{AxBxC,2}$	Opt
2	1	2	2	1	2	1	$E_{A,2}$	$E_{B,1}$	$E_{C,2}$	$E_{AxB,2}$	$E_{AxC,1}$	$E_{BxC,2}$	$E_{AxBxC,1}$	Opt
2	2	1	1	2	2	1	$E_{A,2}$	$E_{B,2}$	$E_{C,1}$	$E_{AxB,1}$	$E_{AxC,2}$	$E_{BxC,2}$	$E_{AxBxC,1}$	Opt
2	2	2	1	1	1	2	$E_{A,}$	$E_{B,2}$	$E_{C,2}$	$E_{AxB,1}$	$E_{AxC,1}$	$E_{BxC,1}$	$E_{AxBxC,2}$	Opt

2.3. Comparison of Results

A summary of results from all ANOVA and optimization analysis was shown in a table like Table 2.19. The results were compared to determine similarities and differences between measurement methods of relative bond strength and relative effective plasticity.

Table 2.19 Predicted Optimum Levels for Relative Bond Strength and Relative Effective Plasticity

Property under study	Measuring Method	Powder Process	Predominant Microstructure	Phase
Bond Strength	Total Transgranular fracture	Level	Level	Level
	Al_2O_3 Transgranular facture	Level	Level	Level
	TiB_2 Transgranular fracture	Level	Level	Level
	Nano-indentation Reduced Modulus	Level	Level	Level
Effective Plasticity	Nano-indentation Final Displacement	Level	Level	Level
	Nano-indentation Fracture Toughness	Level	Level	Level

3. Results and Discussion

This section presents results and discussion for relative bond strength and relative effective plasticity analysis. Fracture surfaces created during previous notched edge fracture toughness testing were examined to determine relative amounts of transgranular and intergranular fracture for Al_2O_3 grains and TiB_2 grains in each sample. Nano-indentation was conducted on polished samples in Al_2O_3 grains and in TiB_2 grains. Indent locations were verified using SEM. Nano-indentation reduced modulus, final displacements, and fracture toughness were determined for indents in Al_2O_3 grains and in TiB_2 grains from nano-indentation curves. Relative amounts of transgranular fracture and nano-indentation reduced modulus were used as measures of relative bond strength. Nano-indentation final displacements and fracture toughness were used as measures of relative effective plasticity. Statistical analysis was conducted to determine the effect of processing parameters on relative bond strength and relative effective plasticity. A comparison was performed to determine similarities and differences between effects of processing parameters on relative bond strength and relative effective plasticity using the different measurement methods.

3.1. Bond Strength

This section presents results and discussion of bond strength analysis. Fracture surfaces created during previous notched edge fracture toughness testing were examined using SEM and EDS. Relative amounts of transgranular fracture and intergranular fracture were determined for Al_2O_3 grains and TiB_2 grains in each sample. The relative amount of transgranular fracture was used as a measure of relative bond strength in each sample. Nano-indentation was conducted on polished areas in Al_2O_3 grains and in TiB_2 grains. Indent locations were verified using SEM. Nano-indentation reduced modulus, for indents in Al_2O_3 grains and in TiB_2 grains, was determined from nano-indentation curves. Statistical analysis was conducted to determine the effect of processing parameters on relative bond strength.

3.1.1. Transgranular Fracture and Intergranular Fracture

This section presents results and discussion of determinations for relative amounts of transgranular fracture and intergranular fracture for Al_2O_3 grains and TiB_2 grains in each sample. Fracture surfaces created during previous notched edge fracture toughness testing were examined using SEM and EDS. Several interior locations on each sample were imaged using SEM and EDS. Relative amounts of transgranular and intergranular fracture for Al_2O_3 grains and TiB_2 grains were determined using SEM and EDS micrographs. Statistical analysis was conducted to determine the effect of processing parameters on relative bond strength as measured by relative amounts of transgranular fracture.

3.1.1.1. Determination of Amounts of Transgranular Fracture and Intergranular Fracture

This section presents results and discussion of determinations for relative amounts of transgranular fracture and intergranular fracture for Al_2O_3 grains and TiB_2 grains in each sample. Fracture surfaces created during prior notched edge fracture toughness testing were examined using SEM and EDS. Several interior locations on each sample were imaged using SEM and EDS. Relative amounts of transgranular and intergranular fracture for Al_2O_3 grains and TiB_2 grains were determined using SEM and EDS micrographs.

Typical fracture surface micrographs for each sample are shown in Figure 3.1. In general, the dark phase is Al_2O_3 and the light phase is TiB_2. Sample A, shown in Figure 3.1(a) has large dark areas which indicates large Al_2O_3 grains and small light areas indicating small TiB_2 grains. There is a very large Al_2O_3 grain in the upper left corner, which has striations indicating transgranular cleavage fracture. Transgranular cleavage in Al_2O_3 is consistent with previous research, which showed cleavage on the basal plane in single crystal Al_2O_3. The small TiB_2 grains are grouped rather than spaced throughout the sample. There are several nearly black holes, which indicate pores or areas of intergranular pullout. There are other areas, which are very angular black holes indicating intergranular pullout.

Sample B, shown in Figure 3.1(b) has large dark areas which indicates large Al_2O_3 grains and small light areas indicating small TiB_2 grains with the same general size as found in Sample A. Most of the Al_2O_3 area appears to be continuous. There are several nearly black holes, which indicate pores or areas of intergranular pullout. Most of the holes are not as regular in shape as the holes in Sample A which may indicate that there is more intergranular pullout in Sample B than in Sample A. There are several areas of Al_2O_3, which are cracked near TiB_2 grains. The circular crack near the bottom right of the micrograph may encircle an area of eutectic microstructure. The cracks may have been caused by the difference in coefficient of thermal expansion between Al_2O_3 and TiB_2 especially in areas of eutectic microstructure.

Sample C, shown in Figure 3.1(c) appears to be mostly continuous with no distinctions in color between one phase and another. There appears to be large areas of transgranular fracture and areas where the sample could have intergranular pullout or intergranular fracture. The intergranular fracture locations appear to highlight where grains would be located on the other fracture surface rather than leaving grains to be present in the fracture surface under study. The intergranular fracture areas indicate grain sizes on the same order as the TiB_2 grains in Samples A and B. There is one large crack in the center of the sample and one small round hole indicating a small pore.

Sample D, shown in Figure 3.1(d) appears to be many separate grains with no clear distinctions in color between one phase and another. There are striations on several of the larger grains indicating transgranular cleavage fracture. There are several nearly black holes, which indicate pores or areas of intergranular pullout. Many of the intergranular

pullout areas are rounded rather than angular indicating that some of the grain on the fracture surface under study may have been pulled out with the grain on the other fracture surface.

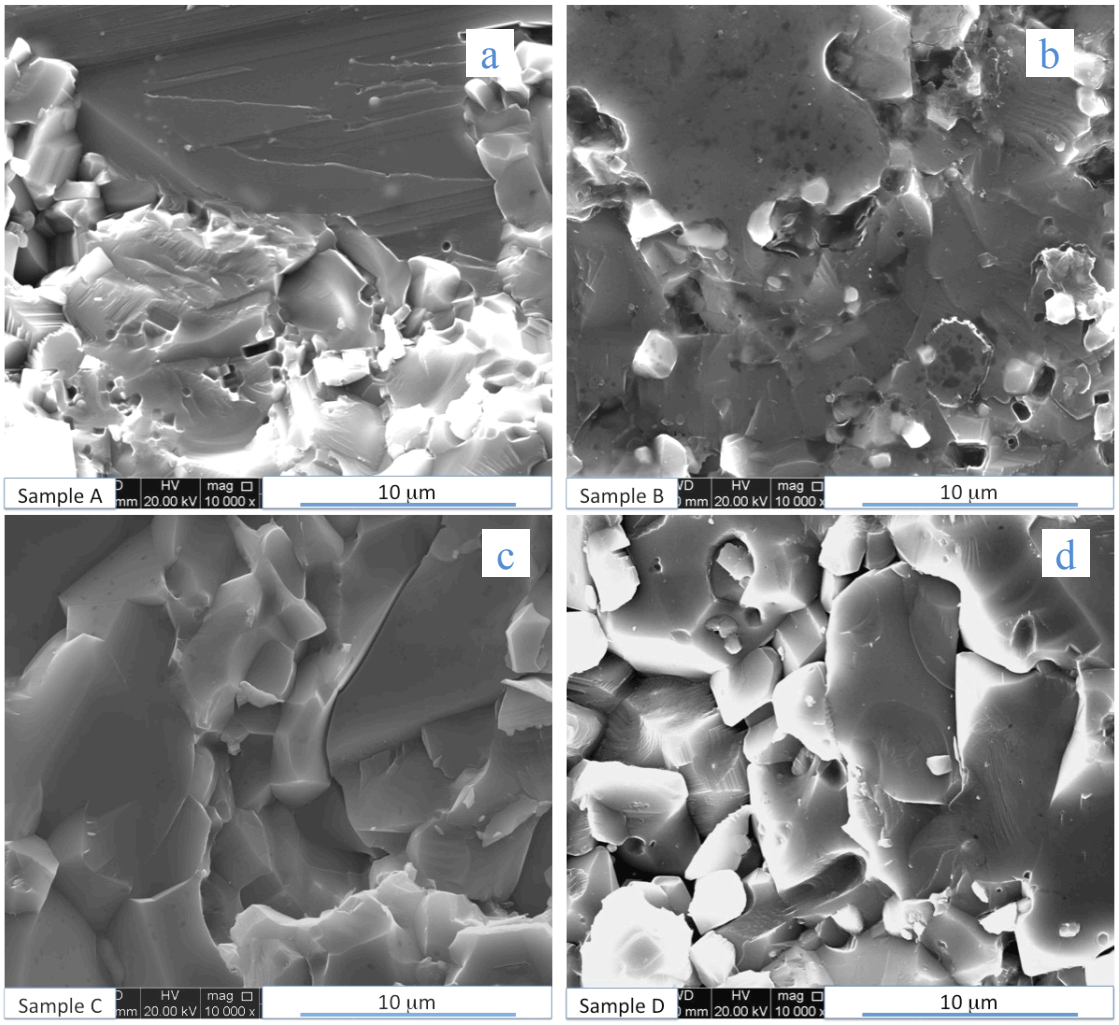

Figure 3.1 SEM Micrograph of Fractured Surface in (a) Sample A (b) Sample B (c) Sample C and (d) Sample D

EDS was used to confirm phase identification. An example of an EDS scan for Sample A is shown in Figure 3.2. The red color denotes the presence of Al. The green color denotes the presence of Ti. EDS scans were conducted at half the magnification of the individual SEM micrographs because of time limitations.

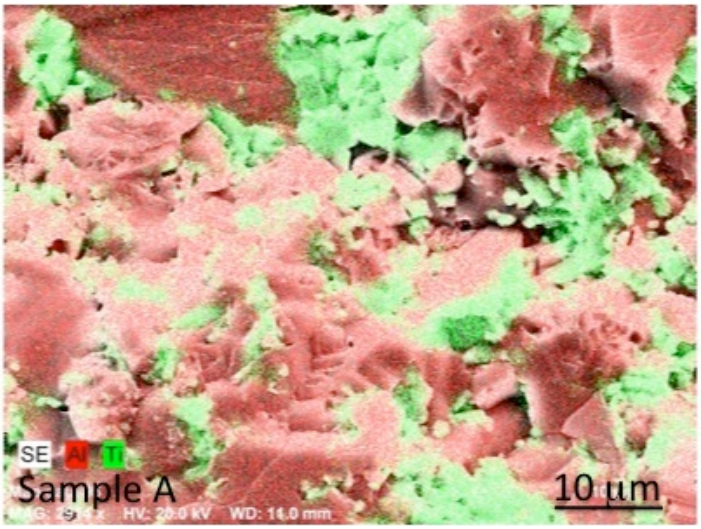

Figure 3.2 EDS Scan of Fracture Surface for Sample A

When the EDS scans were examined with the SEM micrographs, a further study of the microstructures in Figure 3.1 could be conducted. Sample A, in Figure 3.1(a), shows cleavage fracture in a TiB_2 grain in the upper left corner of the micrograph. This was unexpected because cleavage fracture is generally transgranular and TiB_2 grains were expected to show intergranular fracture. TiB_2 grains in Sample A were grouped together rather than spaced throughout the sample. Most of the areas of intergranular pullout occurred in the Al_2O_3 grains, which may indicate that there were TiB_2 grains in the indicated locations on the opposite fracture surface. There was a very clear delineation between the Al_2O_3 grains and the TiB_2 grains, which may indicate that the grain boundary strength between Al_2O_3 grains and the TiB_2 grains was not as strong as the grain strength within Al_2O_3 grains or TiB_2 grains. Al_2O_3 does not appear to show distinct grains, which may be because the Al_2O_3 melted and solidified rather than sintering from separate grains. The melting of Al_2O_3 may have occurred during the SHS reaction since the adiabatic temperature of the reaction is near 2200°C, which is greater than 2050°C, the melting temperature of Al_2O_3.

Sample B, in Figure 3.1(b), shows that the cracks in the sample did not occur around TiB_2 grains. The fracture origin may have been an interface between Al_2O_3 grains and TiB_2 grains but the propagation of the crack does not appear to have a specific pattern. It was very difficult to identify separate Al_2O_3 grains in Sample B because the Al_2O_3 appeared to have melted and solidified. TiB_2 grains were distinct, small grains, with very few TiB_2 grains in groups. TiB_2 grains were scattered throughout the sample. The EDS scan shows TiB_2 grains in locations where the SEM scan shows large continuous surfaces of Al_2O_3. TiB_2 grains may be beneath the surface of Al_2O_3 grains. If the grain boundary strength between Al_2O_3 grains and TiB_2 grains was weak, then intergranular fracture between the subsurface TiB_2 grains and the Al_2O_3 grain would be expected. Since the SEM scan shows a continuous surface of Al_2O_3, the grain strength within Al_2O_3 was weaker than the grain boundary strength between Al_2O_3 and TiB_2 grains.

Sample C, in Figure 3.1(c), shows most of the intergranular pullout or intergranular fracture in TiB_2 grains. It was expected that the large crack would separate Al_2O_3 grains and TiB_2 grains, but the analysis shows that the large crack separates Al_2O_3 grains. The crack forming between Al_2O_3 grains may indicate that the grain strength within Al_2O_3 grains was weaker than the grain boundary strength between Al_2O_3 grains and TiB_2 grains. Most of the TiB_2 grains surround the Al_2O_3 grains that are cracked. The TiB_2 grains are not distinct, instead appearing to be continuous, which is consistent with melting not sintering. Since TiB_2 melts at 3225°C and Sample C was created by manual mixing followed by hot pressing at 1600°C, sintering not melting could have occurred. The indistinct grain boundaries may be due to other phenomenon such as diffusion. But diffusion would not be expected to be significant in the limited time (150-240 minutes) at 1600°C.

Sample D, in Figure 3.1(d), shows some of the large grains are TiB_2 grains, which was unexpected in comparison with the other samples. The large grain which has transgranular cleavage as well as what may be a crack or a layer of transgranular cleavage, towards the upper right hand corner, is a TiB_2 grain. The TiB_2 grains are not grouped together. The TiB_2 grains were much larger in Sample D than in any of the other three samples. The rounded intergranular pullout occurred in Al_2O_3 grains. It is possible that the pulled out grains were TiB_2 grains, which were connected to Al_2O_3 grains. The unusually rounded intergranular pullout may have been due to higher grain boundary strength between the TiB_2 grains and Al_2O_3 grains than the grain strength within the Al_2O_3 grains.

Qualitative visual observation of fracture modes using all eight SEM micrographs and both EDS scans for each sample was conducted. A summary of the qualitative observation of fracture modes is shown in Table 3.1.The fracture of the Al_2O_3 grains in Sample A appeared to be mainly transgranular with some intergranular fracture, which was expected because the Al_2O_3 grains were large. Al_2O_3 grains in Sample B appeared to show transgranular and intergranular fracture. Al_2O_3 grains in Sample C appeared to show mainly intergranular with some transgranular fracture. Al_2O_3 grains in Sample D appeared to show mainly intergranular fracture with some transgranular fracture.

Fracture modes in TiB_2 grains in Sample A and B appeared to be mainly intergranular with a minor amount of transgranular fracture, which was expected because the TiB_2 grains were fairly small. TiB_2 grains in Sample C and D appeared to show intergranular and transgranular fracture.

It was expected that fracture modes would follow the same pattern as observed by Carney since single notched edge fracture bars were tested with the same general method that was used to test the MOR bars in Carney's research. Results stated above show general agreement with Carney's research with the exception that Carney reported less transgranular fracture of TiB_2 grains in each sample.

Table 3.1 Qualitative Visual Observation of Fracture Modes

Sample	Powder Processing	Predominant Microstructure	Al_2O_3 grains	TiB_2 grains
A	SHS	TiB_2 grains surround Al_2O_3 grains	Mainly transgranular	Mainly intergranular
B	SHS	TiB_2 grains distributed amongst Al_2O_3 grains	Transgranular and intergranular	Mainly intergranular
C	MM	TiB_2 grains surround Al_2O_3 grains	Mainly intergranular	Intergranular and transgranular
D	MM	TiB_2 grains distributed amongst Al_2O_3 grains	Mainly intergranular	Intergranular and transgranular

A comparison of possible relative grain boundary strengths and grain strengths in each sample was conducted. In Sample A, the grain boundary strength between Al_2O_3 grains and the TiB_2 grains may not have been as strong as the grain strength within Al_2O_3 grains or TiB_2 grains. The grain strength within Al_2O_3 may have been weaker than the grain boundary strength between Al_2O_3 and TiB_2 grains in Samples B, C, and D.

Quantitative analysis of fracture modes was conducted to determine relative amounts of transgranular fracture and intergranular fracture for Al_2O_3 grains and TiB_2 grains on SEM and EDS micrographs. A summary of the measured fracture areas for each sample is shown in Table 3.2.

Table 3.2 Summary of Measured Fracture Areas

Sample	Location	Al_2O_3 grains			TiB_2 grains		
		Total area	Trans-granular area	Inter-granular area	Total area	Trans-granular area	Inter-granular area
A	Upper middle	88668	67429	21239	30830	5575	25255
A	Lower middle	87704	77618	10086	31496	3379	28117
B	Upper middle	80873	54461	26412	38625	2650	35975
B	Lower middle	85075	71210	13865	33827	2841	30986
C	Upper middle	77390	55004	22386	41512	3206	9451
C	Lower middle	75247	56480	18767	43357	35093	8264
D	Upper middle	87354	16430	70924	31250	17904	13346
D	Lower middle	77252	25872	51380	41054	10182	30872

3.1.1.2. Relative Bond Strength from Transgranular Fracture

This section describes results of determinations of relative bond strength from amounts of transgranular fracture in each sample. Example calculations can be found in the Appendix.

A summary of transgranular fracture and intergranular fracture percentages for Al_2O_3 grains and TiB_2 grains (when all four are added together to show 100%) is shown in Figure 3.3. The largest area on Samples A, B, and C was transgranular fracture in Al_2O_3 grains. The largest area on Sample D was intergranular fracture in Al_2O_3 grains. The next largest area for Samples A, B, and D was intergranular fracture in TiB_2 grains. The next largest area for Sample C was transgranular fracture in TiB_2 grains.

Sample C had the lowest variability between fracture modes found in upper middle and lower middle areas, which may indicate that the fracture origin was equidistant from the two measured areas. Sample D had the largest variability between fracture modes found in upper middle and lower middle areas, which may mean that the fracture origin was closer to one of the measured areas.

The difference in fracture modes of Al_2O_3 grains and TiB_2 grains in the different samples may be due to the differences in the sizes of the grains as well as the grain boundary strengths between the Al_2O_3 grains and TiB_2 grains and the grain strengths within the Al_2O_3 grains and TiB_2 grains. The Al_2O_3 grains were generally large in Samples A, B, and C, which is consistent with more transgranular fracture of Al_2O_3 than intergranular fracture of Al_2O_3 in Samples A, B, and C. Sample D had Al_2O_3 grains that were smaller than the other three samples, therefore intergranular fracture of Al_2O_3 grains may be expected. Transgranular fracture of TiB_2 grains in Sample C may be expected because the size of the TiB_2 grains is larger than the TiB_2 grains in Samples A and B. The TiB_2 grains in Sample D were also larger than the TiB_2 grains in Samples A and B, and had more transgranular fracture of TiB_2 grains than Samples A and B, but not as much transgranular fracture of TiB_2 grains in Sample C.

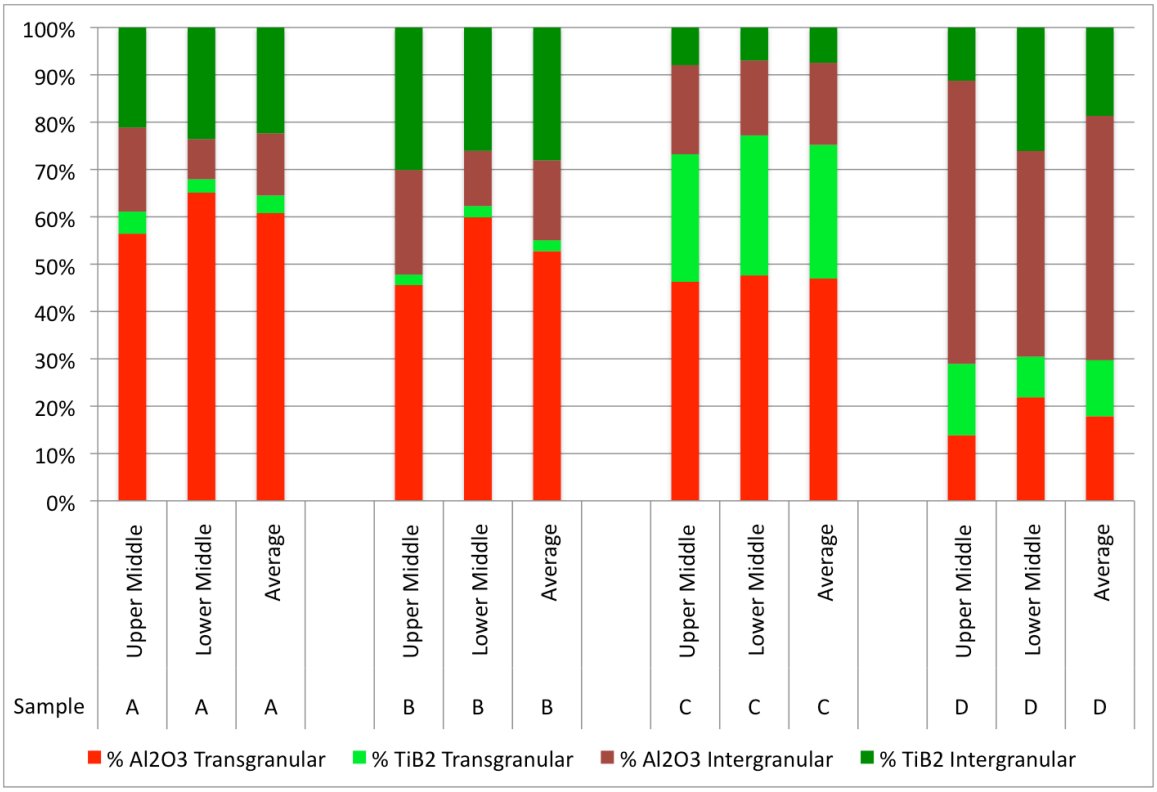

Figure 3.3 Percent Transgranular and Intergranular Fracture in Al_2O_3 and TiB_2

A summary of the quantitative results is shown in Table 3.3. There were some significant differences between the qualitative analysis and the quantitative analysis. More transgranular fracture was measured quantitatively than was observed qualitatively in Al_2O_3 grains in Samples B and C. More transgranular fracture was measured quantitatively than was observed qualitatively in TiB_2 grains in Sample C. More intergranular fracture was measured quantitatively than was observed qualitatively in TiB_2 grains in Sample D.

Table 3.3 Quantitative Summary of Fracture Modes

Sample	Powder Processing	Predominant Microstructure	Percent Transgranular in Al_2O_3 grains	Percent Transgranular in TiB_2 grains
A	SHS	TiB_2 grains surround Al_2O_3 grains	82.3	14.4
B	SHS	TiB_2 grains distributed amongst Al_2O_3 grains	75.5	7.6
C	MM	TiB_2 grains surround Al_2O_3 grains	73.1	79.1
D	MM	TiB_2 grains distributed amongst Al_2O_3 grains	26.1	41.0

Samples A and B were produced using an SHS reaction, but each had different hot pressing parameters. The resulting microstructures were different in that Sample A had

TiB_2 grains surrounding Al_2O_3 grains and Sample B had TiB_2 grains distributed amongst Al_2O_3 grains. Samples C and D were produced using a MM process, but each had different hot pressing parameters. The resulting microstructures were different in that Sample C had TiB_2 grains surrounding Al_2O_3 grains and Sample D had TiB_2 grains distributed amongst Al_2O_3 grains. The quantitative analysis shows that the fracture modes for Samples A and B were similar, but that fracture modes for Samples C and D were not similar. Similarities between fracture modes in Samples A and B, with differences between Samples A and B compared with Samples C and D indicates that powder processing method is important in determining fracture mode. But, Samples C and D were not similar which indicates that predominant microstructure had an impact on fracture mode. The final result is that powder processing and predominant microstructure may have an interaction, which is important in determining fracture mode.

It was expected that fracture modes for Al_2O_3 grains and in TiB_2 grains in each sample would confirm Carney's research results. These results did confirm that more intergranular fracture for Al_2O_3 grains was observed in Sample D than was found in Logan's as well as Keller and Zhou's research. One of the differences between the results shown in Table 3.3 and Carney's results is that this research found more transgranular fracture in Al_2O_3 grains in Sample C as was shown in Logan's results as well as Keller and Zhou's results. Results shown in Table 3.3 also showed more intergranular fracture in TiB_2 grains for Sample D and transgranular fracture in TiB_2 grains for Sample C, which is the opposite of Carney's results, but may be more consistent with Logan's results as well as Keller and Zhou's results.

One reason for differences between results in this research and previous research may be the scale at which the analysis was conducted. Analysis in this research was performed with a field of view of approximately 50 μm. Carney's analysis was performed on micrographs with a lower magnification, which may have been half of the magnification used in this research. Other reasons for differences between this research and previous research may be differences caused by the qualitative nature of previous analysis and possible differences in relative amounts of transgranular fracture in the sample depending upon the location of analysis relative to the fracture origin.

3.1.1.3. Effect of Processing Parameters on Relative Bond Strength using Transgranular Fracture

This section presents results and discussion for determining the effect of processing parameters on relative bond strength as determined by relative amounts of transgranular fracture. Statistical analysis was conducted to determine the effect of processing parameters on relative bond strength.

Minitab was used to perform ANOVA on L4 Taguchi arrays. Results of relative bond strength determinations were organized to match the factor levels shown in Table 3.4 for each test run. The L4 array was input with powder processing (SHS and MM) and predominant microstructure (TiB_2 grains surrounding Al_2O_3 grains and TiB_2 grains

distributed amongst Al_2O_3 grains) as the factors under study as shown in Table 3.4. ANOVA analysis was initially conducted using relative bond strength as measured by total transgranular fracture as the response under study.

Table 3.4 L4 for Effect of Processing Parameter on Relative Bond Strength as Measured by Total Transgranular Fracture

	Factor A Column 1	Factor B Column 2	Factor AxB Column 3	Results	
Test Run	Powder processing	Predominant Microstructure	Interaction between powder processing and predominant microstructure	Upper	Lower
1	SHS	TiB_2 grains surround Al_2O_3 grains	Level not controlled – Interaction determined from calculations	61.09	67.95
2	SHS	TiB_2 grains distributed amongst Al_2O_3 grains	Level not controlled – Interaction determined from calculations	47.79	62.28
3	MM	TiB_2 grains surround Al_2O_3 grains	Level not controlled – Interaction determined from calculations	73.22	77.21
4	MM	TiB_2 grains distributed amongst Al_2O_3 grains	Level not controlled – Interaction determined from calculations	28.95	30.48

Example calculations are shown in Appendix A. A summary of confidence level results is shown in Figure 3.4. The red line represents the 90% confidence level. The Minitab results show that factor A: Powder Processing was significant at an 84.7% confidence level, B: Predominant Microstructure is significant at a 99.7% confidence level, and the interaction between factors AxB: Powder processing and predominant microstructure were significant at a confidence level of 98.8%. Factor A: Powder Processing had an confidence level smaller than the critical level which means that the probability of powder processing affecting relative bond strength was less than 90%. It was unexpected to find that the interaction had a higher probability of affecting relative bond strength as measured by total transgranular fracture than one of the main factors.

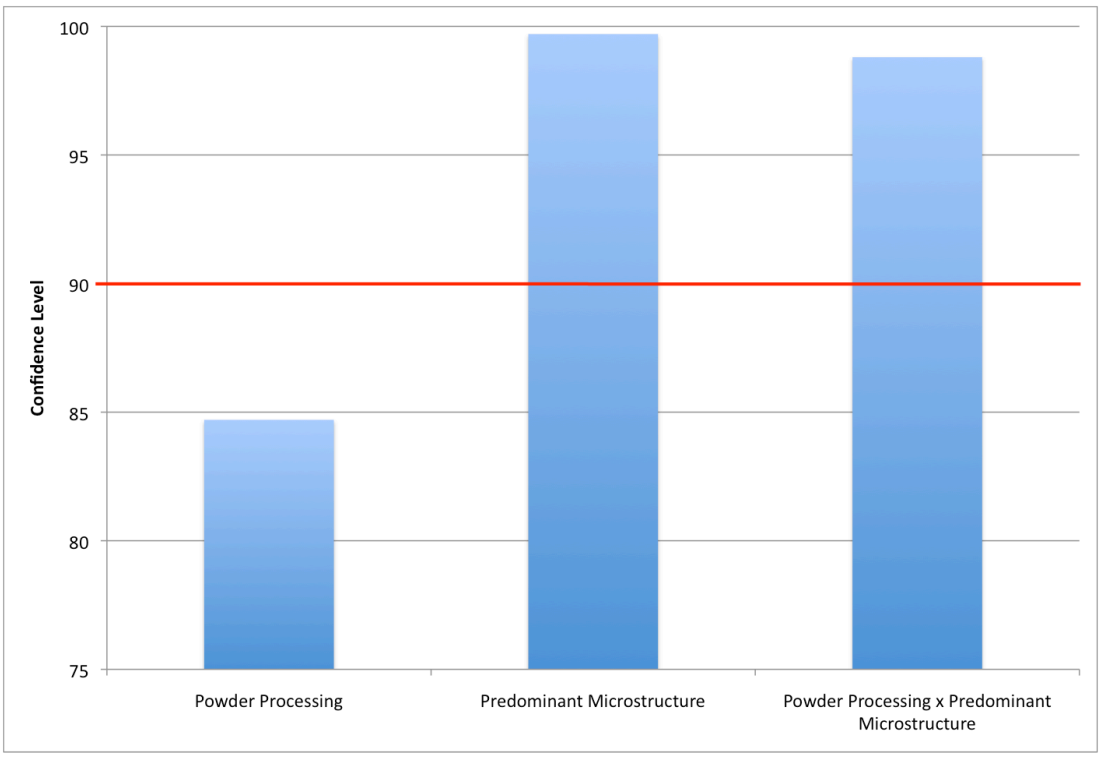

Figure 3.4 Confidence Levels for Factors for Effect of Processing Parameters on Bond Strength as Measured by Total Transgranular Fracture

The manual calculations and Minitab calculations show good agreement. Therefore Minitab was used to perform ANOVA calculations in this research including determinations of the effect of processing parameters on relative bond strength as measured by transgranular fracture using amounts of transgranular fracture in Al_2O_3 grains and transgranular fracture in TiB_2 grains as separate measures of relative bond strength.

A summary of the effect of each factor and interaction is shown in Table 3.5. The effects of Factor B: Predominant Microstructure had the largest effect on relative bond strength. The effect of the interaction had the opposite sign as the effect of the main factors.

Table 3.5 Effects of Each Factor for Relative Bond Strength as Measured by Total Transgranular Fracture

Factor	Average, Level 1	Average, Level 2	Effect (2→1)	Effect (1 → 2)
A	59.78	52.46	-7.31	7.31
B	69.87	42.37	-27.50	27.50
AxB	47.12	65.13	18.01	-18.01

A summary of optimization calculations is shown in Table 3.6. The optimum value, defined as the maximum value determined through optimization calculations, for relative bond strength as measured by total transgranular fracture was obtained when the factor levels were A=2, B=1, and AxB=2 to obtain an optimum value of 94.31. The factor levels correspond to processing parameters of manually mixed powders with TiB_2 grains

surrounding Al_2O_3 grains, which matches sample C. The average value for relative bond strength as measured by total transgranular fracture for Sample C was 75.22 during the experiment.

Table 3.6 Optimization of Relative Bond Strength as Measured by Total Transgranular Fracture

A	B	AxB	Effect A	Effect B	Effect AxB	Optimize
1	1	1	7.31	27.50	-18.01	72.92
1	2	2	7.31	-27.50	18.01	53.95
2	1	2	-7.31	27.50	18.01	94.31
2	2	1	-7.31	-27.50	-18.01	3.30

The same analysis method was conducted to determine the effect of processing parameters on relative bond strength as measured by transgranular fracture using amounts of transgranular fracture in Al_2O_3 grains. A summary of confidence level results is shown in Figure 3.5. The red line represents the 90% confidence level. The Minitab results show that factor A: Powder Processing was significant at a 99.0% confidence level, B: Predominant Microstructure was significant at a 98.6% confidence level, and the interaction between factors AxB: Powder processing and predominant microstructure was significant at a confidence level of 96.5%. Both factors and the interaction between factors have confidence levels larger than the critical value. This means that both factors and their interaction have a high probability of affecting relative bond strength as measured by Al_2O_3 transgranular fracture.

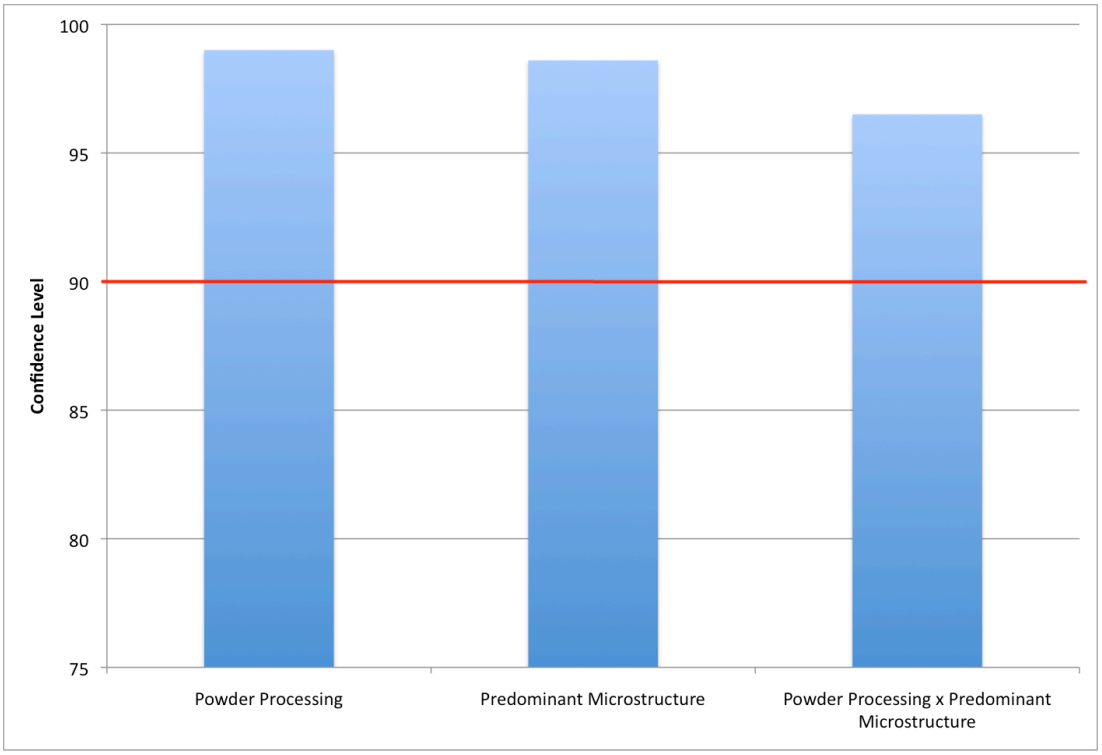

Figure 3.5 Confidence Levels for Factors for Effect of Processing Parameters on Bond Strength as Measured by Al_2O_3 Transgranular Fracture

A summary of the effects of each factor is shown in Table 3.7. The Factor A: Powder Processing had the largest effect on relative bond strength, with the effect of Factor B: Predominant Microstructure being slightly less.

Table 3.7 Effects of Each Factor for Relative Bond Strength as Measured by Al_2O_3 Transgranular Fracture

Factor	Average, Level 1	Average, Level 2	Effect (2→1)	Effect (1 → 2)
A	78.90	49.61	-29.29	29.29
B	77.67	50.84	-26.83	26.83
AxB	54.21	74.29	20.08	-20.08

The overall average of results was 64.23. A summary of optimization calculations is shown in Table 3.8. The optimum value for relative bond strength as measured by Al_2O_3 transgranular fracture was obtained when the factor levels are A=1, B=1, and AxB=1 to obtain an optimum value of 100.29. This corresponds to processing parameters of SHS produced powders with TiB_2 grains surrounding Al_2O_3 grains, which matches sample A. The average value for relative bond strength as measured by Al_2O_3 transgranular fracture for Sample A was 82.27 during the experiment.

Table 3.8 Optimization of Relative Bond strength as Measured by Al_2O_3 Transgranular Fracture

A	B	AxB	Effect A	Effect B	Effect AxB	Optimize
1	1	1	29.29	26.83	-20.08	100.29
1	2	2	29.29	-26.83	20.08	86.79
2	1	2	-29.29	26.83	20.08	81.88
2	2	1	-29.29	-26.83	-20.08	-11.95

The same analysis method was conducted to determine the effect of processing parameters on bond strength as measured by transgranular fracture using amounts of transgranular fracture in TiB_2 grains. A summary of confidence level results is shown in Figure 3.6. The red line represents the 90% confidence level. The Minitab results show that factor A: Powder Processing is significant at a 99.6% confidence level, B: Predominant Microstructure is significant at a 94.4% confidence level, and the interaction between factors AxB: Powder processing and predominant microstructure is significant at a confidence level of 86.4%.

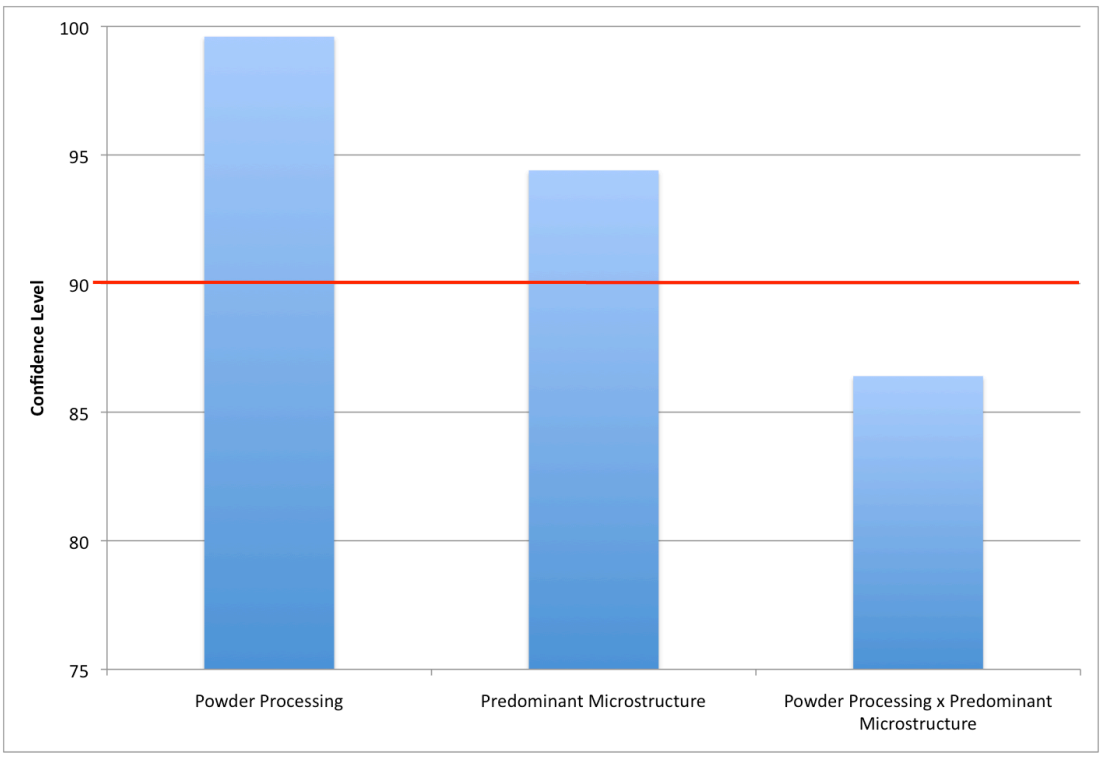

Figure 3.6 Confidence Levels of Factors for Effect of Processing Parameters on Bond Strength as Measured by TiB_2 Transgranular Fracture

A summary of the effects of each factor is shown in Table 3.9. Factor A: Powder Processing had the largest effect on relative bond strength as measured by TiB_2 transgranular fracture.

Table 3.9 Effects of Each Factor for Relative Bond Strength as Measured by TiB_2 Transgranular Fracture

Factor	Average, Level 1	Average, Level 2	Effect (2→1)	Effect (1 → 2)
A	11.02	60.07	49.05	-49.05
B	46.75	24.33	-22.41	22.41
AxB	27.73	43.36	15.63	-15.63

The overall average of results was 35.54. A summary of optimization calculations is shown in Table 3.10. The optimum value was obtained when the factor levels were A=2, B=1, AxB=2 to obtain an optimum value of 122.63. This corresponds to processing parameters of manually mixed powders with TiB2 grains surrounding Al2O3 grains, which matches Sample C. The average value for relative bond strength as measured by TiB2 transgranular fracture of Sample C was 79.09 during the experiment.

Table 3.10 Optimization of Relative Bond Strength as Measured by TiB_2 Transgranular Fracture

A	B	AxB	Effect A	Effect B	Effect AxB	Optimize
1	1	1	-49.05	22.41	-15.63	-6.73
1	2	2	-49.05	-22.41	15.63	-20.28
2	1	2	49.05	22.41	15.63	122.63
2	2	1	49.05	-22.41	-15.63	46.55

A summary of the confidence levels for the effects of each factor and interaction on bond strength for all three measures of relative bond strength is shown in Table 3.11. Factor A: Powder Processing showed as significant at or above a 99% level for transgranular facture in Al_2O_3 grains and transgranular fracture in TiB_2 grains. Factor B: Predominant Microstructure showed as significant at or above a 94% level for all three fracture measurement methods. The interaction between factors A & B showed as significant at or above a 96% level for total transgranular fracture and transgranular fracture in Al_2O_3 grains.

Table 3.11 Confidence Level for Each Factor and Interaction Effect on Bond Strength using Each Fracture Measurement Method

Measurement Method	Factor A: Powder Processing	Factor B: Predominant Microstructure	Interaction AxB: Powder Processing and Predominant Microstructure
Total Transgranular Fracture	84.7	99.7	98.8
Transgranular fracture in Al_2O_3 grains	99.0	98.6	96.5
Transgranular fracture in TiB_2 grains	99.6	94.4	86.4

Each measurement method is measuring relative bond strength in a slightly different way; therefore differences between measurement results may be expected. The total transgranular fracture is a measure of the grain strength of Al_2O_3 and TiB_2 compared to the grain boundary strength between Al_2O_3 and Al_2O_3, Al_2O_3 and TiB_2, as well as between TiB_2 and TiB_2. The Al_2O_3 transgranular fracture is a measure of the grain strength within Al_2O_3 compared to the grain boundary strength between Al_2O_3 and Al_2O_3 as well as between Al_2O_3 and TiB_2. The TiB_2 transgranular fracture is a measure of the grain strength within TiB_2 compared to the grain boundary strength between Al_2O_3 and TiB_2 as well as between TiB_2 and TiB_2. The amount of TiB_2 in each sample is significantly lower than the amount of Al_2O_3, which means that variations in TiB_2 fracture types would have a larger impact on the relative amount of transgranular fracture in TiB_2 than the impact of the same variation of Al_2O_3 fracture type would have on the relative amount of transgranular fracture in Al_2O_3.

A summary of the optimum factor levels for obtaining the highest bond strength using each of the three measures is shown in Table 3.12. The optimum level for Factor A: Powder Processing was 2: Manual Mixing for total transgranular fracture and transgranular fracture in TiB_2 grains. The optimum level for Factor B: Predominant Microstructure was 1: TiB_2 grains surround Al_2O_3 grains for all three fracture measurement methods. The interaction level was a result of the factor levels and could not be controlled independently.

Table 3.12 Optimum Factor Levels, Effects, and Value for Bond Strength using Each Fracture Measurement Method

Measurement Method	Factor A: Powder Processing		Factor B: Predominant Microstructure		Interaction AxB: Powder Processing and Predominant Microstructure		Optimum Value	Cond value during exp
	Level	Effect	Level	Effect	Level	Effect		
Total Transgranular Fracture	2	-7.31	1	27.49	2	18.01	94.31	75.22
Transgranular fracture in Al_2O_3 grains	1	29.29	1	26.83	1	-20.08	100.29	85.27
Transgranular fracture in TiB_2 grains	2	49.05	1	22.41	2	15.63	122.63	79.09

The practical limit of each relative bond strength measure is 100 since the measures were relative amounts of transgranular fracture. An optimum value of greater than 100 indicates that the maximum value should be achievable.

Each of the optimum values was greater than the actual values obtained during the experiment for the optimum factor levels. This difference may indicate that there was more variability in the relative bond strength response than was indicated by the factor levels that were used in the experiment. Further experimentation with a larger sample set and quantitative factor levels for predominant microstructure may provide better understanding as to how powder processing and predominant microstructure influence relative bond strength as measured by relative amount of transgranular fracture. Other factors, which may have confounded results, include sample microstructure characteristics such as phase distribution, phase size, and grain size.

Grain size may be of particular importance because of the influence of grain size on analysis methods used in this research. When there was a small group of grains, as may have been the case for some TiB_2 grains, intergranular rather than transgranular fracture was apparent because of different orientations of grain surfaces. In some large phase areas, as may have been the case for some Al_2O_3 grains, transgranular fracture appeared

to be the fracture mode, but may have been intergranular fracture around a very large grain.

3.1.2. Nano-indentation Reduced Modulus

This section presents results and discussion for analysis of relative bond strength as measured by nano-indentation reduced modulus. Nano-indentation was conducted on polished samples in Al_2O_3 grains and in TiB_2 grains. Indent locations were verified using SEM. Reduced modulus for indents in Al_2O_3 grains and in TiB_2 grains were calculated from nano-indentation curve results. Statistical analysis using ANOVA of a Taguchi array was conducted to determine the effect of processing parameters on relative bond strength as measured by nano-indentation reduced modulus.

3.1.2.1. Determination of Nano-indentation Reduced Modulus

This section presents results and discussion for determination of nano-indentation reduced modulus. Nano-indentation was conducted on polished samples in Al_2O_3 grains and in TiB_2 grains. Indent locations were verified using SEM. Reduced modulii for indents in Al_2O_3 grains and in TiB_2 grains were calculated using nano-indentation curve results.

Indent locations were verified using SEM after samples were coated with Gold-Palladium (Au-Pd) to prevent charging of sample surfaces. Figure 3.7 shows a typical SEM micrograph of an indented sample at a magnification of 10,000x. Red circles show the location of each of the nine indentations. The dark phase is Al_2O_3 and the light phase is TiB_2. Indents into Al_2O_3 may be easier to see than indents in TiB_2.

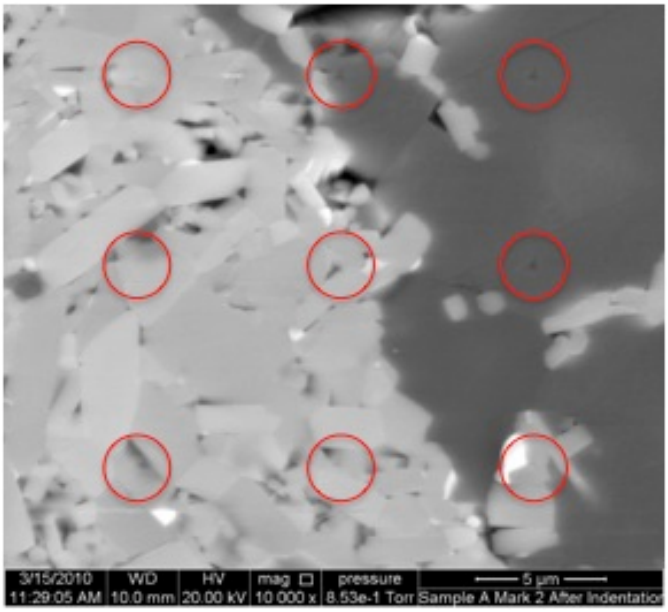

Figure 3.7 Typical SEM Micrograph After Nano-indentation (10,000x)

Representative high magnification (200,000x) micrographs of indents in Al_2O_3 grains and in TiB_2 grains are shown in Figure 3.8. Micrographs magnification higher than 200,000x did not have sufficient resolution to perform reliable analysis. The Au-Pd coating is the cause of textured surface patterns. The indent into Al_2O_3 shown in Figure 3.8(a) may indicate sinking-in at the edges of the indent. Sinking-in may cause the measured plastic displacement to be less than the plastic displacement without sinking-in. Since there is an inverse relationship between the reduced modulus and the plastic displacement, a decreased plastic displacement may cause the measured reduced modulus to be higher than the actual reduced modulus. The indent into TiB_2 shown in Figure 3.8(a) may show piling up at the edges of the indent. Piling-up may cause the measured plastic displacement to be higher than the plastic displacement without piling-up.

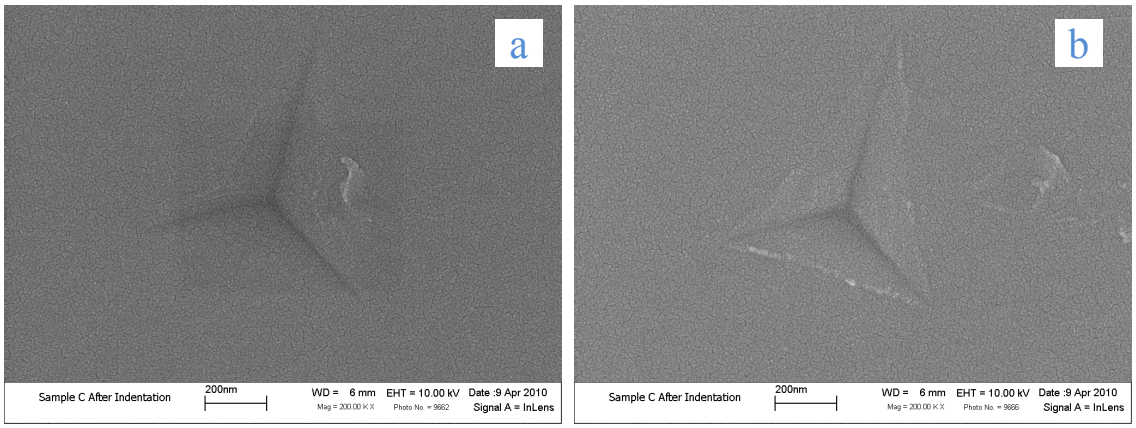

Figure 3.8 Nano-indentation in (a) Al_2O_3 Grains and in (b) TiB_2 Grains (200,000x)

It is possible that the indentation behavior shown in Figure 3.8 was limited to a small number of indents and was not consistent behavior for every indent into each phase. A limited number of high-resolution SEM micrographs were obtained since it was very difficult to obtain imaging for indents at the very high resolution necessary for determinations of sinking-in and piling-up behavior.

Micrographs such as the micrograph shown in Figure 3.7 were used to determine which nano-indentation curves applied to each phase since nano-indentation did not always occur in the intended phase because of the difficulty in choosing nano-indentation locations using an optical microscope.

Five nano-indentation curves were chosen for each phase in each sample, which minimized surface and boundary effects. The reduced modulus for each nano-indentation point was obtained from the appropriate line in the nano-indenter summary output.

One example calculation was performed to verify results obtained from the nano-indentation software. The example calculation is shown in the Appendix. The reduced modulus shown by the nano-indenter software was 172 GPa. The nano-indenter software value was 2/3 of the value calculated, 259 GPa. The nano-indenter software calculations could not be replicated, therefore reduced modulus calculations were conducted manually

rather than using the Nano-indenter software results. A summary of calculated results is shown in Table 3.13.

Table 3.13 Nano-indentation Reduced Modulus from Calculations

Run	Result 1	Result 2	Result 3	Result 4	Result 5
1	257.53	253.17	266.81	264.18	262.74
2	318.42	307.14	302.14	319.48	314.38
3	268.95	258.95	264.90	272.02	206.84
4	334.11	340.40	340.97	368.34	369.77
5	126.26	129.14	128.38	128.37	155.98
6	178.48	180.68	180.95	182.46	185.47
7	182.91	197.32	188.01	191.05	194.13
8	214.94	241.52	231.38	242.07	247.61

Table 3.14 shows a summary of the expected reduced modulii and the reduced modulii calculated from nano-indentation. The calculated reduced modulii were lower than expected. One reason for the differences may be sinking-in and piling-up effects on the indentation response. Taking into account the effects of sinking-in and piling-up, shown in Figure 3.8, the actual reduced modulus for Al_2O_3 would be even lower than the expected reduced modulus, while the actual reduced modulus for TiB_2 would be closer to the expected reduced modulus. Another reason for differences between expected and measured reduced modulii is that expected modulii were calculated for Al_2O_3 in bulk Al_2O_3 and TiB_2 in bulk TiB_2 rather than Al_2O_3 and TiB_2 in Al_2O_3-TiB_2 composites. The elastic modulus and Poisson's ratios were likely different for each component in the composite when compared with each component in each bulk material.

Table 3.14 Calculation of Expected Reduced Modulus for Al_2O_3 and TiB_2

Material	Expected Reduced Modulus (GPa)	Measured Reduced Modulus (GPa)
Al_2O_3	248.2-355.9	210
TiB_2	279.3-381.4	270

3.1.2.2. Effect of Processing Parameters on Relative Bond Strength using Nano-indentation Reduced Modulus

This section presents results and discussion for determining the effect of processing parameters on relative bond energy as determined by nano-indentation reduced modulus. Statistical analysis was conducted to determine the effect of processing parameters on relative bond strength. Minitab was used to perform ANOVA on an L8 Taguchi array.

Example calculations using the data in Table 3.13 were used to verify results obtained from Minitab and are shown in the Appendix. The calculated results and the Minitab results show good agreement. A summary of confidence level results is shown in Figure 3.9. The red line represents the 90% confidence level. The Minitab results show that factor A: Powder Processing, factor B: Predominant Microstructure, and factor C: Indented Phase are significant at a 100.0% confidence level. The interaction between

factors AxB: Powder processing and predominant microstructure is also significant at a confidence level of 100.0%. The interaction between factors AxC: Powder processing and indented phase is significant at a confidence level of 99.7%. The interaction between factors BxC: predominant microstructure and indented phase is significant at a confidence level of 98.0%. The interaction between factors AxBxC: Powder processing, predominant microstructure, and indented phase is significant at a confidence level of 99.2%.

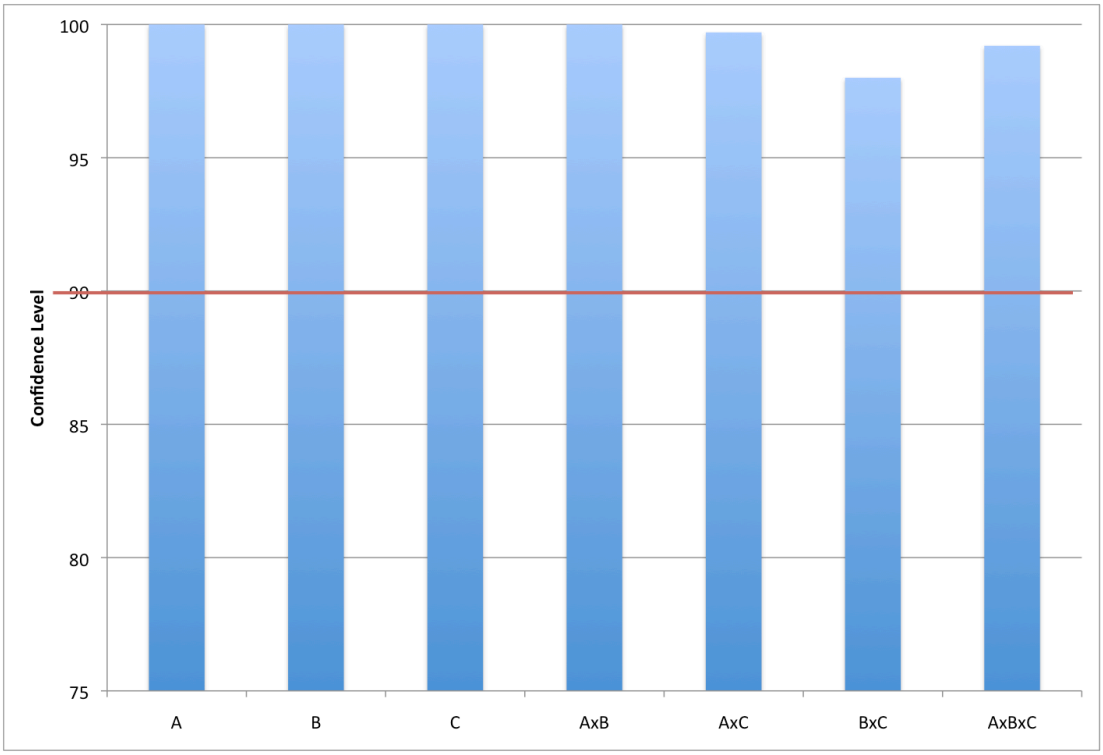

Figure 3.9 F-values of Factors for Effect of Processing Parameters on Relative Bond Strength as Measured by Nano-indentation Reduced Modulus

A summary of the effects of each factor is shown in Table 3.15. Factor A: Powder Processing had the largest effect on relative bond strength as measured by nano-indentation reduced modulus.

Table 3.15 Effects of Each Factor for Relative Bond Strength as Measured by Nano-indentation Reduced Modulus

Factor	Average, Level 1	Average, Level 2	Effect (2→1)	Effect (1 → 2)
A	294.56	185.35	-109.20	109.20
B	222.11	257.81	35.70	-35.70
C	209.88	270.04	60.15	-60.15
AxB	249.85	230.07	-19.77	19.77
AxC	233.08	246.83	13.75	-13.75
BxC	245.18	234.73	-10.45	10.45
AxBxC	245.97	233.94	-12.03	12.03

The overall average of results was 239.96. A summary of optimization calculations is shown in Table 3.16.

Table 3.16 Optimization of Relative Bond Strength as Measured by Nano-indentation Reduced Modulus

A	B	C	A xB	A xC	B xC	A xB xC	E_A	E_B	E_C	E_{AxB}	E_{AxC}	E_{BxC}	E_{AxB}	Opt
1	1	1	1	1	1	1	109.21	-35.70	-60.15	19.77	-13.75	10.45	12.03	281.82
1	1	2	1	2	2	2	109.21	-35.70	60.15	19.77	13.75	-10.45	-12.03	384.66
1	2	1	2	1	2	2	109.21	35.70	-60.15	-19.77	-13.75	-10.45	-12.03	268.70
1	2	2	2	2	1	1	109.21	35.70	60.15	-19.77	13.75	10.45	12.03	461.48
2	1	1	2	2	1	2	-109.21	-35.70	-60.15	-19.77	13.75	10.45	-12.03	27.29
2	1	2	2	1	2	1	-109.21	-35.70	60.15	-19.77	-13.75	-10.45	12.03	123.26
2	2	1	1	2	2	1	-109.21	35.70	-60.15	19.77	13.75	-10.45	12.03	141.41
2	2	2	1	1	1	2	-109.21	35.70	60.15	19.77	-13.75	10.45	-12.03	231.05

The optimum value was obtained when the factor levels were A=1, B=2, C=2 to obtain an optimum value of 461.48. This corresponds to processing parameters of SHS reaction with TiB_2 grains distributed throughout Al_2O_3 grains, and performing nano-indentation into TiB_2 grains, which matches results obtained from nano-indentation into TiB_2 grains of sample B. The average nano-indentation reduced modulus measured for TiB_2 grains of sample B was 350.72 during the experiment.

One possible reason that the optimum value was higher than the experiment value is that there were other factors affecting the measurement results that were not controlled in this research. Possible factors could be related to surface and boundary conditions near the indentation locations. The indentation locations chosen for analysis were chosen to minimize surface and boundary effects, but the indentation response could have been affected by boundary conditions that were not visible from SEM micrographs, which would include a condition where the indented grain was not very thick. Even if the grain below the indented grain were the same phase, the grain boundary would affect the indentation response of the material in that location by inhibiting dislocation movement and increasing resistance to plastic deformation.

A related factor could be the size of the indentation relative to the size grain. If the grain was small, then the grain boundaries would have a higher probability of influencing the indentation response of the material. The indents shown in Figure 3.8 were on the order of 600 nm, which is 0.6 μm. Previous research stated that TiB_2 grains were from 1-10 μm so the indentation response in TiB_2 grains could have been affected depending upon the individual grain size. Previous research stated that Al_2O_3 grain sizes were generally larger, from 10-100 μm, which could decrease the probability that grain size affected the indentation response.

3.2. Effective Plasticity

This section describes results and discussion for effective plasticity analysis. Nano-indentation curves obtained during reduced modulus testing were analyzed to determine

nano-indentation final displacements and nano-indentation fracture toughness. Statistical analysis was conducted to determine the effect of processing parameters on relative effective plasticity using nano-indentation final displacements and fracture toughness as separate measures of relative effective plasticity.

3.2.1. Nano-indentation Final Displacements

This section describes results and discussion for nano-indentation final displacement determinations. Nano-indentation curves used to determine reduced modulus were analyzed to determine nano-indentation final displacements. Statistical analysis was conducted using ANOVA of Taguchi arrays to determine the effect of processing parameters on relative effective plasticity using nano-indentation final displacements as a measure of relative effective plasticity.

3.2.1.1. Determination of Nano-indentation Final Displacements

This section describes results and discussion for nano-indentation final displacement determinations. Nano-indentation curves used to determine nano-indentation reduced modulus were analyzed to determine nano-indentation final displacements. Typical nano-indentation curves for Al_2O_3 grains and for TiB_2 grains in Sample A are shown in Figure 3.10. Nano-indentation curves for other samples were similar with final displacements in TiB_2 grains generally being less than final displacements in Al_2O_3 grains. Smaller final displacements in TiB_2 grains were expected because TiB_2 is generally harder than Al_2O_3.

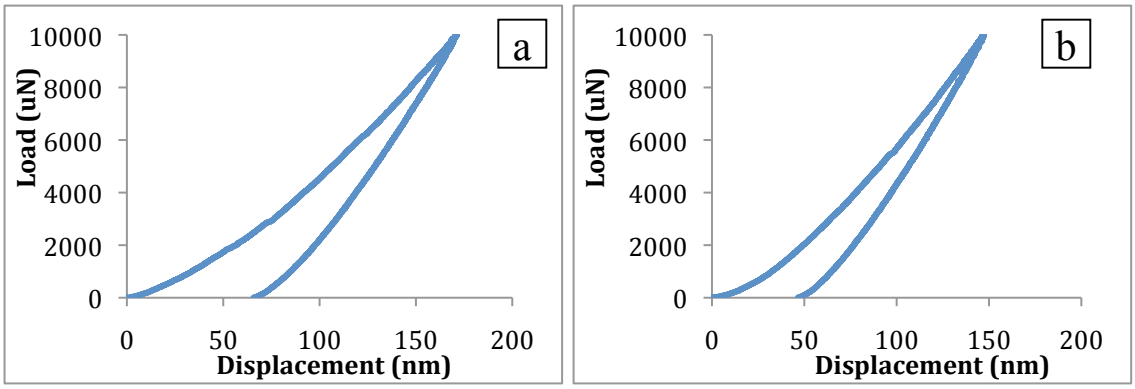

Figure 3.10 Typical Nano-indentation Curves for (a) Al_2O_3 Grains and (b) TiB_2 Grains in Sample A

A summary of final displacements in Al_2O_3 grains and in TiB_2 grains for each sample is shown in Figure 3.11. The "error bar" shows one standard deviation above and below the mean value for each sample. Final displacements in Al_2O_3 grains were higher than in TiB_2 grains. Final displacements in Al_2O_3 grains showed more variation between samples than final displacements in TiB_2 grains for samples B and C. Final displacements in TiB_2 showed more variation between samples than final displacements in Al_2O_3 grains for samples A and D. The highest final displacement in Al_2O_3 grains was in Sample C. The

lowest final displacement in Al_2O_3 grains was in Sample D. The highest final displacement in TiB_2 grains was in Sample A. The lowest final displacement in TiB_2 grains was in Sample D.

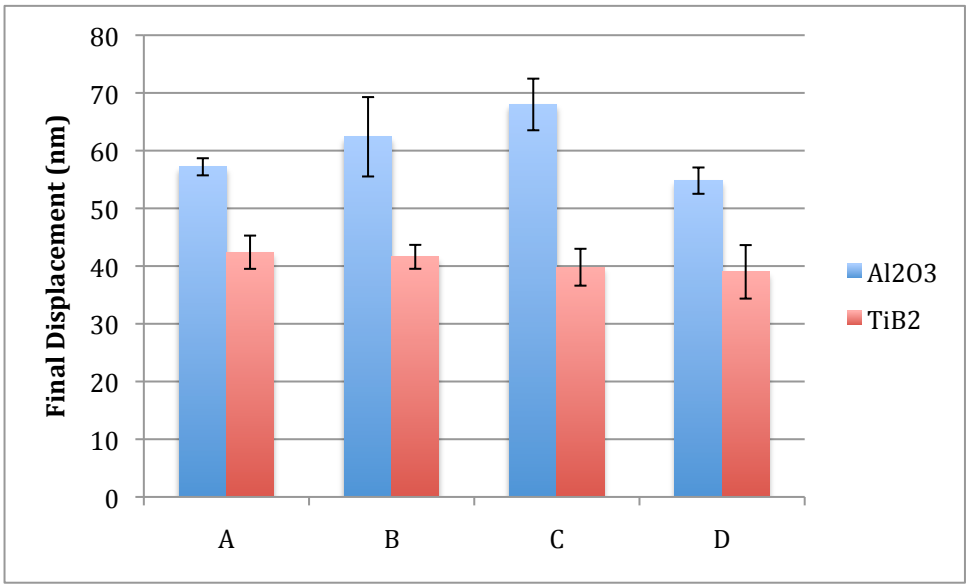

Figure 3.11 Summary of Final Displacement for Each Sample in Each Phase

Differences in final displacements between samples may have been due to the microstructure differences between samples, including differences in grain size and distribution of the phases. Variation may also be due to the fact that there was no way to know the thickness of the grain being indented. If an Al_2O_3 grain was thin and another Al_2O_3 grain was underneath, then the grain boundary would inhibit dislocation movement and decrease the plastic displacement. Since the TiB_2 grains were generally smaller than the Al_2O_3 grains, the influence of grain boundaries may have been more significant for indentations in TiB_2 grains than in Al_2O_3 grains.

3.2.1.2. Effect of Processing Parameters on Relative Effective Plasticity using Nano-indentation Final Displacements

This section presents results and discussion for determining effect of processing parameters on relative effective plasticity as determined by nano-indentation final displacement. ANOVA using an L8 Taguchi array was conducted using powder processing (SHS and MM), predominant microstructure (TiB_2 grains surrounding Al_2O_3 grains and TiB_2 grains distributed amongst Al_2O_3 grains), and the indented phase (Al_2O_3 and TiB_2) as the factors under study, as shown in Table 3.17. The ANOVA analysis was conducted using relative effective plasticity as measured by nano-indentation final displacements for the response under study.

Table 3.17 L8 of Effective Plasticity as Measured by Final Displacements

Test Run	Result 1	Result 2	Result 3	Result 4	Result 5
1	58	59	57	57	55
2	47	40	42	40	40
3	56	62	61	59	74
4	41	40	45	42	40
5	74	70	68	66	62
6	40	44	35	40	40
7	57	52	57	55	53
8	45	36	43	35	36

A summary of confidence level results for the effect of processing parameters on relative effective plasticity as measured by final displacements is shown in Figure 3.12. The red line represents the 90% confidence level. The Minitab results show that factor A: Powder Processing is significant at 22.3%. The factor B: Predominant Microstructure is significant 92.5%. The factor C: Indented Phase is significant at a 100.0% confidence level. The interaction between factors AxB: Powder processing and predominant microstructure is also significant at a confidence level of 100.0%. The interaction between factors AxC: Powder processing and indented phase is significant at a confidence level of 87.9%. The interaction between factors BxC: predominant microstructure and indented phase is significant at a confidence level of 83.7%. The interaction between factors AxBxC: Powder processing, predominant microstructure, and indented phase is significant at a confidence level of 99.9%.

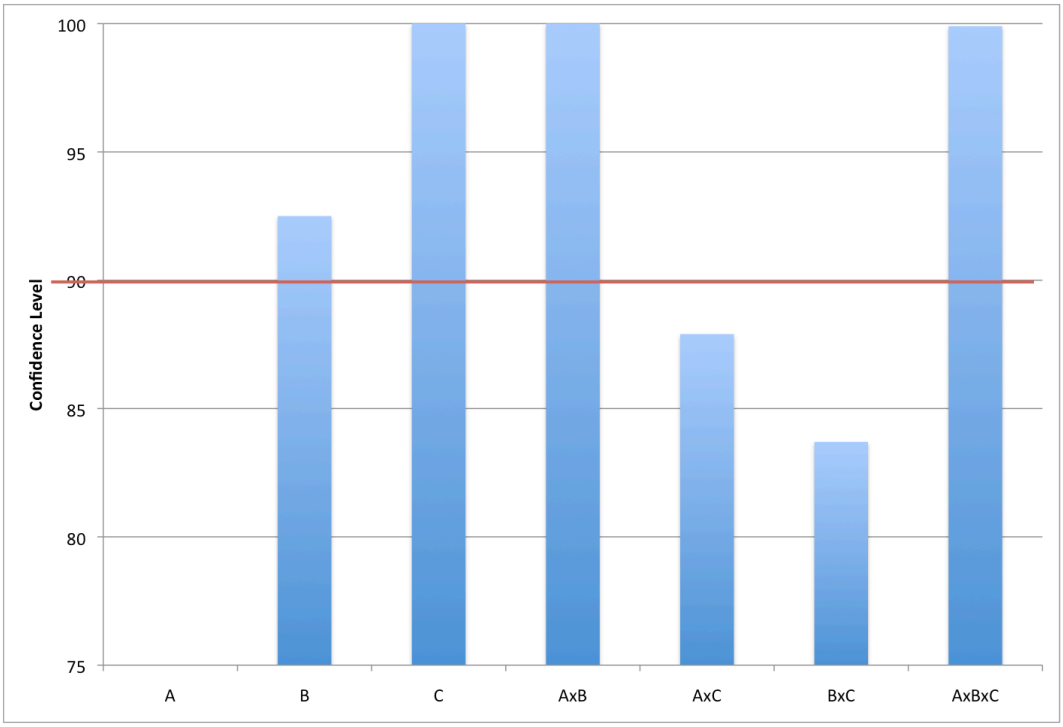

Figure 3.12 Confidence Level of Factors for Effect of Processing Parameters on Effective Plasticity as Measured by Nano-indentation Final Displacements

It was expected that phase would be a significant factor because of differences in properties between the two phases, specifically hardness, which would influence final displacements. It was unexpected that the interaction between all three factors had a much higher probability of significance than one of the three main factors, Factor A: Powder processing.

A summary of the effects of each factor is shown in Table 3.18. Factor C: Indented Phase had the largest effect on relative effective plasticity as measured by nano-indentation final displacement.

Table 3.18 Effects of Each Factor for Effective Plasticity as Measured by Nano-indentation Final Displacement

Factor	Average, Level 1	Average, Level 2	Effect (2→1)	Effect (1 → 2)
A	50.75	50.40	-0.35	0.35
B	51.70	49.45	-2.25	2.25
C	60.60	40.55	-20.05	20.05
AxB	48.20	52.95	4.75	-4.75
AxC	49.60	51.55	1.95	-1.95
BxC	51.45	49.70	-1.75	1.75
AxBxC	48.35	52.80	4.45	-4.45

The overall average of results was 50.58. A summary of optimization calculations is shown in Table 3.19.

Table 3.19 Optimization of Effective Plasticity as Measured by Nano-indentation Final Displacements

A	B	C	A xB	A xC	B xC	A xB xC	E_A	E_B	E_C	E_{AxB}	E_{AxC}	E_{BxC}	E_{AxBxC}	Opt
1	1	1	1	1	1	1	0.35	2.25	20.05	-4.75	-1.95	1.75	-4.45	63.83
1	1	2	1	2	2	2	0.35	2.25	-20.05	4.75	1.95	-1.75	4.45	33.03
1	2	1	2	1	2	2	0.35	-2.25	20.05	4.75	-1.95	-1.75	4.45	74.23
1	2	2	2	2	1	1	0.35	-2.25	-20.05	4.75	1.95	1.75	-4.45	32.63
2	1	1	2	2	1	2	-0.35	2.25	20.05	4.75	1.95	1.75	4.45	85.43
2	1	2	2	1	2	1	-0.35	2.25	-20.05	4.75	-1.95	-1.75	-4.45	29.03
2	2	1	1	2	2	1	-0.35	-2.25	20.05	-4.75	1.95	-1.75	-4.45	59.03
2	2	2	1	1	1	2	-0.35	-2.25	-20.05	-4.75	-1.95	1.75	4.45	27.43

The optimum value was obtained when the factor levels were A=2, B=1, C=1 to obtain an optimum value of 85.43. This corresponds to processing parameters of Manually Mixed powders with TiB_2 grains surrounding Al_2O_3 grains, and performing nano-indentation into Al_2O_3 grains, which matches results obtained from nano-indentation into Al_2O_3 grains of sample C. The average nano-indentation final displacement measured on Sample C for Al_2O_3 was 68.0 during the experiment.

3.2.2. Nano-indentation Fracture Toughness

This section presents results and discussion for determining nano-indentation fracture toughness. Nano-indentation curves obtained during reduced modulus testing were analyzed to determine nano-indentation fracture toughness. Statistical analysis was conducted to determine the effect of processing parameters on relative effective plasticity as measured by nano-indentation fracture toughness.

3.2.2.1. Determination of Nano-indentation Fracture Toughness

This section presents results and discussion for determining nano-indentation fracture toughness. Nano-indentation curves obtained during reduced modulus testing were used to determine nano-indentation fracture toughness. The same five curves for Al_2O_3 grains and five curves for TiB_2 grains for each sample used to determine final displacements were used to determine fracture toughness for each phase in each sample.

Example calculations are shown in the Appendix. A summary of fracture toughness results for all samples and indented phases is shown in Table 3.20. There is no apparent trend in the results.

Table 3.20 Summary of Fracture Toughness Results for All Samples

Sample	Indented Phase	Kc ($MPa/m^{1/2}$) First	Kc ($MPa/m^{1/2}$) Second
A	Al_2O_3	25.35	7.63
A	TiB_2	21.95	60.65
B	Al_2O_3	5.69	3.28
B	TiB_2	59.51	3.14
C	Al_2O_3	15.50	0.61
C	TiB_2	60.95	22.39
D	Al_2O_3	7.82	22.34
D	TiB_2	2.02	11.48

3.2.2.2. Effect of Processing Parameters on Effective Plasticity using Nano-indentation Fracture Toughness

This section presents results and discussion for determining effect of processing parameters on relative effective plasticity as determined by nano-indentation fracture toughness. Statistical analysis was conducted to determine the effect of processing parameters on effective plasticity as measured by nano-indentation fracture toughness. Minitab was used to perform ANOVA on an L8 Taguchi array. The L8 array was input using powder processing (SHS vs. MM), predominant microstructure (TiB_2 grains surrounding Al_2O_3 grains vs. TiB_2 grains distributed amongst Al_2O_3 grains), and the indented phase (Al_2O_3 vs. TiB_2) as the factors under study.

A summary of confidence level results for the effect of processing parameters on relative effective plasticity as measured by nano-indentation fracture toughness is shown in Figure 3.13. The red line represents the 90% confidence level. The Minitab results show that factor A: Powder Processing is significant at a confidence level of 38.7%. The factor B: Predominant Microstructure is significant at a confidence level of 73.3%. The factor C: Indented Phase is significant at a confidence level of 89.7%. The interaction between factors AxB: Powder processing and predominant microstructure is also significant at a confidence level of 10.9%. The interaction between factors AxC: Powder processing and indented phase is significant at a confidence level of 45.4%. The interaction between factors BxC: predominant microstructure and indented phase is significant at a confidence level of 63.2%. The interaction between factors AxBxC: Powder processing, predominant microstructure, and indented phase is significant at a confidence level of 67.6%. This means that none of the factors were significant in this experiment. This may be due to large variability in the responses obtained.

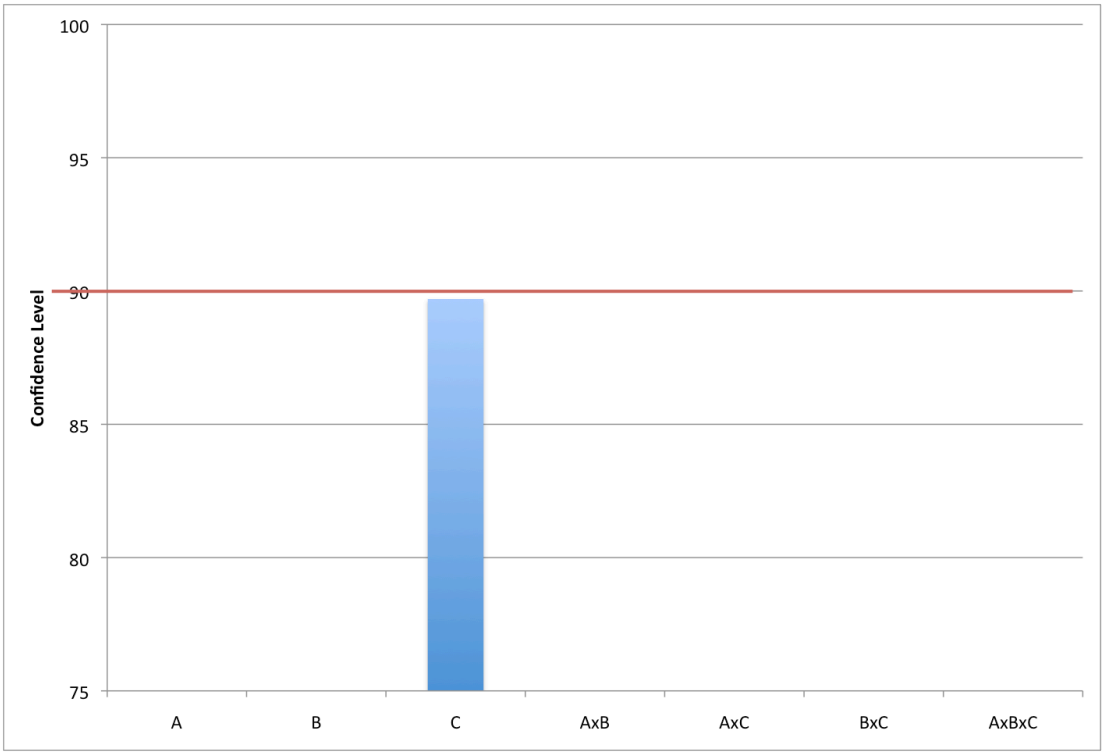

Figure 3.13 Confidence Levels of Factors for Effect of Processing Parameters on Effective Plasticity as Measured by Nano-indentation Fracture Toughness

The original derivation for determinations of crack length using changes in slope of nano-indentation curves was conducted using a cube corner indenter rather than a Berkovich indenter. The difference in the material response to the different indenter geometry may have contributed to the large error obtained during this research. Another factor, which may have contributed to the large error, is that it was assumed that all pop-in events were due to crack formation rather than other mechanisms. Both Al_2O_3 and TiB_2 could exhibit twinning, which would also appear as a pop-in event. Other factors that may have influenced the results are the thickness of the material below the indentation, and the

grain size of the material. Finally, a much larger sample size may be necessary to determine differences between materials using this method due to high variability in results.

A summary of the effects of each factor is shown in Table 3.21. Factor C: Indented Phase had the largest effect on relative effective plasticity as measured by nano-indentation fracture toughness.

Table 3.21 Effects of Each Factor for Effective Plasticity as Measured by Nano-indentation Fracture Toughness

Factor	Average, Level 1	Average, Level 2	Effect (2→1)	Effect (1 → 2)
A	23.40	17.89	-5.51	5.51
B	26.88	14.41	-12.47	12.47
C	11.03	30.26	19.23	-19.23
AxB	19.91	21.38	1.48	-1.48
AxC	17.35	23.94	6.59	-6.59
BxC	15.66	25.63	9.98	-9.98
AxBxC	26.14	15.15	-10.99	10.99

The overall average of results was 20.64. A summary of optimization calculations is shown in Table 3.22. The optimum value is obtained when the factor levels are A=2, B=1, C=2 to obtain an optimum value of 62.70. This corresponds to processing parameters of Manually Mixed with TiB_2 grains surrounding Al_2O_3 grains, and performing nano-indentation into TiB_2 grains, which matches results obtained from nano-indentation into TiB_2 grains of sample A. The average nano-indentation fracture toughness in TiB_2 grains of sample A was 41.67 during the experiment.

Table 3.22 Optimization of Bond strength as Measured by Nano-indentation Fracture Toughness

A	B	C	A xB	A xC	B xC	A xB xC	E_A	E_B	E_C	E_{AxB}	E_{AxC}	E_{BxC}	E_{AxB}	Opti
1	1	1	1	1	1	1	5.51	12.47	-19.23	-1.48	-6.59	-9.98	10.99	12.34
1	1	2	1	2	2	2	5.51	12.47	19.23	-1.48	6.59	9.98	-10.99	61.96
1	2	1	2	1	2	2	5.51	-12.47	-19.23	1.48	-6.59	9.98	-10.99	-11.67
1	2	2	2	2	1	1	5.51	-12.47	19.23	1.48	6.59	-9.98	10.99	42.01
2	1	1	2	2	1	2	-5.51	12.47	-19.23	1.48	6.59	-9.98	-10.99	-4.53
2	1	2	2	1	2	1	-5.51	12.47	19.23	1.48	-6.59	9.98	10.99	62.70
2	2	1	1	2	2	1	-5.51	-12.47	-19.23	-1.48	6.59	9.98	10.99	9.52
2	2	2	1	1	1	2	-5.51	-12.47	19.23	-1.48	-6.59	-9.98	-10.99	-7.14

3.3. Comparison of Results

This section presents results and discussion for a comparison of the results obtained during the determinations of the effect of processing parameters on relative bond strength and relative effective plasticity. ANOVA analysis using Taguchi arrays was conducted to determine the effect of processing parameters on relative bond strength and relative

effective plasticity. A comparison of the significant factors and optimization levels obtained using each measurement method was conducted.

A summary showing the factors and interactions, which were significant at a confidence level greater than 90%, is shown in Table 3.23. Factor A: Powder Processing was significant for most of the relative bond strength measures, but was not significant for the relative effective plasticity measures. There are a couple differences between the powder processing methods SHS and MM. One difference is that the SHS method causes the temperature of the material to increase to around 2000°C. The increased temperature of the SHS reaction makes it possible that a eutectic phase will form between Al_2O_3 and TiB_2. A eutectic phase would have much different strength within grains and between grains than Al_2O_3 or TiB_2. The difference in strengths within grains and between grains may have a stronger influence on the relative bond strength than on the relative effective plasticity.

Factor B: Predominant Microstructure was significant for all measures except relative effective plasticity as measured by fracture toughness, for which none of the factors and interactions was significant. The predominant microstructures were classified as TiB_2 grains surrounding Al_2O_3 grains and TiB_2 grains distributed amongst Al_2O_3 grains. In the samples with TiB_2 grains surrounding Al_2O_3 grains, the TiB_2 grains were agglomerated to form larger areas of TiB_2 grains, whereas the samples that had TiB_2 grains distributed amongst Al_2O_3 grains had more individual TiB_2 grains in many locations. The distribution of the grains would have an impact on the predominant types of interfaces in each sample. Samples with agglomerated TiB_2 grains would be more likely to have TiB_2-TiB_2 interfaces, which may have different grain boundary strengths than Al_2O_3-TiB_2 interfaces and Al_2O_3-Al_2O_3 interfaces. The difference in grain boundary strengths may have a stronger influence on the relative bond strength than on the relative effective plasticity. The influence of predominant microstructure may be confounded by characteristics of the microstructure that were not controlled in this experiment such as grain size of each phase.

The interaction AxB: Powder Processing and Predominant Microstructure was significant for most of the relative bond strength measures and for relative effective plasticity as measured by final displacements. The influence of the interaction between the two factors could have been confounded by distinctions between the four samples, which were not directly controlled through the two main factors. Examples of the distinctions between the four samples include the grain size of each phase, location of measurements relative to the crack initiation site, and relative locations of indents compared to surface and boundary effects.

Factor C: Indented Phase was significant for the nano-indentation measures except nano-indentation fracture toughness, although the significance for nano-indentation fracture toughness was 89.7%. The indented phase, Al_2O_3 or TiB_2, was expected to have a significant effect on relative bond strength and relative effective plasticity since there are significant differences between the properties of the two phases which relate to bond strength and effective plasticity.

The interactions AxC: Powder Processing and Indented Phase and BxC: Predominant Microstructure and Indented Phase were only significant for the relative bond strength measure using nano-indentation reduced modulus. The main factors were also significant for relative bond strength measured using nano-indentation reduced modulus. The significance of the interactions may indicate that instead of the main factors being independent, the main factors are both based on other factors which are influencing the relative bond strength measured using nano-indentation reduced modulus, such as grain size of each phase and thickness of each phase near the indentation location.

The interaction AxBxC: Powder Processing, Predominant Microstructure, and Indented Phase were significant for all the nano-indentation measures except nano-indentation fracture toughness. The main factor A: Powder Processing was not significant for relative effective plasticity as measured by final displacement. The significance of the interaction between the three main factors when one of the main factors was not significant may indicate that instead of the main factors being independent, the main factors are all based on other factors.

Table 3.23 Significant Effects for Bond Strength and Effective Plasticity

Factor/ Interaction	Bond Strength				Effective Plasticity	
	Total Trans Fracture	Al_2O_3 Trans Fracture	TiB_2 Trans Fracture	Reduced Modulus	Final Displ	Fracture Tough
A	No	Yes	Yes	Yes	No	No
B	Yes	Yes	Yes	Yes	Yes	No
AxB	Yes	Yes	No	Yes	Yes	No
C	N/A	N/A	N/A	Yes	Yes	No
AxC	N/A	N/A	N/A	Yes	No	No
BxC	N/A	N/A	N/A	Yes	No	No
AxBxC	N/A	N/A	N/A	Yes	Yes	No

A summary of the predicted optimum levels for factors under study is shown in Table 3.24. The optimum levels for the largest relative bond strength and relative effective plasticity include the effects of the interactions as well as the main factors. It is possible that the highest positive effect of one main factor was counteracted by the highest positive effect of another factor and the interaction between the two factors. Therefore, an analysis of the optimum levels for each factor cannot ignore the interactions between the factors or the effects of each main factor and interaction.

Table 3.24 Predicted Optimum Levels for Bond Strength and Effective Plasticity

Property under study	Measuring Quantity	Powder Process	Predominant Microstructure	Phase
Bond Strength	Total Transgranular fracture	2	1	N/A
	Al_2O_3 Transgranular fracture	1	1	N/A
	TiB_2 Transgranular fracture	2	1	N/A
	Nano-indentation Reduced Modulus	1	2	2
Effective Plasticity	Nano-indentation Final Displacements	2	1	1
	Nano-indentation Fracture Toughness	2	1	2

The optimum level for Powder Processing was predominantly 2: Manual Mixing. SHS produced material had higher positive effect on relative bond strength as measured by total transgranular fracture, but the effect of the predominant microstructure and the interaction between the two variables caused the final optimized levels to include level 2, MM, for factor A.

SHS produced material had higher optimum values for relative bond strength when measured using Al_2O_3 transgranular fracture and nano-indentation reduced modulus, with a larger positive effect for total transgranular fracture. The SHS reaction temperature could reach 2200°C, which is higher than the melting temperature of Al_2O_3. The melting and resolidification of Al_2O_3 could cause there to be stronger grain boundary interfaces between Al_2O_3 grains and between Al_2O_3 and TiB_2 grains, especially if a eutectic microstructure was formed. The SHS reaction temperature may not have significantly affected the TiB_2 because the melting temperature of TiB_2 is significantly higher than the SHS temperature.

The nano-indentation final displacements and fracture toughness had higher optimum values for MM produced material. This may be due to the potentially stronger grain boundaries produced in SHS reactions causing a decrease in the ease of dislocation movement, which caused a decrease in the plasticity of the material below the plasticity of the MM produced material.

The optimum level for Predominant Microstructure was predominantly 1: TiB_2 grains surrounding Al_2O_3 grains. TiB_2 grains surrounding Al_2O_3 grains produced a higher optimum value for relative bond strength as measured by all three types of transgranular fracture, but TiB_2 grains distributed throughout Al_2O_3 grains produced a higher optimum value for relative bond strength as measured by nano-indentation reduced modulus. It may be that the grain boundary strength of TiB_2-TiB_2 interfaces, Al_2O_3-TiB_2 interfaces,

and Al_2O_3-Al_2O_3 interfaces are very different. It is possible that when there are more Al_2O_3-TiB_2 interfaces, the relative bond strength as measured by transgranular fracture decreases because the grain boundary strength of the Al_2O_3-TiB_2 interfaces is lower than the grain boundary strength of TiB_2-TiB_2 interfaces and Al_2O_3-Al_2O_3 interfaces.

The difference in the relative bond strength as measured by nano-indentation reduced modulus may have been due to the locations of the indentations, which were chosen for the analysis. In order to reduce the influence of boundary effects, indentation locations were chosen as far away from the other phase as possible. In samples that had TiB_2 grains distributed throughout Al_2O_3 grains, the probability that the indentations were closer to the other phase was higher. Indentations close to the other phase may have had higher nano-indentation reduced modulus due to the grain boundary inhibiting dislocation movement and increasing the nano-indentation reduced modulus.

The optimum level for Indented Phase was predominantly 2: TiB_2, which was expected since TiB_2 has a higher resistance to deformation. For the same reason, TiB_2 was expected to have a lower relative effective plasticity, since higher resistance to deformation means less effective plasticity, which means that it was expected that Al_2O_3 would have a higher relative effective plasticity. The one part of the predicted response, which does not match the optimum results, is the relative effective plasticity as measured by nano-indentation fraction toughness. The unexpected results may be due to the high error obtained during the experiment. Error could have been caused by the formation of pop-in events due to twinning or other effects rather than crack formation. Error could also be introduced through influences of surface and boundary effects including thickness of the material and grain size.

4. Conclusions

This section presents conclusions for relative bond strength and relative effective plasticity analysis. The relative amount of transgranular fracture and the nano-indentation reduced modulus were used as measures of relative bond strength in each sample. The nano-indentation final displacement and fracture toughness were used as measures of relative effective plasticity in each sample.

4.1. Bond Strength

This section presents conclusions for relative bond strength analysis. Fracture surfaces created during previous notched edge fracture toughness testing were examined using SEM and EDS. Relative amounts of transgranular fracture and intergranular fracture were determined for Al_2O_3 grains and TiB_2 grains in each sample. Nano-indentation was conducted on polished areas in Al_2O_3 grains and in TiB_2 grains. Nano-indentation reduced modulii, for indents in Al_2O_3 grains and in TiB_2 grains, were determined from nano-indentation curves. The relative amount of transgranular fracture and the nano-indentation reduced modulus were used as measures of relative bond strength in each sample. Statistical analysis was conducted to determine the effect of processing parameters on relative bond strength.

4.1.1. Transgranular and Intergranular Fracture

This section presents conclusions for transgranular fracture analysis used to determine the effect of processing parameters on relative bond strength. Fracture surfaces created during previous notched edge fracture toughness testing were examined using SEM and EDS. Relative amounts of transgranular and intergranular fracture for Al_2O_3 grains and TiB_2 grains were determined using SEM and EDS micrographs. Statistical analysis was conducted to determine the effect of processing parameters on relative bond strength as measured by relative amounts of transgranular fracture.

*Transgranular cleavage of Al_2O_3 grains was found in SEM micrographs of the fracture surface. Transgranular cleavage of Al_2O_3 grains is consistent with previous research, which showed cleavage on the basal plane in single crystal Al_2O_3. A eutectic microstructure may have been formed during the Al_2O_3-TiB_2 SHS reaction.

*Most of the areas of intergranular pullout in Sample A occurred in Al_2O_3 grains, which may indicate that there were TiB_2 grains in the indicated locations on the opposite fracture surface.

*In Samples A and B, the Al_2O_3 did not appear to show distinct grains, which may be because the Al_2O_3 melted and solidified.

*For Sample B, the grain strength within Al_2O_3 was weaker than the grain boundary strength between Al_2O_3 and TiB_2 grains.

*For Sample C, the grain strength within Al_2O_3 grains appeared to be weaker than the grain boundary strength between Al_2O_3 grains and TiB_2 grains.

*In Sample C, the indistinct grain boundaries may be due to other phenomenon such as diffusion, which would not be expected in the limited time (150-240 minutes) at 1600°C.

*In Sample D, the unusually rounded intergranular pullout may have been due to higher grain boundary strength between the TiB_2 grains and Al_2O_3 grains than the grain strength within the Al_2O_3 grains.

*Differences in amounts of transgranular fracture between upper and lower sample areas on each may have been due to the location of the facture origin in comparison with the measurement location.

*Differences between the fracture modes of Al_2O_3 grains and TiB_2 grains in the different samples may be due to the differences in the sizes of the grains as well as the grain boundary strengths between the Al_2O_3 grains and TiB_2 grains and the grain strengths within the Al_2O_3 grains and TiB_2 grains.

*Differences between these results and previous research may be due to the scale at which the analysis was conducted, the qualitative nature of previous analysis, and differences in relative amounts of transgranular fracture in the sample depending upon the location of analysis relative to the fracture origin.

*Powder processing showed as significant for relative bond strength as measured by transgranular facture in Al_2O_3 grains and transgranular fracture in TiB_2 grains.

*Predominant microstructure showed as significant for relative bond strength as measured by total transgranular fracture, transgranular fracture in Al_2O_3 grains, and transgranular fracture in TiB_2 grains.

*The interaction between powder processing and predominant microstructure showed as significant for relative bond strength as measured by total transgranular fracture and transgranular fracture in Al_2O_3 grains.

*Each measurement method is measuring relative bond strength in a slightly different way; therefore differences between measurement results may be expected.

*Each of the optimum values was greater than the actual values obtained during the experiment for the optimum factor levels indicating that there may have been more variability in the relative bond strength response than was indicated by the factor levels that were used in the experiment.

*Other factors, which may have confounded fracture mode analysis results, include sample microstructure characteristics such as phase distribution, phase size, and grain size.

4.1.2. Nano-indentation Reduced Modulus

This section presents conclusions for relative bond strength as measured by nano-indentation reduced modulus. Nano-indentation was conducted on polished samples in Al_2O_3 grains and in TiB_2 grains. Indent locations were verified using SEM. Reduced modulus for indents in Al_2O_3 grains and in TiB_2 grains were calculated from nano-indentation curve results. Statistical analysis using ANOVA of a Taguchi array was conducted to determine the effect of processing parameters on relative bond strength as measured by nano-indentation reduced modulus.

*High resolution SEM showed sinking-in in Al_2O_3 grains and piling-up in TiB_2 grains.

*Sinking-in and piling-up may have contributed to the differences between calculated and expected reduced modulii.

*Another reason for differences between expected and measured reduced modulii is that expected modulii were calculated for Al_2O_3 in bulk Al_2O_3 and TiB_2 in bulk TiB_2 rather than Al_2O_3 and TiB_2 in an Al_2O_3-TiB_2 composite.

*The elastic modulus and Poisson's ratios were likely different for each component in the composite when compared with each component in each bulk material.

*The optimum value was higher than the experimental value possibly due to other factors affecting the measurement results that were not controlled in this research, which could be related to surface and boundary conditions near the indentation locations, which include the thickness of the indented phase as well as the size of the indent relative to the grain size.

4.2. Effective Plasticity

This section describes conclusions from effective plasticity analysis. Nano-indentation curves obtained during reduced modulus testing were analyzed to determine nano-indentation final displacements and nano-indentation fracture toughness. Statistical analysis was conducted to determine the effect of processing parameters on relative effective plasticity using nano-indentation final displacements and fracture toughness as separate measures of relative effective plasticity.

4.2.1. Nano-indentation Final Displacements

This section describes results and discussion for nano-indentation final displacement determinations. Nano-indentation curves used to determine reduced modulus were analyzed to determine nano-indentation final displacements. Statistical analysis was conducted using ANOVA of Taguchi arrays to determine the effect of processing parameters on relative effective plasticity using nano-indentation final displacements as a measure of relative effective plasticity.

*Final displacements in TiB_2 grains were generally less than final displacements in Al_2O_3 grains.

*Differences in final displacements between samples may have been due to the microstructure differences between samples, including differences in grain size, distribution of the phases, and thickness of the grain being indented.

*One of the main factors, powder processing, was not significant at a 90% confidence level but the interaction between all three factors was significant.

4.2.2. Nano-indentation Fracture Toughness

This section presents conclusions from determining nano-indentation fracture toughness. Nano-indentation curves obtained during reduced modulus testing were analyzed to determine nano-indentation fracture toughness. Statistical analysis was conducted to determine the effect of processing parameters on relative effective plasticity as measured by nano-indentation fracture toughness.

*There were no apparent trends in the results for the nano-indentation fracture toughness measurement results.

*None of the main factors or interactions showed as statistically significant at a 90% confidence level, which may be due to large variability in the responses obtained.

*The large error obtained during this research may be due to the difference in the material response to a Berkovich rather than cube corner indenter, the assumption that all pop-in events were due to crack formation rather than other mechanisms, such as twinning, or sample characteristics such as the thickness of the material below the indentation, and the grain size of the indented material.

4.3. Comparison of Results

This section presents conclusions from a comparison of the results obtained during the determinations of the effect of processing parameters on relative bond strength and relative effective plasticity. A comparison of the significant factors and optimization levels obtained using each measurement method was conducted.

*In Sample A, the grain boundary strength between Al_2O_3 grains and the TiB_2 grains may not have been as strong as the grain strength within Al_2O_3 grains or TiB_2 grains.

*The grain strength within Al_2O_3 may have been weaker than the grain boundary strength between Al_2O_3 and TiB_2 grains in Samples B, C, and D.

*Powder Processing was significant for most of the relative bond strength measures, but was not significant for the relative effective plasticity measures.

*The difference in strengths within grains and between grains caused by the formation of a eutectic phase may have had a stronger influence on the relative bond strength than on the relative effective plasticity.

*Predominant microstructure was significant for all measures except relative effective plasticity as measured by fracture toughness, for which none of the factors and interactions was significant.

*Differences in the distribution of the phases in each sample could cause a difference in the amount of each type of interface, TiB_2-TiB_2, Al_2O_3-TiB_2, and Al_2O_3-Al_2O_3, in each sample.

*The interaction between powder processing and predominant microstructure was significant for most of the relative bond strength measures and for relative effective plasticity as measured by final displacements.

*Indented phase was significant for the nano-indentation measures except nano-indentation fracture toughness, although the significance for Nano-indentation fracture toughness was 89.7%.

*The interaction between powder processing and indented phase and between predominant microstructure and indented phase were only significant for the relative bond strength measure using nano-indentation reduced modulus.

*The interaction between powder processing, predominant microstructure, and indented phase were significant for all the nano-indentation measures except nano-indentation fracture toughness.

*The main factor powder processing was not significant for relative effective plasticity as measured by final displacement.

*The influence factors and interactions may have been confounded by characteristics of the microstructure that were not controlled in this experiment such as the grain size of each phase, location of measurements relative to crack initiation site, and relative location of indentation compared to surface and boundary effects.

*The significance of the interactions may indicate that instead of the main factors being independent, the main factors are based on other factors which were not controlled during this research, such as grain size of each phase and thickness of each phase near the indentation location.

*The most common optimum level for powder processing was MM.

*SHS produced material had higher optimum values for relative bond strength when measured using Al_2O_3 transgranular fracture and nano-indentation reduced modulus, with the higher positive effect for total transgranular fracture.

*The nano-indentation final displacements and fracture toughness had higher optimum values for MM produced material, which may be due to the potentially stronger grain boundaries produced in SHS reactions causing a decrease in the ease of dislocation movement, which caused a decrease in the plasticity of the material.

*TiB_2 grains surrounding Al_2O_3 grains produced a higher optimum value for relative bond strength as measured by all three types of transgranular fracture, but TiB_2 grains distributed throughout Al_2O_3 grains produced a higher optimum value for relative bond strength as measured by nano-indentation reduced modulus.

*The difference in the optimum value of predominant microstructure for relative bond strength as measured by nano-indentation reduced modulus may have been due to the locations of the indentations that were chosen for the analysis.

*The optimum phase for relative bond strength was TiB_2, and for relative effective plasticity, with the exception of relative effective plasticity as measured by nano-indentation fracture toughness, was Al_2O_3 due to each material's response to deformation.

*The high error obtained during measurement of nano-indentation fracture toughness may have been caused by the formation of pop-in events from twinning rather than crack formation or through influences of surface and boundary effects including thickness of the material and grain size of the indented phase.

5. Future Work

This section presents recommendations for future work to understand the effect of processing parameters on relative bond strength and relative effective plasticity in Al_2O_3-TiB_2 composites.

An examination of fracture modes for both sides of a fracture surface would provide a more definitive description of the fracture. If both fracture surfaces were examined, it would be possible to match transgranular fracture on one surface with transgranular fracture on the matching surface, which would confirm that the fracture was in fact transgranular fracture.

An analysis of fracture mode with regards to the types of interfaces, Al_2O_3-Al_2O_3, Al_2O_3-TiB_2, and TiB_2-TiB_2, could provide information about the grain boundary strength compared to the grain strength of each phase. A quantification of the types of interfaces could be obtained by quantitatvely characterizing the distribution of the phases rather than the qualitative characterization used in this research.

An investigation of the change in fracture mode in comparison with the fracture origin could be conducted on each sample to determine if there are differences in fracture mode at different distances from the fracture origin. An exploration of the fracture modes at different length scales (by changing the magnification on SEM scans) would provide information that could explain differences in observed fracture modes between results obtain in this research and previous research.

A comparison of fracture mode with grain size throughout the samples may provide clarity about the effect of grain size on the fracture mode of the samples used in this research. A statistical analysis of grain size similar to the previous analysis of phase size would provide a basis for the fracture mode and grain size analysis.

Conducting nano-indentation fracture toughness testing using a cube corner indenter instead of a Berkovich indenter would eliminate the type of indenter as a source of error for nano-indentation fracture toughness measurements. Performing nano-indentation fracture toughness analysis using a larger sample size may provide a better statistical analysis with a smaller error. Performing nano-indentation with a larger maximum load may cause formation of cracks, which are visible in an SEM, which would allow a standard calculation of fracture toughness rather than trying to use pop-in events that may be caused by other mechanisms.

Examination of the phase thickness at the indentation site, by cutting the sample perpendicular to the surface through the center of the indent, would provide information to determine the impact of phase thickness on nano-indentation results. Conducting nano-indentation into grains of the same size for each phase could provide information that could be used to determine the influence of grain size and the influence of phase on nano-indentation response. A comparison of surface and grain boundary effects on nano-

indentation response could be conducting using the information for indents that were not analyzed in this research.

A comparison of nano-indentation response in Al_2O_3-TiB_2 with nano-indentaion response in bulk Al_2O_3 and in TiB_2 may provide insight into reasons why calculated nano-indentation reduced modulus did not match expected nano-indentation reduced modulus.

A further exploration of the formation of a eutectic during the SHS production of Al_2O_3-TiB_2 composites could provide new ways to control the properties of Al_2O_3-TiB_2 composites.

References

[1] Michael Ashby, Hugh Shercliff, and David Cebon. Materials Engineering, Science, Processing and Design. Elsevier Ltd, Oxford, UK, 2010.
[2] William D. Callister, Jr. Materials Science and Engineering. John Wily & Sons, Inc., New York, NY, 2000.
[3] C. Barry Carter and M. Grant Norton. Ceramic Materials Science and Engineering. Springer Science+Business Media, LLC., New York, NY, 2007.
[4] Norman E. Dowling. Mechanical Behavior of Materials. Prentice-Hall, Inc., Upper Saddle River, NJ, 1999.
[5] Frank A. McClintock and Ali S. Argon. Mechanical Behavior of Materials. Addison-Wesley Publishing Company, Inc., Reading, MA, 1966.
[6] John B. Wachtman, W. Roger Cannon, M John Matthewson. Mechanical Properties of Ceramics. John Wiley & Sons, Inc., New Jersey, 2009.
[7] Donald H. Buckley. Friction and Wear Behavior of Glasses and Ceramics. In *Surfaces and Interfaces of Glass and Ceramics* edited by V. D. Frechette, W. C. LaCourse, and V. L. Burdick, Materials Science Research Volume 7, Proceedings of the 1973 International Symposium on Special Topics in Ceramics, Plenum Press, New York, 1974.
[8] Barbara L Gabriel. SEM:A User's Manual for Materials Science, American Society for Metals, Metals Park, OH 1985.
[9] G. F. Pittinato, V. Kerlins, A. Phillips, and M. A. Russo. SEM/TEM Fractography Handbook, McDonnel Douglas Astronautics Company, Huntington Beach, CA, 1975.
[10] Wein-Joe Yang, Chang-Te Yu, and Albert S. Kobayashi. SEM Quantification of Transgranular vs. Intergranular Fracture. *Journal of the American Ceramic Society*, **1991**, 74 [2] 290-295.
[11] Ronald J. Kerans and Triplicane A. Parthasarathy. Fiber Coating Design Parameters for Ceramic Composites as Implied by Considerations of Debond Crack Roughness. In *Ceramic Microstructures*. Antoni P. Tomsia and Andreas M. Glaeser, Eds. Plenum Press, New York, NY, 1998.
[12] J. Cook, J. E. Gordon, C. C. Evans, and D. M. Marsh. A Mechanism for the Control of Crack Propagation in All-Brittle Systems. *Proceedings of the Royal Society of London, Series A, Mathematical and Physical Sciences*, **1964**, 282 [1391] 508-520.
[13] K. V. Logan. Elastic-Plastic Behavior of Hot Pressed Composite Titanium Diboride/Alumina Powders Produced Using Self-Propagating High Temperature Synthesis. PhD thesis, Georgia Institute of Technology, 1992.
[14] Roy W. Rice. Fracture Topography of Ceramics. In Surfaces and Interfaces of Glass and Ceramics edited by V. D. Frechette, W. C. LaCourse, and V. L. Burdick, Materials Science Research Volume 7, Proceeding of the 1973 International Symposium on Special Topics in Ceramics, Plenum Press, New York, 1974.
[15] John J. Gilman. Chemistry and Physics of Mechanical Hardness. John Wiley & Sons, Inc, Hoboken, NJ, 2009.
[16] Derek Hull. Fractography: Observing, Measuring and Interpreting Fracture Surface Topography. Cambridge University Press, Cambridge UK, 1999.
[17] A. Gatto. Critical Evaluation of Indentation Fracture Toughness Measurements with Vickers Indenter on Ceramic Matrix Composite Tools. *Journal of Materials Processing Technology*, **2002**, 85 [1] 65-67.
[18] Brian R. Lawn. Physics of Fracture. *Journal of American Ceramic Society*, Feb **1983**, 66 [2] 83-91.
[19] Gayle S. Painter, Paul F. Becher, and Ellen Y. Sun. Bonding Energies at Intergranular Interfaces in Alumina-Doped Silicon Nitride. *Journal of the American Ceramic Society*, **2002**, 85 [1] 65-67.
[20] D. B. Marshal and P. E. D. Morgan. Interface Materials for Oxide Composites. In *Ceramic Microstructures Control at the Atomic Level*. Antoni P. Tomsia and Andreas M. Glaeser, eds. Plenum Press, New York, 1998.
[21] Alison Fox Carney. The Effect of Microstructure on the Mechanical Properties of a 30% Titanium Diboride/ 70% Alumina Composite. MS thesis, Georgia Institute of Technology, 1997.
[22] Eugene Medvedoski. Alumina Ceramics for Ballistic Protection. *American Ceramic Society Bulletin*, **2002**, 81 [3] 27-32.

[23] Ronald G. Munro. Evaluated Material Properties for a Sintered alpha-Alumina. Journal of American Ceramic Society, **1997**, 80 [8] 1919-1928.
[24] Ronald J Gillespie, Donald R Eaton, David A Humphreys, and Edward A Robinson. Atoms, Molecules, and Reactions: An Introduction to Chemistry. Prentice Hall, Englewood Cliffs, NJ, 1994.
[25] M. W. Chen, J. W. McCauley, D. P. Dandekar, and N. K. Bourne. Dynamic Plasticity and Failure of High-Purity Alumina under Shock Loading. *Nature Materials*, August **2006**, 5, 614-618.
[26] G. I. Watt, S. B. Bhaduri, R. Radhakrishnan, and P. R. Taylor. Consolidation of TiB_2 Powders Produced by Plasma Synthesis of Cheap Raw Materials. In *Advanced Synthesis and Processing of Composites and Advanced Ceramics.*
[27] V. Sundaram, K. V. Logan, and R. F. Speyer. Reaction Path in the Formation of Titanium Diboride by a Magnesium Thermite Process. In *Advanced Synthesis and Processing of Composites and Advanced Ceramics.*
[28] Ronald G. Munro. Materials Properties of Titanium Diboride. *Journal of Research of the National Institute of Standards and Technology*, **2000**, 105 [5] 709-720.
[29] L. Lundstrom. Transition Metal Borides. In *Boron and Refractory Borides*, V. I. Matkovich, ed, Springer-Verlag, Berlin, 1977.
[30] M. Criakoglu, S. Bhaduri, S. B. Bhaduri. Combustion Synthesis Processing of Functionally Graded Materials in the Ti B Binary System. *Journal of Alloys and Compounds*, **2002**, 347, 259-265.
[31] Shingo Nakane, Yoshihiko Takano, Masaru Yoshinaka, Ken Hirota, and Osama Yumaguchi. Fabrication and Mechanical Properties of Titanium Diboride Ceramics. *Journal of the American Ceramic Society*, **1999**, 82 [6] 1627-1628.
[32] J. Castaing and P. Costa. Properties and Uses of Diboride. In *Boron and Refractory Borides*, V. I. Matkovich ed, Springer-Verlag, Berlin, 1977.
[33] Xiaoyan Ma, Changrong Li, Zhenmin Du, and Weijing Zhang. Thermodynamic Assessment of the Ti-B system. *Journal of Alloys and Compounds*, **2004**, 370, 149-158.
[34] B. Basu, G. B. Raju, and A. K. Suri. Processing and Properties of Monolithic TiB_2 Based Materials. International Materials Reviews, **2006**, 51 [6] 352-374.
[35] M. De Graef, J. P. A. Lofvander, C. McCullough, and C. G. Levi. The Evolution of Metastable B_f Borides in a Ti-Al-B Alloy. Acta Metallurgica et Materialia, **1992**, 40 [12] 3395-3406.
[36] Andrew R. Keller and Min Zhou. Effect of Microstructure on Dynamic Failure Resistance of Titanium Diboride/ Alumina Ceramics. *Journal of the American Ceramic Society*, **2003**, 86 [3] 449-457.
[37] T. P. DeAngelis and D. S. Weiss. Advanced Ceramics Via SHS. In Combustion and Plasma Synthesis of High-Temperature Materials, Z. A. Munir and J. B. Holt, Eds., VCH, New York, NY.
[38] Laszlo J. Kecskes, Andrus Niiler, Thomas Kottke, Kathryn V. Logan, and Guillermo R. Villalobos. Dynamic Consolidation of Combustion-Synthesis Alumina-Titanium Diboride Composite Ceramics. Journal of the American Ceramic Society, October **1996**, 79 [10] 2687-2695.
[39] Isabel K. Lloyd, Kevin J. Doherty, and Gary A. Gilde. Phase Equilibrium Studies in Al2O3-TiB2. In *Ceramic Armor Materials by Design* pg 623-628.
[40] Kathryn V. Logan. Effect of Microstructure on the Dynamic Behavior of Composite Alumina/Titanium Diboride. In *Ceramic Armor Materials by Design* pg 611-622.
[41] Kathryn V. Logan and Guillermo R. Villalobos. Thermodynamic behavior of selected SHS reactions. In *Heat Transfer in Fire and Combustion Systems*, Volume 250 of HTD, p. 249-257. 1993.
[42] M. A. Meyers, E. A. Olevsky, J. Ma, and M. Jamet. Combustion Synthesis/Densification of an Al_2O_3-TiB_2 composite. *Materials Science and Engineering*, A311:83-99, 2001.
[43] Paul F. Becher. Microstructural Design of Toughened Ceramics. *Journal of the American Ceramic Society.* **1991**, 74 [2] 255-269.
[44] Kathryn V. Logan. Process for Controlling the Microstructural Bias of Multi Phase Composites. Patent US 6,440,343 B2. August 27, 2002, filed April 14, 2000.
[45] D. E. Grady. Impact Strength and Indentation Hardness of High-Strength Ceramics. In *Shock Waves in Condensed Matter.* Elsevier, Amsterdam, 1993.
[46] Matt K. Ferber, Paul F. Becher, and Cabell B. Finch. Effect of Microstructure on the Properties of TiB2 Ceramics. *Journal of the American Ceramic Society*, **1983**, 66 [1] C-2 – C-3.
[47] Alida Bellosi, Goffredo De Portu, and Stefano Guicciardi. Preparation and Properties of Electroconductive Al_2O_3-based Composite. *Journal of European Ceramic Society*, **1992**, 10, 307-315.

[48] J. Korey Phillips. Effects of Hot Press Parameters on Microstructure and the Effects of Microstructure on Electronic Properties of a 70% Al_2O_3/ 30% TiB_2 Composite. Independent Research Report, June 8, 1996.
[49] Louis Ferranti, Jr. Processing and Characterization of Microstructurally Biased Two-Phase Titanium Diboride/Alumina Ceramic (TiB_2 +Al_2O_3). MS thesis, Georgia Institute of Technology, 2001.
[50] Greg Kennedy, Louis Ferranti, Rodney Russell, Min Zhou, and Naresh Thadhani. Influence of Microstructural Bias on the Hugoniot Elastic Limit and Spall Strength of Two-Phase TiB_2+Al_2O_3 Ceramics. *AIP Conference Proceedings*, **2002**, 220, 755-758.
[51] K. V. Logan and J. D. Walton. TiB_2 Formation Using Thermite Ignition. *Ceramic Engineering and Science Proceedings*, **1985**, 5 [7] 712-738.
[52] Roy W. Rice. Ceramic Processing: An Overview. AIChE Journal, **1990**, 36 [4] 481-510.
[53] Andrew R. Keller. An Experimental Analysis of the Dynamic Failure Response of TiB_2/Al_2O_3 Composites. MS thesis, Georgia Institute of Technology, 2000.
[54] David C. Joy. Scanning Electron Microscopy. In *Characterization of Materials Part I.* Eric Lifshin Ed. VCH Publishing Verlagsgesellschat mbH, Weinheim, Germany, 1992.
[55] Anthony C. Fischer-Cripps. Nanoindentation. Springer-Verlag New York, LLC, New York, NY, 2004.
[56] John J. Gilman. Chemistry and Physics of Mechanical Hardness. John Wiley & Sons, Inc, Hoboken, NJ, 2009.
[57] Andrew Gouldstone, Nuwong Chollacoop, Ming Dao, Ju Li, Andrew M Minor, and Yu-Lin Shen. Indentation across size scales and disciplines: Recent developments in experimentation and modeling. *Acta Materialia,* **2007**, 55, 4015-4039.
[58] TriboIndenter Manual NRL-M-100 v8.2
[59] G.R. Anstis, P. Chantikul, B.R. Lawn, and D.B. Marshall. Critical Evaluation of Indentation Techniques for Measuring Fracture Toughness: I, Direct Crack Measurements. *Journal of American Ceramic Society*, September **1981**,Vol 64, [9], 533-538.
[60] A. Leonardi, F. Furgouele, S. Syngellakis, and R. Wood. Analytical Approaches to Stress Intensity Factor Evaluation for Indentation Cracks. *J. Am. Ceram. Soc*., **2009**, 92 [5] 1093-1097.
[61] S. Field, M. V. Swain, and R. D. Dukino. Determination of Fracture Toughness from the Extra Penetration Produced by Indentation-Induced Pop-in. *Journal of Materials Research*, **2003**, 18 [6] 1412-1419.
[62] Jiju Antony. Design of Experiments for Engineers and Scientists. Butterworth-Heinemann, Burlington, MA, 2003.
[63] Douglas C. Montgomery. Design and Analysis of Experiments. John Wiley & Sons, Inc., New York, NY, 2009.
[64] Ranjit K. Roy. Design of Experiments Using the Taguchi Approach. John Wiley & Sons, Inc., New York, NY, 2001.
[65] Genichi Taguchi, Subir Chowdhury, Yuin Wu. Taguchi's Quality Engineering Handbook. John Wiley & Sons, Inc. Hoboken, NJ, 2005.

Appendix

Example Calculations from Section 3.1.1.2: Relative Bond Strength from Transgranular Fracture

Example calculations are shown using measurements from the upper middle location of sample A. Total amounts of transgranular fracture in each location were determined by adding the area of transgranular fracture in Al_2O_3 grains and transgranular fracture in TiB_2 grains as shown in Equation A.1.

$$A_{Trans,Total} = A_{Trans,Al_2O_3} + A_{Trans,TiB_2} = 67429 + 5575 = 73004 \quad \text{(A.1)}$$

The relative amount of transgranular fracture in each location was calculated by dividing the total amount of transgranular fracture by the total area, then converting the decimal to a percent, as shown in Equation A.2.

$$A_{Rel,Trans} = A_{Trans,Total} = 73004/119498 = 61.092\% \quad \text{(A.2)}$$

The total area was calculated as shown in Equation A.3. The relative amount of total transgranular fracture in each location was one measure used to determine the relative bond strength for each sample.

$$A_{Total} = A_{Trans,Al_2O_3} + A_{Trans,TiB_2} + A_{Inter,Al_2O_3} + A_{Inter,TiB_2} = 119498 \quad \text{(A.3)}$$

The relative amount of transgranular fracture of Al_2O_3 grains was determined by dividing the relative amount of transgranular fracture for Al_2O_3 grains by the total area of Al_2O_3 grains for each location, then converting the decimal to a percent, as shown in Equation A.4.

$$A_{Rel,Trans,Al_2O_3} = A_{Trans,Al_2O_3} / A_{Total,Al_2O_3} = 67429/88668 = 76.047\% \quad \text{(A.4)}$$

The same calculations were performed for transgranular fracture in TiB_2 grains as shown in Equation A.5.

$$A_{Rel,Trans,TiB_2} = A_{Trans,TiB_2} / A_{Total,TiB_2} = 5575/30830 = 18.08\% \quad \text{(A.5)}$$

Example Calculations and Minitab Analysis Results from Section 3.1.1.3: Effect of Processing Parameters on Relative Bond Strength using Transgranular Fracture

The first step in the ANOVA analysis was to determine the total sum of the squares, SS_T, as shown in Equation A.6. The total number of results, N, was calculated from the total number of runs, a, and the total number of results for each run, b, as shown in Equation A.7.

$$SS_T = \left(\sum_{i=1}^{4}\sum_{j=1}^{2} y_{ij}^2\right) - \frac{y_{total}^2}{N} = \left(61.09^2 + ... + 30.48^2\right) - \frac{449.00^2}{8} \qquad (A.6)$$
$$= 27601.6 - 25197 = 2404.79$$

$$N = a * b = 4 * 2 = 8 \qquad (A.7)$$

In order to calculate the sum of the squares for each factor, it was necessary to determine which result values corresponded with each level of that factor. For the Factor A, the values y_{11}, y_{12}, y_{21}, and y_{22} corresponded to level 1 of factor A. The values y_{31}, y_{32}, y_{41}, and y_{42} corresponded to level 2 of factor A. The sum of the squares for factor A was calculated by adding the values for the first level, then squaring that total, then adding the values for the second level and squaring the second level total. Then the whole total was divided by the number of results for each run, c, and then subtracting the grand total squared divided by the total number of results. The sum of the squares was calculated using Equation A.8. The number of results for each run, c, was calculated using Equation A.9.

$$SS_A = \frac{1}{c}\begin{bmatrix}\left(y_{11} + y_{12} + y_{21} + y_{22}\right)^2 \\ +\left(y_{31} + y_{32} + y_{41} + y_{42}\right)^2\end{bmatrix} - \frac{y_{total}^2}{N}$$
$$= \frac{1}{4}\begin{bmatrix}\left(61.09 + 67.95 + 47.79 + 62.28\right)^2 \\ +\left(73.22 + 77.21 + 28.95 + 30.48\right)^2\end{bmatrix} - \frac{449.00^2}{8} = 2404.79 \qquad (A.8)$$

$$c = \frac{a}{2} * b = \frac{4}{2} * 2 = 4 \qquad (A.9)$$

This method was continued to calculate the sum of the squares for the other factors, SS_B and SS_{AxB}, as shown in Equations A.10 and A.11.

$$SS_B = \frac{1}{c}\left[\left(y_{11} + y_{12} + y_{31} + y_{32}\right)^2 + \left(y_{21} + y_{22} + y_{41} + y_{42}\right)^2\right] - \frac{y_{total}^2}{N} \qquad (A.10)$$

$$SS_{AxB} = \frac{1}{c}\left[\left(y_{11} + y_{12} + y_{41} + y_{42}\right)^2 + \left(y_{21} + y_{22} + y_{31} + y_{32}\right)^2\right] - \frac{y_{total}^2}{N} \qquad (A.11)$$

The sum of the squares for the error, SS_E, was calculated using Equation A.12.

$$SS_E = SS_T - SS_A - SS_B - SS_{AxB} = 2404.79 - 107.00 - 1511.97 - 648.69 = 137.13 \quad \text{(A.12)}$$

The number of degrees of freedom, DF_F, for the total was calculated as shown in Equation A.13.

$$DF_T = N - 1 = 8 - 1 = 7 \quad \text{(A.13)}$$

The number of degrees of freedom for each factor, DF_A, DF_B, and DF_{AxB}, was calculated as shown in Equation A.14.

$$DF_A = DF_B = DF_{AxB} = (number\,of\ levels) - 1 = 2 - 1 = 1 \quad \text{(A.14)}$$

The number of degrees of freedom for the error term was calculated as shown in Equation A.15.

$$DF_E = DF_T - \sum DF_{Factor} = 7 - 3 = 4 \quad \text{(A.15)}$$

The mean square for each factor, MS_A, MS_B, and MS_{AxB}, was calculated as shown in Equations A.16, A.17, and A.18.

$$MS_A = SS_A / DF_A = 107.00/1 = 107.00 \quad \text{(A.16)}$$

$$MS_B = SS_B / DF_B = 1511.97/1 = 1511.97 \quad \text{(A.17)}$$

$$MS_{AxB} = SS_{AxB} / DF_{AxB} = 648.69/1 = 648.69 \quad \text{(A.18)}$$

The mean square for the error, MS_E, term was calculated as shown in Equation A.19.

$$MS_E = SS_E / DF_E = 137.13/4 = 34.283 \quad \text{(A.19)}$$

The F-value for each factor, F_A, F_B, and F_{AxB}, was calculated as shown in Equations A.20, A.21, and A.22.

$$F_A = MS_A / MS_E = 107.00/34.283 = 3.1211 \quad \text{(A.20)}$$

$$F_B = MS_B / MS_E = 1511.97/34.283 = 44.103 \quad \text{(A.21)}$$

$$F_C = MS_C / MS_E = 648.69/34.283 = 18.922 \quad \text{(A.22)}$$

The F-value was compared with a tabulated F-value to determine the probability of significance or confidence level, *(1-a)*, of the factor. For a probability of significance of 90%, the confidence interval, *a*, would be 10%, as shown in Equation A.23.

$$\alpha = 100\% - 90\% = 10\% = 0.10 \tag{A.23}$$

The tabulated F-value was determined according to Equation A.24.

$$F_{tabulated} = F_{\alpha, DF_{factor}, DF_{error}} = F_{0.10,1,4} = 4.545 \tag{A.24}$$

The Minitab software displays the confidence interval as the P-value. The Minitab summary of results for effect of processing parameter on relative bond strength as measured by total transgranular fracture is shown in Table A.1.

Table A.1 L4 Results for Effect of Processing Parameters on Bond Strength as Measured by Total Transgranular Fracture

Source of Variation	Sum of Squares	Degrees of Freedom	Mean Square	F_0	P-Value	C.L.
A: Powder Processing	107.00	1	107.00	3.11	0.153	84.7
B: Predominant Microstructure	1512.01	1	1512.01	43.96	0.003	99.7
AxB: Interaction between powder processing and predominant microstructure	648.68	1	648.68	18.86	0.012	98.8
Error	137.57	4	34.39			
Total	2405.26	7				

The effect of factor A, $E_{A,2}$, was determined from the average of the values for each level of factor A, as shown in Equation A.25.

$$E_{A,2} = L_{A,2} - L_{A,1} = 52.464 - 59.779 = -7.314 \tag{A.25}$$

The average of the values for each level of factor A, $L_{A,level}$, was calculated as shown in Equations A.26 and A.27.

$$L_{A,2} = \frac{1}{c}\left(y_{11} + y_{12} + y_{21} + y_{22}\right) = \frac{1}{4}\left(61.09 + 67.95 + 47.79 + 62.28\right) = 59.78 \tag{A.26}$$

$$L_{A,1} = \frac{1}{c}\left(y_{31} + y_{32} + y_{41} + y_{42}\right) = \frac{1}{4}\left(73.22 + 77.21 + 28.95 + 30.48\right) = 52.46 \tag{A.27}$$

Once the effect of each factor was determined, an optimum value was determined as shown in Equation A.28. The optimum value, *Opt*, was calculated by using the overall average value, $Avg_{Overall}$, calculated using Equation A.29.

$$\begin{aligned} Opt &= Avg_{Overall} + E_{A,Level} + E_{B,Level} + E_{AxB,Level} \\ &= 56.12 + (-7.31) + 27.50 + 18.01 = 94.31 \end{aligned} \tag{A.28}$$

$$Avg_{Overall} = \frac{y_{total}}{a*b} = \frac{449.0}{4*2} = 56.12 \quad \text{(A.29)}$$

The Minitab summary of results for the effect of processing parameters on relative bond strength as measured by transgranular fracture in Al_2O_3 grains is shown in Table A.2

Table A.2 L4 Results for Effect of Processing Parameters on Relative Bond Strength as Measured by Al_2O_3 Transgranular Fracture

Source of Variation	Sum of Squares	Degrees of Freedom	Mean Square	F_0	P-Value	C.L.
A: Powder Processing	1715.76	1	1715.76	20.98	0.010	99.0
B: Predominant Microstructure	1440.15	1	1440.15	17.61	0.014	98.6
AxB: Interaction between powder processing and predominant microstructure	806.65	1	806.65	9.86	0.035	96.5
Error	327.11	4	81.78			
Total	4289.67	7				

The Minitab summary of results for the effect of processing parameters on relative bond strength as measured by transgranular fracture in TiB_2 grains is shown in Table A.3.

Table A.3 L4 Results for Effect of Processing Parameters on Relative Bond Strength as Measured by TiB_2 Transgranular Fracture

Source of Variation	Sum of Squares	Degrees of Freedom	Mean Square	F_0	P-Value	C.L.
A: Powder Processing	4811.62	1	4811.62	34.19	0.004	99.6
B: Predominant Microstructure	1004.20	1	1004.20	7.14	0.056	94.4
AxB: Interaction between powder processing and predominant microstructure	488.70	1	488.70	3.47	0.136	86.4
Error	562.94	4	140.74			
Total	6867.45	7				

Example Calculations from Section 3.1.2.1: Determination of Nano-indentation Reduced Modulus

Figure A.1 shows the nano-indentation load-displacement curve for one location in Sample A in an Al_2O_3 grain. The units displayed are Newtons and meters so that slope calculations will be in the desired standard units. The slope of the unloading curve, dP/dh, is shown as 130,077 N/m.

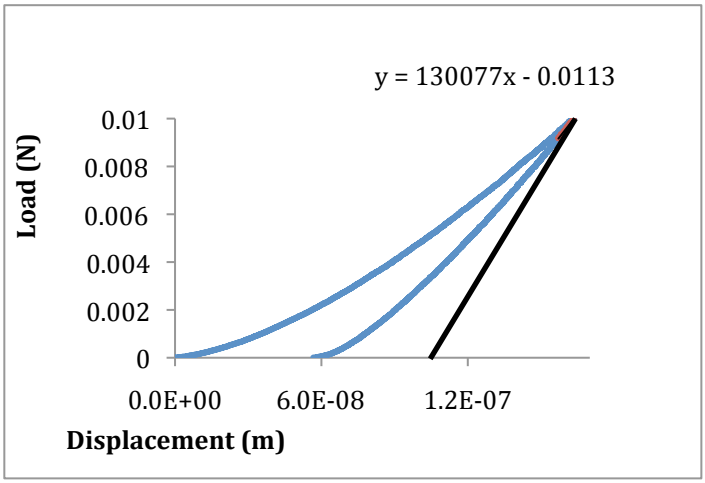

Figure A.1 Nano-indentation Curve in an Al_2O_3 Grain in Sample A

The reduced modulus, E_r, was calculated using Equation A.30.

$$E_r = \frac{1}{2(1.034)h_p}\sqrt{\frac{\pi}{24.494}} * \frac{dP}{dh}_{measured}$$

$$= \frac{1}{2(1.034)(8.69E-8\ m)}\sqrt{\frac{\pi}{24.494}} * 130077\ N/m \qquad \text{(A.30)}$$

$$= 2.59E11\ N/m^2 = 259\ GPa$$

The plastic displacement, h_p, was calculated from the slope of the unloading line as shown in Equation A.31.

$$h_p = x = \frac{y-b}{m} = \frac{0-(slope\ intercept)}{dP/dh} = \frac{0-(-0.0113)}{130077} = 8.69E-8\ m \qquad \text{(A.31)}$$

Example Calculations from Section 3.1.2.2: Effect of Processing Parameters on Relative Bond Strength using Nano-indentation Reduced Modulus

Example calculations were used to verify results obtained from Minitab. The first step in ANOVA analysis was to calculate the grand total, y_{total}, of all results as shown in Equations A.32.

$$y_{total} = \sum_{i=1}^{8}\sum_{j=1}^{5} y_{ij} = 257.53 + 253.17 + ... + 242.07 + 247.61 = 9598.35 \quad \text{(A.32)}$$

Then, the total sum of the squares, SS_T, was calculated as shown in Equation A.33. The total number of results, N, was calculated as shown in Equation A.34, where a is the number of runs and b is the number of results for each run.

$$SS_T = \left(\sum_{i=1}^{4}\sum_{j=1}^{2} y_{ij}^2\right) - \frac{y_{total}^2}{N} = \left(257.53^2 + ... + 247.61^2\right) - \frac{9598.35^2}{40} \quad \text{(A.33)}$$
$$= 2485609 - 2303200 = 182409$$

$$N = a * b = 8 * 5 = 40 \quad \text{(A.34)}$$

The sum of the squares for each factor, SS_A, SS_B, SS_C , SS_{AxB}, SS_{BxC}, SS_{BxC}, and SS_{AxBxC}, was calculated using Equations A.35 through A.42.

$$SS_A = \frac{1}{c}\left[\left(\sum_{i=1}^{4}\sum_{j=1}^{5} y_{ij}\right)^2 + \left(\sum_{i=5}^{8}\sum_{j=1}^{5} y_{ij}\right)^2\right] - \frac{y_{total}^2}{N} \quad \text{(A.35)}$$
$$= \frac{1}{20}\left[\left(257.53 + ... + 369.77\right)^2 + \left(126.26 + ...247.61\right)^2\right] - \frac{9598.35^2}{40} = 119269$$

$$c = \frac{a}{2} * b = \frac{8}{2} * 5 = 20 \quad \text{(A.36)}$$

$$SS_B = \frac{1}{c}\left[\left(\sum_{j=1}^{5} y_{1j} + \sum_{j=1}^{5} y_{2j} + \sum_{j=1}^{5} y_{5j} + \sum_{j=1}^{5} y_{6j}\right)^2 + \left(\sum_{j=1}^{5} y_{3j} + \sum_{j=1}^{5} y_{4j} + \sum_{j=1}^{5} y_{7j} + \sum_{j=1}^{5} y_{8j}\right)^2\right] \quad \text{(A.37)}$$
$$-\frac{y_{total}^2}{N} = \frac{1}{20}\left[\begin{matrix}\left(257.53 + ... + 314.38 + 126.26 + ... + 185.47\right)^2 \\ +(268.95 + ... + 369.77 + 182.91 + ... + 247.61)^2\end{matrix}\right] - \frac{9598.35^2}{40} = 12755$$

$$SS_C = \frac{1}{c}\left[\begin{array}{l}\left(\sum_{j=1}^{5} y_{1j} + \sum_{j=1}^{5} y_{3j} + \sum_{j=1}^{5} y_{5j} + \sum_{j=1}^{5} y_{7j}\right)^2 \\ +\left(\sum_{j=1}^{5} y_{2j} + \sum_{j=1}^{5} y_{4j} + \sum_{j=1}^{5} y_{6j} + \sum_{j=1}^{5} y_{8j}\right)^2\end{array}\right] - \frac{y_{total}^2}{N}$$

$$= \frac{1}{20}\left[\begin{array}{l}\left(257.53 + ... + 262.74 + 268.95 + ... + 206.84 \right.\\ \left.+126.26 + ... + 155.98 + 182.91 + ... + 194.13\right)^2 \\ \left(318.42 + ... + 314.38 + 334.11 + ... + 369.77 \right.\\ \left.+178.48 + ... + 185.47 + 214.94 + ... + 247.61\right)^2\end{array}\right] \qquad \text{(A.38)}$$

$$- \frac{9598.35^2}{40} = 36195$$

$$SS_{AxB} = \frac{1}{c}\left[\begin{array}{l}\left(\sum_{j=1}^{5} y_{1j} + \sum_{j=1}^{5} y_{2j} + \sum_{j=1}^{5} y_{7j} + \sum_{j=1}^{5} y_{8j}\right)^2 \\ +\left(\sum_{j=1}^{5} y_{3j} + \sum_{j=1}^{5} y_{4j} + \sum_{j=1}^{5} y_{5j} + \sum_{j=1}^{5} y_{6j}\right)^2\end{array}\right] - \frac{y_{total}^2}{N}$$

$$= \frac{1}{20}\left[\begin{array}{l}\left(257.53 + ... + 262.74 + 318.42 + ... + 314.38 \right.\\ \left.+182.91 + ... + 194.13 + 214.94 + ... + 247.61\right)^2 \\ \left(268.95 + ... + 206.84 + 334.11 + ... + 369.77 \right.\\ \left.+126.26 + ... + 155.98 + 178.48 + ... + 185.47\right)^2\end{array}\right] \qquad \text{(A.39)}$$

$$- \frac{9598.35^2}{40} = 3920$$

$$SS_{AxC} = \frac{1}{c}\left[\begin{array}{l}\left(\sum_{j=1}^{5} y_{1j} + \sum_{j=1}^{5} y_{3j} + \sum_{j=1}^{5} y_{6j} + \sum_{j=1}^{5} y_{8j}\right)^2 \\ +\left(\sum_{j=1}^{5} y_{2j} + \sum_{j=1}^{5} y_{4j} + \sum_{j=1}^{5} y_{5j} + \sum_{j=1}^{5} y_{7j}\right)^2\end{array}\right] - \frac{y_{total}^2}{N}$$

$$= \frac{1}{20}\left[\begin{array}{l}\left(257.53 + ... + 262.74 + 268.95 + ... + 206.84 \right.\\ \left.+178.48 + ... + 185.47 + 214.94 + ... + 247.61\right)^2 \\ \left(318.42 + ... + 314.38 + 334.11 + ... + 369.77 \right.\\ \left.+126.26 + ... + 155.98 + 182.91 + ... + 194.13\right)^2\end{array}\right] \qquad \text{(A.40)}$$

$$- \frac{9598.35^2}{40} = 1900$$

$$SS_{BxC} = \frac{1}{c}\left[\begin{array}{l}\left(\sum_{j=1}^{5} y_{1j} + \sum_{j=1}^{5} y_{4j} + \sum_{j=1}^{5} y_{5j} + \sum_{j=1}^{5} y_{8j}\right)^2 \\ +\left(\sum_{j=1}^{5} y_{2j} + \sum_{j=1}^{5} y_{3j} + \sum_{j=1}^{5} y_{6j} + \sum_{j=1}^{5} y_{7j}\right)^2\end{array}\right] - \frac{y_{total}^2}{N}$$

$$= \frac{1}{20}\left[\begin{array}{l}\left(\begin{array}{l}257.53 + ... + 262.74 + 334.11 + ... + 369.77 \\ +126.26 + ... + 155.98 + 214.94 + ... + 247.61\end{array}\right)^2 \\ \left(\begin{array}{l}318.42 + ... + 314.38 + 268.95 + ... + 206.84 \\ +178.48 + ... + 185.47 + 182.91 + ... + 194.13\end{array}\right)^2\end{array}\right] \qquad \text{(A.41)}$$

$$- \frac{9598.35^2}{40} = 1100$$

$$SS_{AxBxC} = \frac{1}{c}\left[\begin{array}{l}\left(\sum_{j=1}^{5} y_{1j} + \sum_{j=1}^{5} y_{4j} + \sum_{j=1}^{5} y_{6j} + \sum_{j=1}^{5} y_{7j}\right)^2 \\ +\left(\sum_{j=1}^{5} y_{2j} + \sum_{j=1}^{5} y_{3j} + \sum_{j=1}^{5} y_{5j} + \sum_{j=1}^{5} y_{8j}\right)^2\end{array}\right] - \frac{y_{total}^2}{N}$$

$$= \frac{1}{20}\left[\begin{array}{l}\left(\begin{array}{l}257.53 + ... + 262.74 + 334.11 + ... + 369.77 \\ +178.48 + ... + 185.47 + 182.91 + ... + 194.13\end{array}\right)^2 \\ \left(\begin{array}{l}318.42 + ... + 314.38 + 268.95 + ... + 206.84 \\ +126.26 + ... + 155.98 + 214.94 + ... + 247.61\end{array}\right)^2\end{array}\right] \qquad \text{(A.42)}$$

$$- \frac{9598.35^2}{40} = 1460$$

The sum of the squares for the error, SS_E, was calculated using Equation A.43.

$$\begin{array}{c} SS_E = SS_T - SS_A - SS_B - SS_C - SS_{AxB} - SS_{AxC} - SS_{BxC} - SS_{AxBxC} \\ = 182409 - 119269 - 12755 - 36195 - 3920 - 1900 - 1100 - 1460 = 5810 \end{array} \qquad \text{(A.43)}$$

The number of degrees of freedom, DF_T, for the total was calculated as shown in Equation A.44.

$$DF_T = N - 1 = 40 - 1 = 39 \qquad \text{(A.44)}$$

The number of degrees of freedom for each factor, DF_{Factor}, was calculated as shown in Equation A.45.

$$DF_{Factor} = DF_A = DF_B = ... = DF_{AxBxC} = (number\ of\ levels) - 1 = 2 - 1 = 1 \quad \text{(A.45)}$$

The number of degrees of freedom for the error term was calculated as shown in Equation A.46.

$$DF_E = DF_T - \sum DF_{Factor} = 39 - 7 = 32 \quad \text{(A.46)}$$

The mean square for each factor, MS_{Factor}, was calculated as shown in Equations A.47 to A.53.

$$MS_A = SS_A / DF_A = 119269/1 = 119269 \quad \text{(A.47)}$$

$$MS_B = SS_B / DF_B = 12755/1 = 12755 \quad \text{(A.48)}$$

$$MS_C = SS_C / DF_C = 36195/1 = 36195 \quad \text{(A.49)}$$

$$MS_{AxB} = SS_{AxB} / DF_{AxB} = 3920/1 = 3920 \quad \text{(A.50)}$$

$$MS_{AxC} = SS_{AxC} / DF_{AxC} = 1900/1 = 1900 \quad \text{(A.51)}$$

$$MS_{BxC} = SS_{BxC} / DF_{BxC} = 1100/1 = 1100 \quad \text{(A.52)}$$

$$MS_{AxBxC} = SS_{AxBxC} / DF_{AxBxC} = 1460/1 = 1460 \quad \text{(A.53)}$$

The mean square for the error, MS_E, term was calculated as shown in Equation A.54.

$$MS_E = SS_E / DF_E = 5810/32 = 181.6 \quad \text{(A.54)}$$

The F-value for each factor, F_{factor}, was calculated as shown in Equations A.55 to A.61.

$$F_A = MS_A / MS_E = 119269/181.6 = 656.8 \quad \text{(A.55)}$$

$$F_B = MS_B / MS_E = 12755/181.6 = 70.24 \quad \text{(A.56)}$$

$$F_C = MS_C / MS_E = 36195/181.6 = 199.3 \quad \text{(A.57)}$$

$$F_{AxB} = MS_{AxB} / MS_E = 3920/181.6 = 21.59 \quad \text{(A.58)}$$

$$F_{AxC} = MS_{AxC} / MS_E = 1900/181.6 = 10.46 \quad \text{(A.59)}$$

$$F_{BxC} = MS_{BxC} / MS_E = 1100/181.6 = 6.057 \quad \text{(A.60)}$$

$$F_{AxBxC} = MS_{AxBxC} / MS_E = 1460/181.6 = 8.040 \quad \text{(A.61)}$$

The F-value was compared with a tabulated F-value to determine the probability of significance, *(1-a)*, of the factor. The tabulated F-value was determined according to Equation A.62.

$$F_{tabulated} = F_{\alpha,DF_{factor},DF_{error}} = F_{0.10,1,32} = 2.869 \quad \text{(A.62)}$$

The Minitab summary of results for the effect of processing parameters on relative bond strength as measured by nano-indentation reduced modulus is shown in Table A.4.

Table A.4 Calculation of Sum of the Squares for L8 Taguchi Array using Nano-indentation Reduced Modulus as a Measure of Relative Bond Strength

Source of Variation	Sum of Squares	Degrees of Freedom	Mean Square	F_0	P-Value	C.L.
A: Powder Processing	119261	1	119261	651.9	0	100
B: Predominant Microstructure	12747	1	12747	69.67	0	100
C: Indented Phase	36185	1	36185	197.8	0	100
AxB: Interaction between powder processing and predominant microstructure	3910	1	3910	21.37	0	100
AxC: Interaction between powder processing and indented phase	1892	1	1892	10.34	0.003	99.7
BxC: Interaction between predominant microstructure and indented phase	1092	1	1092	5.97	0.020	98.0
AxBxC: Interaction between powder processing, predominant microstructure, and indented phase	1447	1	1447	7.91	0.008	99.2
Error	5854	32	183			
Total	182389	39				

The effect of each factor, E_{Factor}, was determined from the average of the values for each level of that factor, using factor A as an example, as shown in Equation A.63.

$$E_{A,2} = L_{A,2} - L_{A,1} = 185.35 - 294.56 = -109.21 \quad \text{(A.63)}$$

The average of the values for each level of each factor was calculated as shown in Equations A.64 and A.65, using factor A as an example.

$$L_{A,2} = \frac{1}{c}\left(\sum_{i=5}^{8}\sum_{j=1}^{5} y_{ij}\right) = \frac{1}{20}(126.26 + ... + 247.61) = 185.35 \quad \text{(A.64)}$$

$$L_{A,1} = \frac{1}{c}\left(\sum_{i=1}^{4}\sum_{j=1}^{5} y_{ij}\right) = \frac{1}{20}(257.53 + ... + 369.77) = 294.56 \quad \text{(A.65)}$$

Once the effect of each factor was determined, an optimum value was determined as shown in Equation 3.66. The optimum value, *Opt*, was calculated by using the overall average value, $Avg_{Overall}$, calculated using Equation A.67.

$$\begin{aligned} Opt &= Avg_{overall} + E_{A,level} + E_{B,level} + E_{C,level} + E_{AxB,level} \\ &+ E_{AxC,level} + E_{BxC,level} + E_{AxBxC,level} = 239.958 + 109.21 \\ &-35.70 - 60.15 + 19.77 - 13.75 + 10.45 + 12.03 = 281.818 \end{aligned} \quad \text{(A.66)}$$

$$Avg_{overall} = \frac{y_{total}}{a * b} = \frac{9598.35}{40} = 239.959 \quad \text{(A.67)}$$

Example Calculations from Section 3.2.1.2: Effect of Processing Parameters on Relative Effective Plasticity using Nano-indentation Final Displacements

The Minitab summary of results for the effect of processing parameters on relative effective plasticity as measured by nano-indentation final displacement is shown in Table A.5.

Table A.5 Calculation of Sum of the Squares for L8 Taguchi Array using Nano-indentation Final Displacements as a Measure of Relative Effective Plasticity

Source of Variation	Sum of Squares	Degrees of Freedom	Mean Square	F_0	P-Value	C.L.
A: Powder Processing	1.23	1	1.23	0.08	0.777	22.3
B: Predominant Microstructure	50.6	1	50.6	3.38	0.075	92.5
C: Indented Phase	4020	1	4020	268.23	0	100
AxB: Interaction between powder processing and predominant microstructure	226	1	226	15.05	0	100
AxC: Interaction between powder processing and indented phase	38.0	1	38.0	2.54	0.121	87.9
BxC: Interaction between predominant microstructure and indented phase	30.6	1	30.6	2.04	0.163	83.7
AxBxC: Interaction between powder processing, predominant microstructure, and indented phase	198	1	198	13.21	0.001	99.0
Error	480	32	15.0			
Total	5044	39				

Example Calculations from Section 3.2.2.1: Determination of Nano-indentation Fracture Toughness

A sample calculation using the five nano-indentation load-displacement curves for Al_2O_3 grains in Sample A is shown. The nano-indenter output was used to determine the maximum load, P, and plastic displacement, h_p, used to calculate hardness as shown in Equation A.68.

$$H = \frac{P}{24.494 h_p^2} = \frac{9992E-6\ N}{24.494(58E-9\ m)^2} = 1.21E11\ Pa = 121\ GPa \qquad \text{(A.68)}$$

The five nano-indentation load-displacement curves for Al_2O_3 grains in Sample A were superimposed upon each other to show changes in slope as shown in Figure A.2. The curves for samples #23, 25, and 26 showed slopes that did not change slope and had maximum displacements of 161, 161, and 162 nm respectively. The curve for sample #17 showed a change in slope near 78 nm as shown in Figure A.3(a). The maximum displacement for sample #17 was 163 nm. The curve for sample #14 showed a change in slope near 127 nm and a maximum displacement of 165 nm as shown in Figure A.3(b).

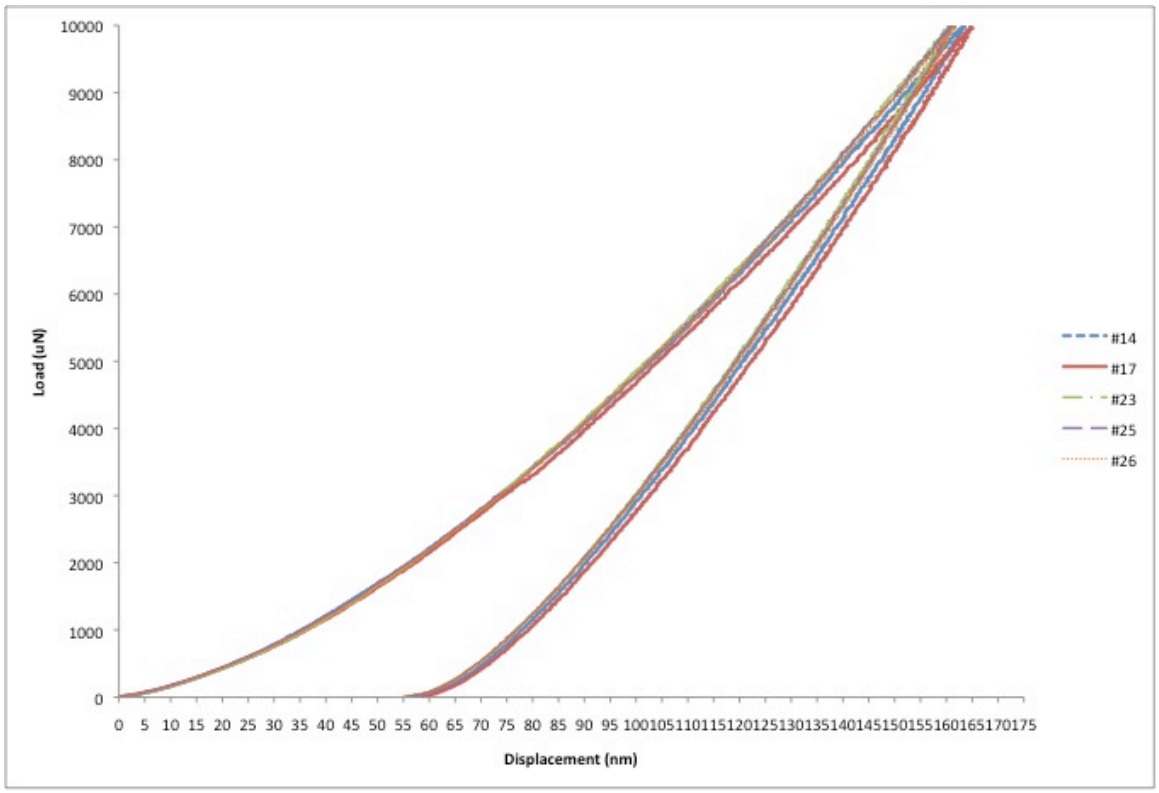

Figure A.2 Load-Displacement Graphs for Al_2O_3 Grains in Sample A

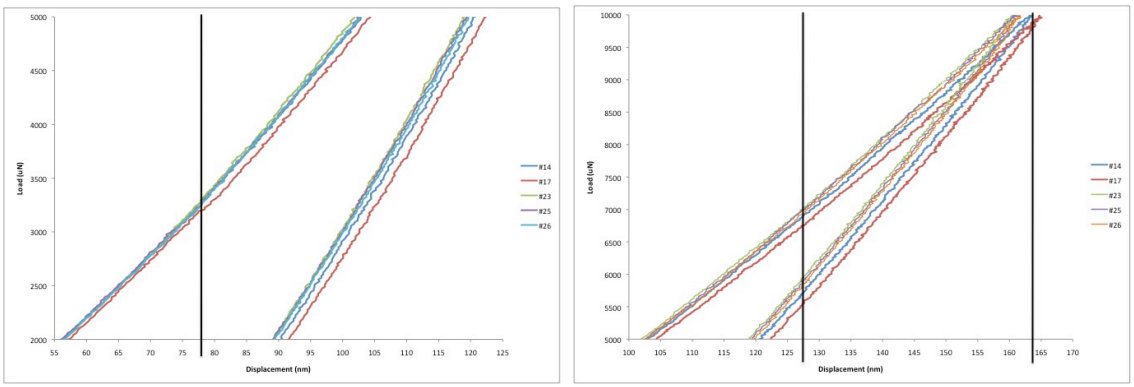

Figure A.3 Load-Displacement Graphs for Al_2O_3 Grains in Sample A Showing Change in Slope for (a) Sample #17 and (b) Sample #14

The value of h_t was obtained from the average of the final displacements for samples that did not change slope, as shown in Equation A.69.

$$h_t = \frac{161 + 161 + 162}{3} = 161.3\ nm \tag{A.69}$$

The value of h_m was obtained from the final displacement for each sample that did change slope. The value for h_x was obtained using Equation A.70.

$$h_x = h_m - h_t = 163 - 161.3\ nm = 1.7\ nm = 1.7E-9\ m \tag{A.70}$$

Equation 3.71 was used to calculate the crack length. The reduced modulus, E_r, was obtained through calculations using Equation A.71.

$$\begin{aligned} c &= \sqrt{2h_m} + \left(Q\frac{E_r}{H} - \sqrt{2}\right)h_x \\ &= \sqrt{2(163E-9\ m)} + \left(4.73 * \frac{257.5}{H} - \sqrt{2}\right) * 1.7E-9\ m \\ &= 7.96E-8\ m \end{aligned} \tag{A.71}$$

The reduced modulus, E_r, along with the bulk modulus of the indenter, E_i, Poisson's ratio of the indenter, u_i, and the Poisson's ratio of the bulk material, u_s, were used to calculate the bulk modulus of the sample, E_s, as shown in Equation A.72.

$$\begin{aligned} E_s &= \frac{E_r E_i\left(1-\nu_s^2\right)}{E_i - E_r\left(1-\nu_i^2\right)} \\ &= \frac{2.58E11\ Pa * 1.14E12\ Pa * (1-0.231^2)}{1.14E12\ Pa - 258E11\ Pa * (1-0.07^2)} \\ &= 3.14E11\ Pa = 314\ GPa \end{aligned} \tag{A.72}$$

The calculated hardness, H, calculated sample bulk modulus, E, and maximum load, P, and calculated crack length, c, were used to determine the fracture toughness, K_c, as shown in Equation A.73.

$$K_c = 0.016\left(\frac{E}{H}\right)^{0.5}\frac{P}{c^{3/2}}$$
$$= 0.016 * \left(\frac{3.14E11\,Pa}{2.48E10\,Pa}\right)^{0.5}\frac{9.99E-3\,N}{(7.96E-8\,m)^{3/2}} \qquad \text{(A.73)}$$
$$= 2.54E7\,N/m^{3/2} = 25.4\,MPa/m^{1/2}$$

The results of calculations for nano-indentation load-displacement curves for Al_2O_3 grains in Sample A are shown in Table A.6.

Table A.6 Summary of Results for Nano-indentation in Al_2O_3 Grains in Sample A

Sample	P (mm)	h_p (nm)	H (GPa)	E_r (GPa)	E_s (GPa)	h_m (nm)	h_t (nm)	c (m)	Kc ($MPa/m^{1/2}$)
14	9992.3	58	121	257	314	163		7.96E-8	25.4
17	9992.8	59	117	253	308	165		1.78E-7	7.63
23	9992.7	57	126	267	329		161		
25	9992.3	57	126	264	325		161		
26	9992.3	55	135	263	323		162		
Avg							161		

The Minitab summary of results for the effect of processing parameters on relative effective plasticity as measured by nano-indentation fracture toughness is shown in Table A.7.

Table A.7 Calculation of Sum of the Squares for L8 Taguchi Array

Source of Variation	Sum of Squares	Degrees of Freedom	Mean Square	F_0	P-Val	C.L.
A: Powder Processing	121	1	121	0.28	0.613	38.7
B: Predominant Microstructure	622	1	622	1.42	0.267	73.3
C: Indented Phase	1480	1	1480	3.38	0.103	89.7
AxB: Interaction between powder processing and predominant microstructure	8.75	1	8.75	0.02	0.891	10.9
AxC: Interaction between powder processing and indented phase	174	1	174	0.40	0.546	45.4
BxC: Interaction between predominant microstructure and indented phase	398	1	398	0.91	0.368	63.2
AxBxC: Interaction between powder processing, predominant microstructure, and indented phase	483	1	483	1.10	0.324	67.6
Error	3502	8	483			
Total	6789	15				